Optical Design Guidelines for Spectral Splitting Photovoltaic Systems: A Sensitivity Analysis Approach

by

David Berney Needleman

B.S. in Physics
University of Oregon, 2007

Submitted to the Department of Mechanical Engineering
in partial fulfillment of the requirements for the degree of
Master of Science in Mechanical Engineering

at the

MASSACHUSETTS INSTITUTE OF TECHNOLOGY

June 2014

Author……
Department of Mechanical Engineering
May 9, 2014

Certified by……
Tonio Buonassisi
Assistant Professor of Mechanical Engineering
Thesis Supervisor

Accepted by……..……
David E. Hardt
Professor of Mechanical Engineering
Chairman, Department Committee on Graduate Theses

Optical Design Guidelines for Spectral Splitting Photovoltaic Systems:

A Sensitivity Analysis Approach

by

David Berney Needleman

Submitted to the Department of Mechanical Engineering
on May 9, 2014 in Partial Fulfillment of the
Requirements for the Degree of Master of Science in
Mechanical Engineering

ABSTRACT

Solar power has unmatched ability to provide greater security and reduced environmental impact for the energy sector. Photovoltaic (PV) systems provide the most popular method used today for harnessing this power. However, the costs of these systems are still higher than traditional fossil fuel generation, leading to limited adoption. One of the major drivers of cost is the efficiency with which PV systems convert solar energy to electricity.

Systems that rely on a single semiconducting material to absorb sunlight are fundamentally limited in how efficiently they can convert it to electricity, so efforts have been made to incorporate multiple absorber materials into a single system. One approach is to use an optical component to split the solar spectrum and guide high-energy light to absorber materials with a wide band gap and low-energy light to absorbers with a narrower band gap.

This thesis uses two-dimensional technology computer aided design (TCAD) simulations to develop design guidelines for optical components used for this purpose. Two optical parameters, spectral fidelity—the fraction of photons that are absorbed by the intended material—and spatial uniformity—the uniformity of light intensity over the surface of the solar cell—are considered. A sensitivity analysis of these parameters is performed for a system using two absorber materials: crystalline silicon (Si) and cuprous oxide (Cu_2O). The spectral fidelity of the low-energy spectral band was found to have a strong impact on device performance, the fidelity of the high-energy spectral band was found to have a small impact, and the spatial uniformity was found to have almost no impact. While the detailed analysis is valid strictly for this combination of absorbers, the findings bear relevance for systems with more absorbers and different materials, and the sensitivity analysis approach can be applied to any system.

Thesis Supervisor: Tonio Buonassisi
Title: Associate Professor of Mechanical Engineering

ACKNOWLEDGEMENTS

I would first like to acknowledge the vast amount of assistance I was given by everyone in the MIT PV Lab. Jonathan Mailoa provided optical modeling; Riley Brandt provided information about Cu_2O, ZnO, and devices that use them as well as lots of good advice; Dr. Niall Mangan, in addition to giving me lots of both general and specific advice about simulations, may be the only person to actually read every word of my thesis cover to cover and gave invaluable feedback on the text and figures; Prof. Buonassisi helped guide my research questions, kept me on track with my timeline, and ensured that the quality of my research was always high. Everyone else helped with my research along the way and kept me sane and relatively cheerful.

I also have to thank MIT Lincoln Laboratory, who largely funded this work, and specifically Drs. Ted Bloomstein and Gary Swanson, whose idea to employ a novel set of diffractive optics to the spectral splitting PV problem got me started, and who contributed optical modeling and feedback along the way.

Thanks to the 35-135 crew, especially those also working on theses this semester: Amanda Yousef, Stephanie Scott, Scott Nill, Brandon Evans, Josh Nation, Adam Libert, and Larissa Nietner. We probably all would have gotten through it alone, but it was so much better together.

Thanks to my parents and family whose love and support have made me who I am and gotten me to where I am.

Finally, and most importantly, thanks to Rosie who lightens my burdens, brightens my days, and makes me want to do and be my best and more. Truly, without her, none of this would have happened.

CONTENTS

FIGURES

TABLES

CHAPTER

1

INTRODUCTION

1.1 Solar Energy

Climate change and energy security are increasingly important issues worldwide, leading to growing demand and importance for cost-effective, clean energy technologies that can be developed locally without relying on international partners. Sunlight is the most abundant renewable resource, with more solar energy striking the Earth every hour than is currently demanded by all human activities each year [1].

Photovoltaic (PV) panels are a common way of harnessing solar energy. They operate by converting sunlight directly into electricity. They are an appealing technology because they have a proven track-record of reliability [2] and bankability [3]. Furthermore, the panel form allows for easy scalability, making PV relevant for new markets where central power production does not exist and may not be economically viable, distributed generation on residential and commercial properties in areas with developed electrical infrastructure, and utility-scale power production.

The installed capacity of PV has been increasing dramatically in recent years, with a cumulative average growth rate of 48% from 2002 to 2012, while prices fell at an average rate of 13% in the same period [4]. Yet further cost reductions are needed to make PV technology competitive with traditional fossil fuels solely based on costs. Higher energy conversion efficiency has been shown to be the strongest lever for decreased costs [5]. This thesis examines one way of increasing efficiencies beyond the limits of traditional PV technology: using optics to split the solar spectrum before it is absorbed.

1.2 Spectral Splitting Photovoltaics

1.2.1 PV Solar Cell Basics

Solid materials have allowable energy levels for electrons that are separated into bands in which the energy levels are virtually continuous with gaps in between them. Since electrons are Fermions and obey the Pauli exclusion principle, which states that each energy level can only be occupied by a maximum of two electrons (one with each spin), the occupation of these energy levels follows the Fermi-Dirac distribution:

$$f(E) = \frac{1}{1 + e^{E - E_F / kT}} \tag{1.1}$$

Where f is the probability that an energy level is occupied, E is the energy level, E_F is the "Fermi level," the highest fully occupied energy level at 0 K, k is Boltzmann's constant, and T is the temperature of the solid.

Figure 1.1 shows the position of the highest occupied state in metals, insulators, and semiconductors. In metals, E_F falls within an energy band (Figure 1.1, left). Since electrons must gain energy to conduct electricity, the availability of states with very small gains in energy makes these materials conductive. In insulators, E_F is at the top of a band and the "band gap" between the highest occupied band (valence band) and band with the next lowest energy level (conduction band) is much greater than kT, such that the occupation probably of the conduction band is essentially zero (Figure 1.1, center). The band gap is large enough that electrons cannot gain sufficient energy to reach the next available state and the material therefore cannot conduct electricity. A semiconductor is an insulator with a small band gap (Figure 1.1, right), such that at room temperature, some of the available states in the conduction band are occupied. A limited number of electrons can gain enough energy to be promoted to the conduction band, so the material can be made to conduct electricity with the application of additional energy (thermal, photonic, etc.).

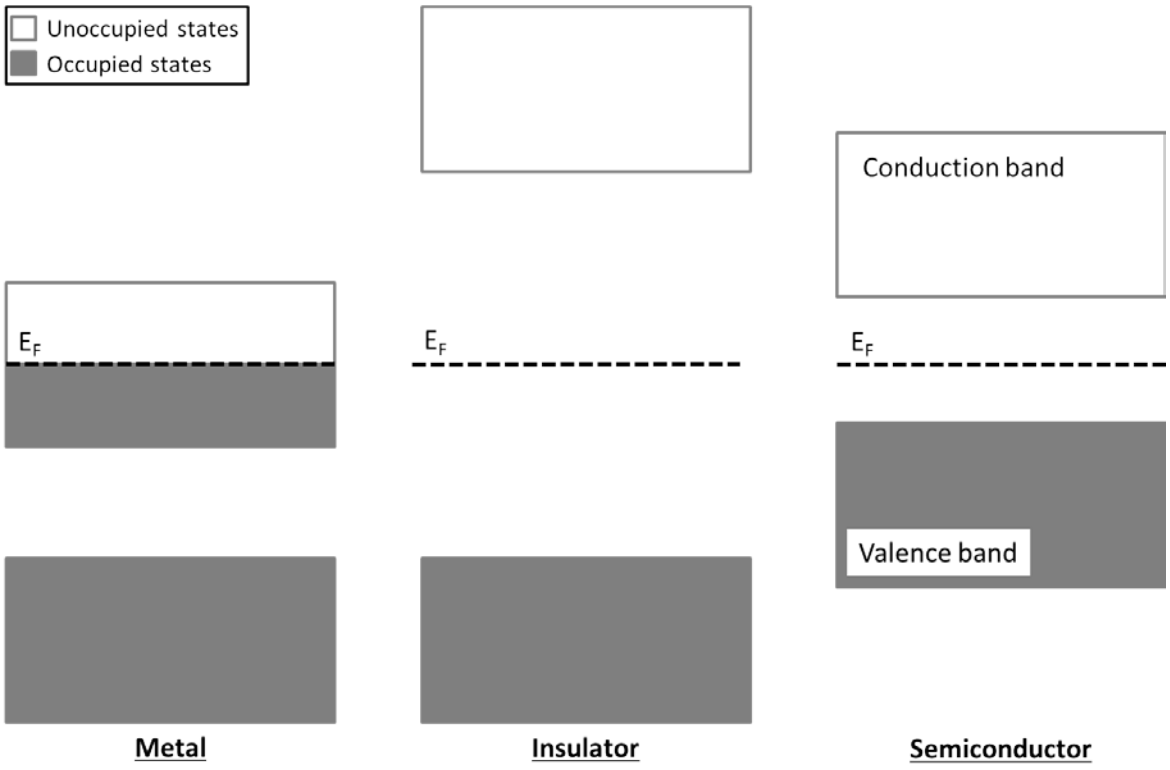

Figure 1.1: Band structure of solids

Band structure of metals, insulators, and semiconductors are shown. Metals have available states for electrons with virtually no additional energy because the Fermi level falls within an energy band. Insulators have essentially no available states because the band gap is too large and the Fermi level falls in the forbidden energy gap. Semiconductors have available states if additional energy is supplied; the Fermi level again falls in the band gap.

The conductivity of a semiconductor can be engineered through a process called "doping," in which electrons are added to the conduction band or removed from the valence band. Removing an electron from a state in the valence band allows the remaining electrons to move around. This can be viewed instead as the motion of the vacancy, analogous to a bubble in a liquid. In this formulation, the vacant state is called a "hole" and is treated as a charge carrier with positive charge of equal magnitude to the electron charge.

As shown in Figure 1.2, doping is achieved by creating electron states within the band gap. These states must either be occupied and near the bottom of the conduction band ($E_C - E < kT$ where E_C is the lowest energy level in the conduction band), as shown on the right side of the figure, or unoccupied and near the top of the valence band ($E - E_V < kT$ where E_V is the highest energy level in the valence band), as shown on the left side of the figure. An occupied energy

level in the gap is called a "donor." With $E_C - E < kT$ as described, the donor will "ionize," and the electron occupying it will be thermally excited into the conduction band, thus creating free negative charge. An unoccupied energy level in the gap is called an "acceptor." With $E - E_V < kT$ as described, the acceptor will ionize, and an electron in the valence band will be thermally excited into it, leaving a hole in the valence band and creating free positive charge. A semiconductor that is doped with donors, creating negative free charge is called "*n*-type," and a semiconductor that is doped with acceptors, creating positive free charge is called "*p*-type." Electrons outnumber holes in an *n*-type semiconductor and holes outnumber electrons in a *p*-type semiconductor. The more numerous charge carrier in a doped semiconductor is called the "majority carrier," and the less numerous charge carrier is called the "minority carrier."

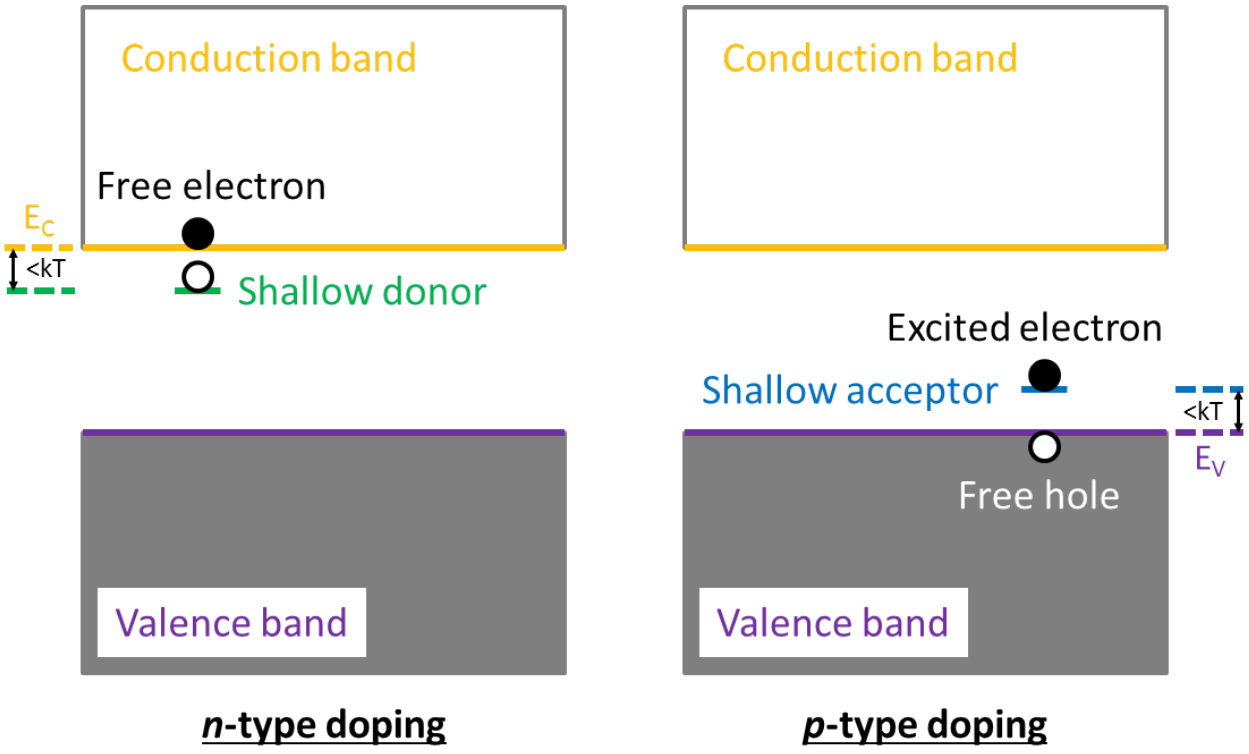

Figure 1.2: Doping of a semiconductor

Semiconductors are doped by the addition of an occupied state just below E_C, which donates an electron to the conduction band (*n*-type doping) or by the addition of an unoccupied state just above E_V, which accepts an electron from the valence band and leaves behind a free hole (*p*-type doping).

As shown in the top portion of Figure 1.3, when an *n*-type semiconductor and a *p*-type semiconductor are joined by a metallurgical junction, electrons diffuse from the *n*-type side

where there is a greater concentration to the *p*-type side where there is a lower concentration (and vice versa for holes). Since each semiconductor was originally charge neutral, as free carriers diffuse across the junction, fixed charge remains on each side (positive on the *n*-type side and negative on the *p*-type side). In detail, each un-ionized dopant state is charge neutral. When it ionizes, fixed charge of equal magnitude and opposite sign remains at the dopant site. If the free carrier diffuses away, only the fixed charge remains, as shown in the lower portion of Figure 1.3. The charged area that is depleted of free carriers is called the "depletion region."

Fixed charge in the depletion region creates an electric field. Carriers in this field will be accelerated ("drift") in the opposite direction that they are diffusing. That is, the field repels holes from the *n*-type side and electrons from the *p*-type side. There is net carrier diffusion across the junction until the depletion region has grown large enough that drift and diffusion balance, and steady state is reached.

The *p*-*n* junction can also be understood with the help of an energy band diagram like the one in Figure 1.4. Band diagrams graph energy *vs.* position of E_C, E_V, and the chemical potential, which is also often (including in this thesis) called the Fermi level and denoted by E_F (note that the confusion arises because a strict definition of the Fermi level is the chemical potential at 0 K, but the term has come to be used for the chemical potential at any temperature). When a semiconductor is doped, the occupation probability of a given energy level changes, so E_F shifts. This shift is toward the conduction band for *n*-type doping and toward the valence band for *p*-type doping. However, in thermal equilibrium, the Fermi level must be constant because electrons will move to the configuration that minimizes their energy, so if there is a gradient in the Fermi level, electrons will move down the gradient, raising the Fermi level where it is low and lowering it where it is high until equilibrium is reached. Since far from the junction, the Fermi level is near the band edges and near the junction it is constant, the bands must bend in the junction region. Bending of the bands indicates the presence of the electric field.

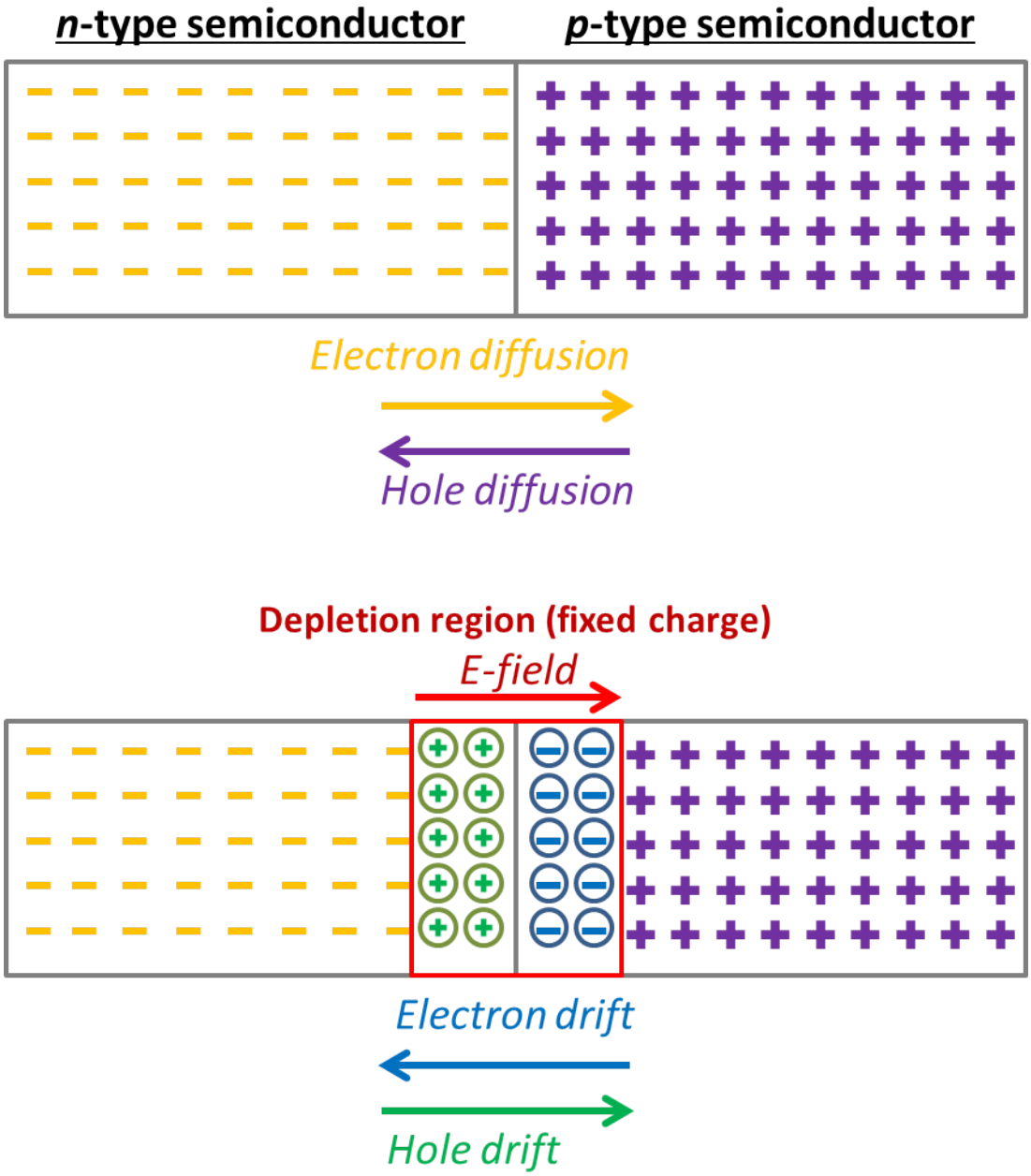

Figure 1.3: *p-n* junction

When a metallurgical junction is formed between an *n*-type and a *p*-type semiconductor, majority carriers diffuse across the junction, leaving behind opposite fixed charge and creating an electric field. This process continues until enough fixed charge remains for carrier drift to balance carrier diffusion.

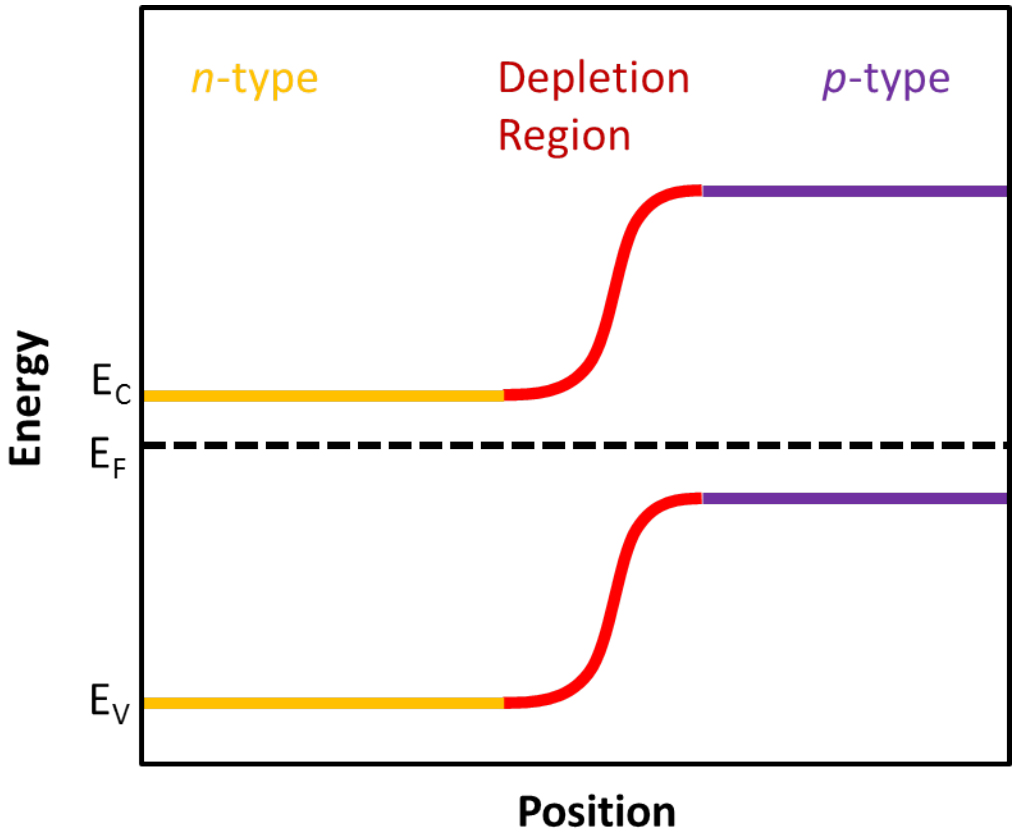

Figure 1.4: Energy band diagram of a *p*-*n* junction

Energy of the valence band maximum and conduction band minimum and the Fermi level are plotted as a function of position for an *n*-type and *p*-type semiconductor in electrical contact. The Fermi level remains constant in thermal equilibrium requiring the bands to bend, indicating the presence of an electric field near the junction.

One of the ways electrons can be excited from the valence band to the conduction band of a semiconductor is by absorption of a photon with energy greater than the band gap. As shown in Figure 1.5, band-to-band excitation generates a free electron in the conduction band and a free hole in the valence band, typically called an "electron-hole pair." When photoexcitation occurs in a doped semiconductor that is part of a *p*-*n* junction and electrical contacts are applied to the ends of the semiconductor, the electron-hole pair are separated with a net flow of electrons toward the contact on the *n*-type side of the junction and a net flow of holes toward the contact on the *p*-type side of the junction, as indicated by the green arrows in Figure 1.5. This electrical current can be dropped across a resistive load shown in red in Figure 1.5 and thereby used to do work. This is the operating principle of a PV solar cell.

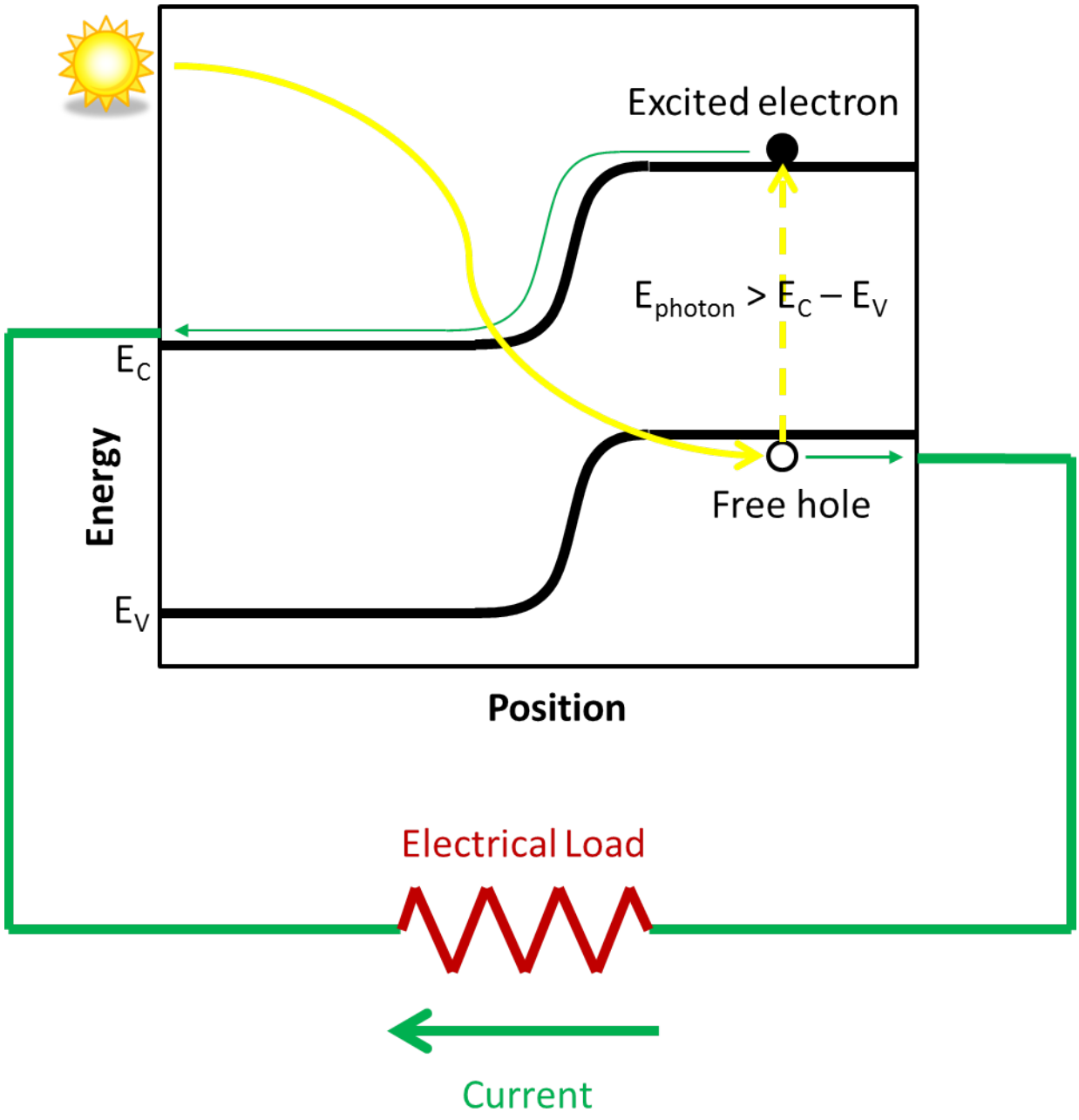

Figure 1.5: Solar cell operation

Photons with energy greater than the band gap strike the solar cell, generating an electron-hole pair. Electrons flow on aggregate toward the *n*-type side of the junction and holes toward the *p*-type side, where they are collected by the external circuit. This current is used to do work on an electrical load.

1.2.2 Thermalization Losses

When photons are absorbed by a semiconductor, the excited electrons shed energy in excess of the band gap through collisions with lattice atoms and each other. This decay process occurs on a timescale shorter than picoseconds, so it is almost impossible to avoid and limits the energy at which excited carriers can be extracted. As noted above, semiconductors also cannot absorb single photons with energy less than their band gap. The sun, however, is a broadband light source, emitting in significant numbers photons with wavelengths ranging from 280 nm to 4000 nm, as shown on the left axis of Figure 1.6. Wavelength can be converted to photon energy using the de Broglie relation:

$$E = h\upsilon \tag{1.2}$$

Where h is Planck's constant and ν is the wavelength of the light. Thus, the solar spectrum ranges from 0.31 eV to 4.4 eV, which are the units used on the *x*-axis of Figure 1.6.

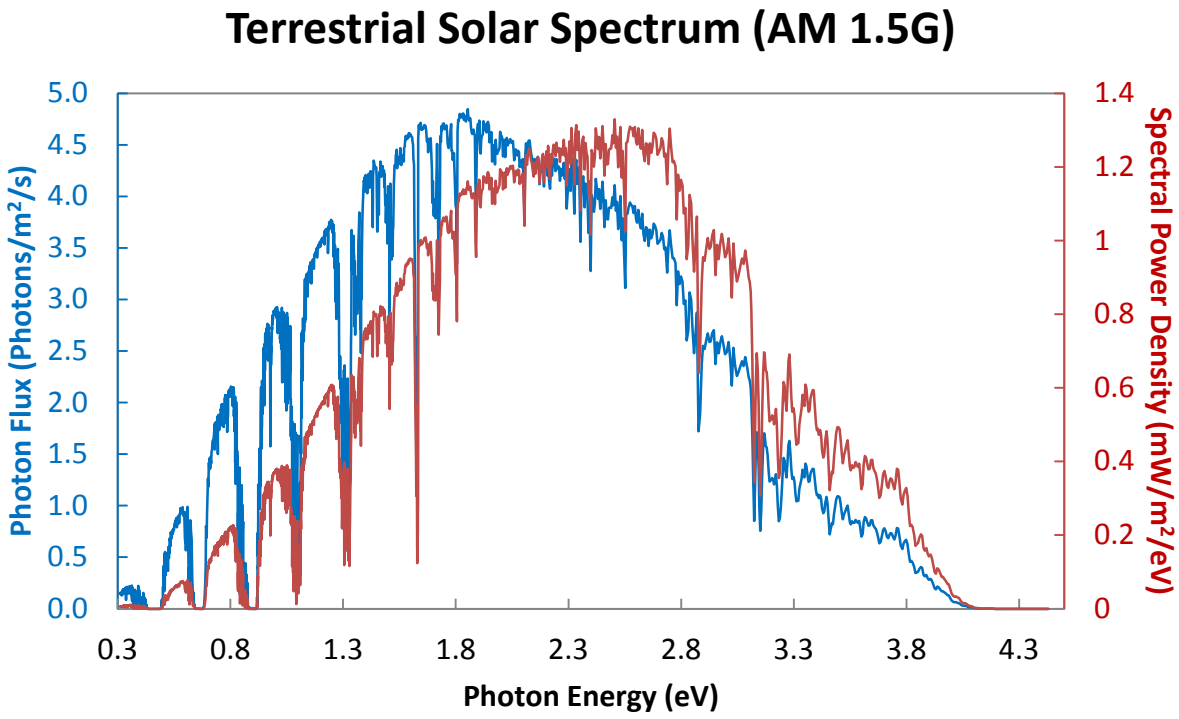

Figure 1.6: Terrestrial solar spectrum

Average photon flux (left axis, blue curve) and spectral power density (right axis, red curve) from the sun to the surface of the Earth using the Air Mass 1.5 Global (AM 1.5G) solar spectrum is plotted *vs.* photon energy.

PV devices that use a single semiconductor to absorb the solar spectrum are therefore limited by two things: their inability to absorb photons with energy less than the band gap of the semiconductor used and their inability to extract energy in excess of the band gap of the semiconductor used from individual photons. Shortly after the first solar cell was invented, Shockley and Queisser calculated the theoretical maximum efficiency of a solar cell with a single absorber material in the "detailed balance limit," which accounts for non-absorption of below-band gap photons, thermalization of high-energy photons to the band edge, and the radiative balance between between solar radiation and the black body radiation of the PV device assuming the PV device absorbs and emits photons symmetrically [6]. This efficiency is often referred to as either the detailed balance or the Shockley-Queisser limit. When performed using the American Society of Testing and Materials (ASTM) standard for the AM 1.5G solar spectrum, these calculations yield a maximum single-junction efficiency of 33.8% [7].

1.2.3 Multi-Junction Devices and Spectral Splitting

If every solar photon is absorbed and absorbed by a semiconductor with a band gap exactly equal to the photon's energy, the Shockley-Queisser limit is 68% [7]. This new limit suggests that significant efficiency gains are possible by adding additional absorber materials to absorb a broader spectral band of photons while reducing thermalization losses. Applying the principles of Shockley and Queisser [6] and the method of Henry [8], code was developed in Matlab to enable calculation of this efficiency limit as well as the optimal absorber band gaps for 2 – 5 independent absorbers (Table 1.1).

Table 1.1: Calculated maximum efficiency for PV devices with multiple absorber materials

Number of absorbers	Absorber band gaps (eV)	Maximum efficiency
1	1.4	34%
2	1.8, 1.0	44%
3	2.1, 1.4, 0.9	50%
4	2.5, 1.9, 1.4, 0.9	54%
5	2.5, 1.9, 1.5, 1.1, 0.7	56%

The results of these calculations show that adding absorbers can increase efficiency rapidly with diminishing gains as the number of absorbers continues to increase. Thus, the potential to

increase PV device efficiency by adding a small number of absorbers is quite large. This fact has spawned several approaches to adding additional absorbers. The most popular has been the stacked multijunction (MJ) solar cell [9], [10]. In this scheme, a series of typically 3 – 5 diodes using absorber layers of varying band gaps are placed directly on top of each other. The wide band gap cells serve both to absorb and convert high energy photons and to serve as long pass filters for the narrower band gap cells below them.

There are many challenges to this approach. The easiest way to create the complex series of metallurgical junctions required to stack several cells is to grown each layer epitaxially on top of the layer below it. This approach requires complicated growth techniques and lattice-matched materials. III-V compound semiconductors have been the materials of choice because they have similar lattice constants, tunable band gaps, and high-quality controlled composition films can be grown in a single-reactor. Germanium is often used a template and bottom cell material. Unfortunately, several critical elements for III-V compounds quite rare, calling into question the ability of devices based on them to reach TW or tens of TW-scale deployment [11].

Stacked MJ cells also require current transport between the layers. This necessity adds further complexity to the device design, usually requiring tunnel junctions between the cells. It also requires the current produced by each diode in the stack to be equal, as series-connected devices will produce a total current equal to the smallest current of an individual cell. Current-matching is quite challenging, especially when daily and seasonal variations in the spectral character of solar radiation are considered.

Despite these challenges, stacked MJ solar cells have been pursued aggressively. They are the standard choice for space applications and have achieved the highest conversion efficiencies of any device architecture with certified efficiencies of 38.8% under non-concentrated light and 44.4% with an illumination intensity of 300 suns [12]. While concentration of light adds costs in the form of optical components and trackers, it increases cell efficiencies and reduces the necessary size (and therefore costs) of the solar cell itself, which is important for III-V devices that, as discussed above, require expensive fabrication techniques.

Another approach to MJ devices is to use an optical component to split the solar spectrum into several spectral energy bands and direct each of these spectral bands to a material with an appropriate band gap, as illustrated schematically in Figure 1.7. This approach has gained popularity in recent years [13], [14] because it provides significantly more flexibility in device

design. Tunnel junctions, current-matching, and epitaxial growth with its inherent materials limitations can all be avoided. Furthermore, the additional costs associated with the necessary optical components are less taxing since concentrating optics are already included in most stacked MJ designs, and there is hope that the spectral splitting optical component would not add significantly to the cost of the optical system.

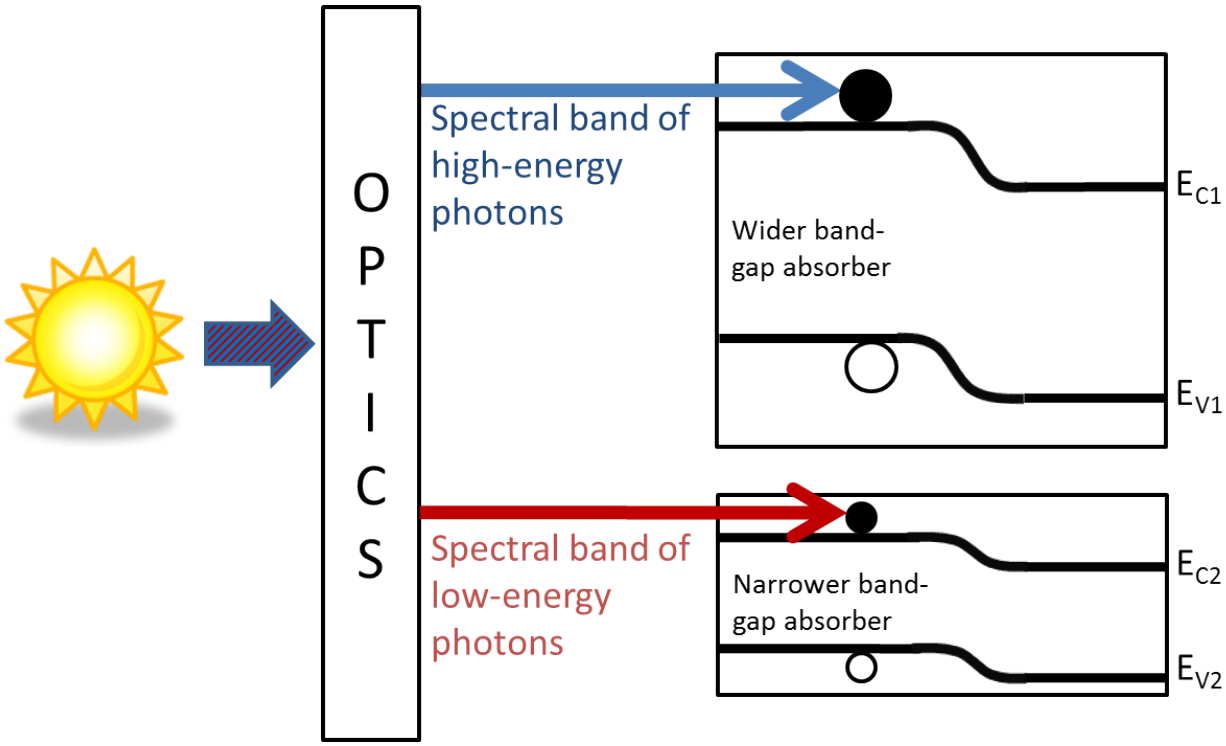

Figure 1.7: Schematic of a generic spectral splitting PV system

Significant efficiency gains have been achieved with spectral splitting PV systems, with several systems reaching efficiencies greater than 30% and a current record efficiency of 38.5% [12], [15]. These efforts build on decades of previous research [16]. The idea for multi-junction devices was first proposed by Trivich and Flinn in 1955 [17], and achieving this result by splitting the solar spectrum spatially by Jackson in 1958 [18]. It languished until the mid-1970's when increasing the efficiency and reducing the cost of PV devices through concentration of sunlight began to draw interest. It was noted that performance under concentration was very sensitive to cell efficiency and that the concentrators themselves were a substantial cost, reducing the importance of the cell cost to the whole system and increasing the importance of efficiency [19]. Furthermore, increased cell heating from higher-density absorption of sub-band gap photons by the lattice and thermalization losses of above-band gap photons under concentrated

illumination would lead to degraded performance. MJ devices, including those employing spectral splitting optics, offered a potential means of increasing efficiency while reducing heating effects, and therefore drew renewed interest [20]–[22].

Early efforts were largely limited by the performance of the individual cells in the system and focused on developing efficient devices with an appropriate range of band gaps [23]. There are now several materials with appropriate band gaps and sufficiently high efficiency to be cost effective (see Table 1.2). However, later efforts have been hampered by inefficient optics [24], [25]. Computational optics has enabled new optical components, a more thorough exploration of the optical designs, and has led to resurgent interest [13]–[15], [26]–[28].

Table 1.2: High-efficiency single-junction solar cell materials with different band gaps [29]

Material	Bandgap (eV)	Record efficiency (%)	Fraction of theoretical max
InGaP	1.9	20.8	0.83
AlGaAs	1.75	17.2 (AM0)	0.63
CdTe	1.5	18.3	0.62
GaAs	1.4	28.8	0.9
InP	1.35	21.2	0.66
Si	1.1	25.6	0.83

While resurgent, there has been little effort to apply a uniform approach to designing spectral splitting PV systems. While very recent efforts have attempted to create a set of metrics to use for this type of evaluation [30], the parameter-space has not been explored. Particularly, optical and device simulations seem to be limited to specific designs under consideration and tend to be limited in the parameter-range they consider.

This thesis explores a part of the optical parameter-space to determine the sensitivity of system performance metrics to system optical properties. This sensitivity analysis is performed for a model system, in which the solar spectrum is split into two spectral bands (tandem device structure) with the low-energy spectral band converted by a PV cell with a silicon (Si) absorber and the high-energy spectral band converted by a PV cell with an absorber layer whose properties are an idealized version of cuprous oxide (Cu_2O). Some of the results from this model

system are quite general and the approach can be applied to any optical scheme and combination of materials.

CHAPTER

2

MODELING APPROACHES

2.1 Device Modeling

2.1.1 Device Architectures

Two device architectures were simulated for both Si and the Cu_2O solar cells. One higher efficiency and one lower efficiency architecture were used, in order to determine differences in the impacts of optical performance based on device architecture or material quality. For Si, the lower efficiency device represents the performance of a high-end turnkey line [31]. The higher efficiency device has similar efficiency to the best-performing commercially-available solar cells [32], [33]. Under a perfectly split solar spectrum, a tandem structure with Cu_2O and Si will have better efficiency than a Si device alone if the full-spectrum efficiency of the Cu_2O device is about 10%. Therefore, even though current record efficiency for Cu_2O is 5.4% [34], the simulated low-efficiency device was just above this breakeven point. The simulated high efficiency was near the limiting performance of a Cu_2O-zinc oxide (ZnO) heterojunction.

The lower-efficiency Si device, shown in Figure 2.1, had a *p*-type base with a diffused *n*-type emitter. Silver front contacts were spaced 1.2 mm apart. The entire rear of the device was treated as an ideal contact to simulate full rear-side metallization. A rear boron diffusion was included to act as a back surface field (BSF), reducing recombination at the back surface. As is standard in Si devices, a silicon nitride (SiN_x) layer was included on the top surface as both an anti-reflective coating and to reduce the surface recombination velocity of (passivate) the front Si surface.

The higher-efficiency Si device, shown in Figure 2.2, was based on a passivated emitter rear totally diffused (PERT) architecture [35]–[37]. A *p*-type base was used with a lightly diffused *n*-type emitter and heavy *n*-type doping under the front contacts. The front contacts were silver and spaced 600 μm apart. A light rear boron diffusion was also included across the whole back

surface with a heavy diffusion under the rear aluminum contacts which were point contacts also spaced 600 μm apart. In both cases, the unit cell simulated was the smallest distance between two lines of symmetry. In the case of the Si cells, this was from the mid-point of one contact halfway to the next contact. Detailed properties for both architectures are listed in Table 2.1.

Table 2.1 Parameters for simulated Si device architectures

	Standard Diffused Junction	**PERT**
Base Thickness	200 μm	200 μm
Base Doping	2×10^{15} cm^{-3}	2.4×10^{16} cm^{-3}
Emitter Doping Peak Concentration	6×10^{19} cm^{-3}	6×10^{18} cm^{-3}
Emitter Depth	425 nm	360 nm
BSF Doping Peak Concentration	1×10^{19} cm^{-3}	1×10^{18} cm^{-3}
BSF Depth	8.5 μm	4 μm
Contact Doping Peak Concentration	N/A	1×10^{20} cm^{-3}
Front Contact Doping Depth	N/A	435 nm
Rear Contact Doping Depth	N/A	6 μm
Contact Spacing	600 μm	300 μm
Contact Width	10 μm	2 μm
Contact Thickness	1 μm	1 μm
Bulk Lifetime	1000 μs	1000 μs
Front Surface Recombination Velocity	1000 cm/s	5 cm/s
AM 1.5G Efficiency	19.4%	24.0%
AM 1.5G Short-Circuit Current (J_{SC})	35.2 mA/cm^2	39.7 mA/cm^2
AM 1.5G Open-Circuit Voltage (V_{OC})	0.66 V	0.72 V
AM 1.5G Fill Factor (FF)	83.4%	84.4%

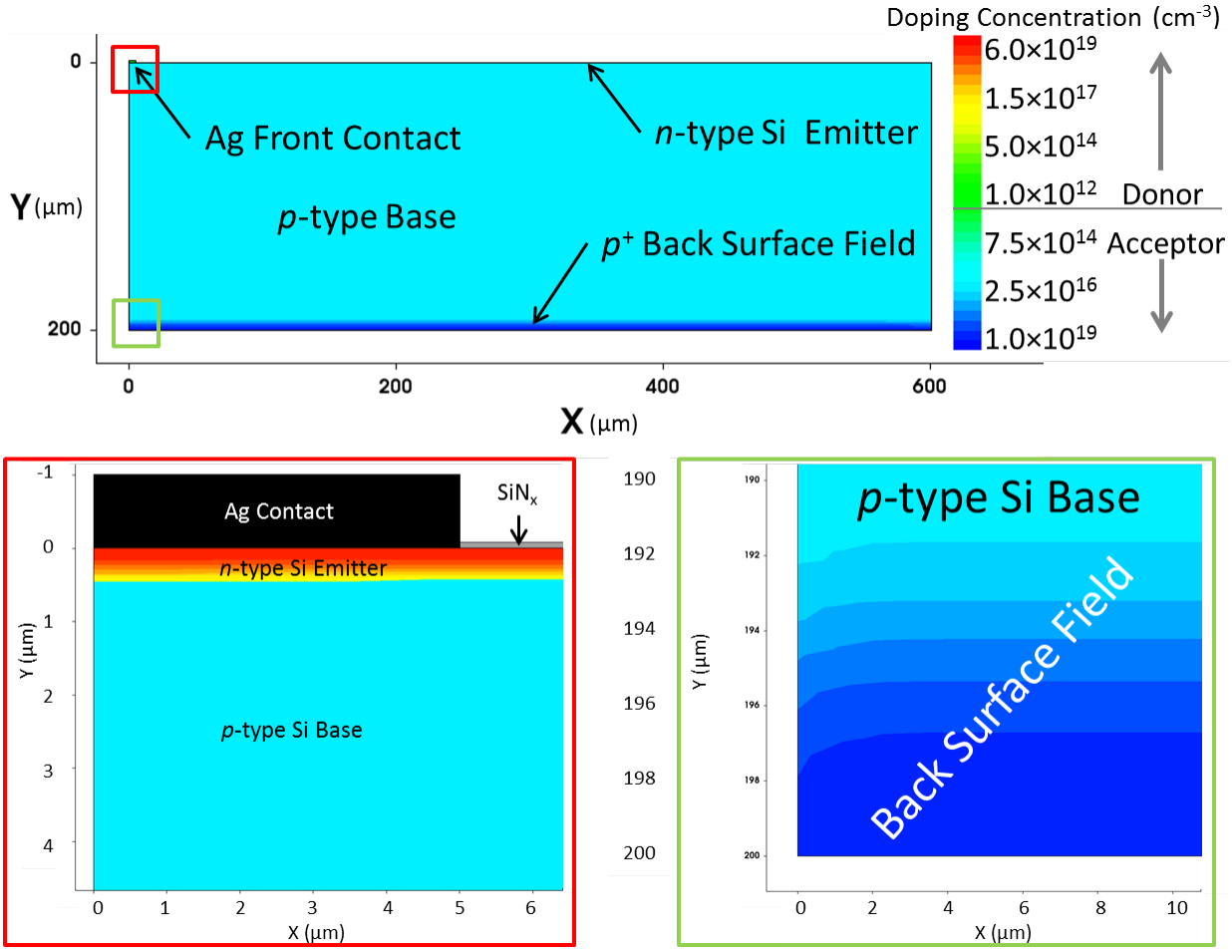

Figure 2.1: Simulated standard diffused junction Si device architecture

Front point contacts (Ag) and full rear contact (not shown), diffused emitter and BSF, SiN_x anti-reflective coating and passivation layer. Full simulated device (top) and zoomed-in view of front contact (bottom left) and rear BSF and contact region (bottom right). Contact covers whole rear of cell, metal not included in simulation.

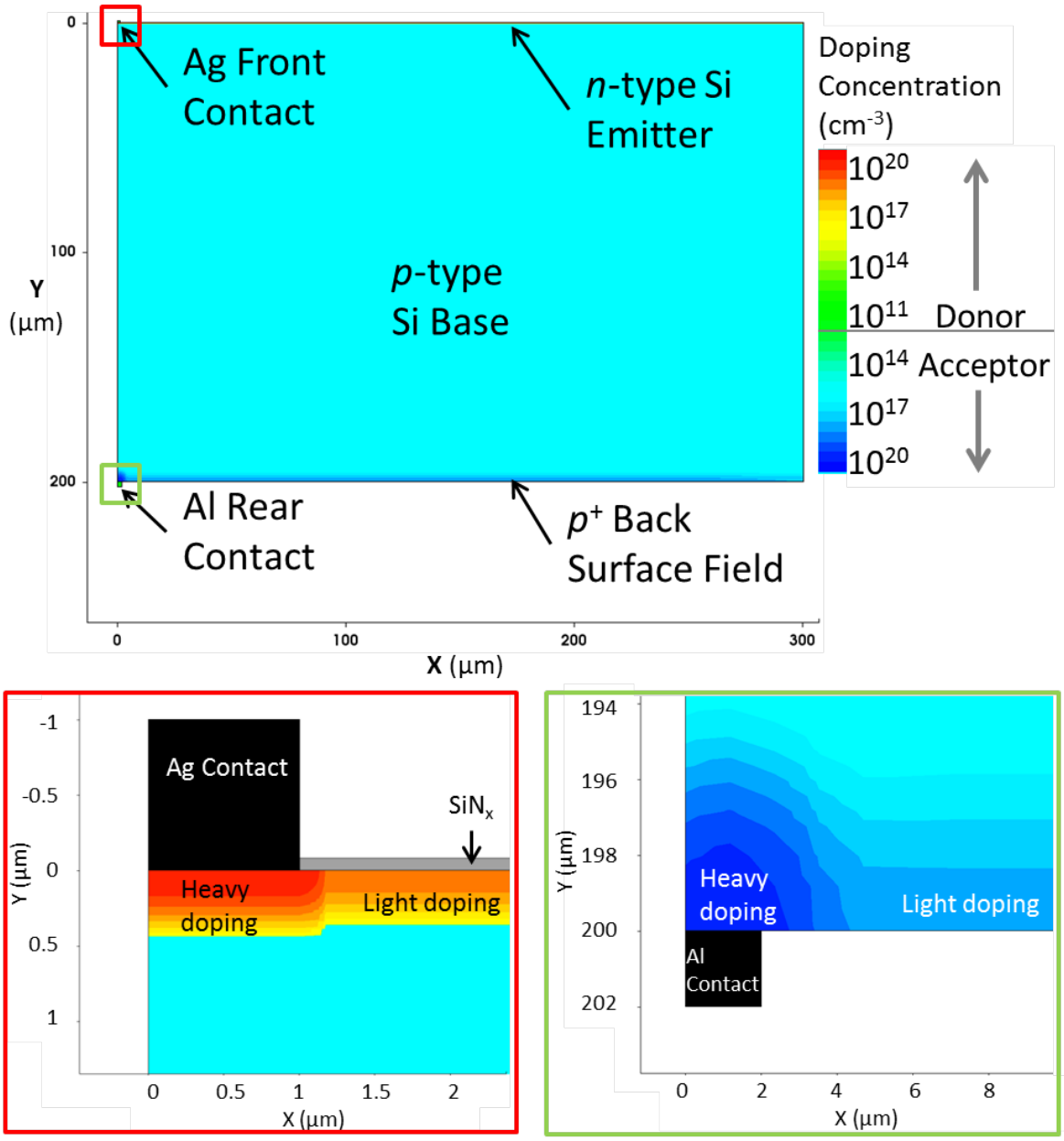

Figure 2.2: Simulated PERT device architecture

Front and rear point contacts (Ag and Al respectively), lightly doped emitter and BSF, selective heavy doping under contacts, SiN_x anti-reflective coating and passivation layer. Full simulated device (top) and zoomed-in view of front (bottom left) and rear (bottom right) contacts.

Both Cu_2O devices had the same architecture, shown in Figure 2.3, with a Cu_2O base and ZnO emitter. Several simplifications of realistic devices were made. The grains in Cu_2O create natural surface texture, but the layers were treated as planar. To properly account for this type of surface texture, the device must be modeled in 3-D. A 2-D simulation would correspond to ripples rather

than peaks, as the third dimension in a 2-D cartegian simulation is extended directly into the third dimension. Surface texture would create variations in the electric field, but these were not expected to impact the simulation results. This assumption could be investigated in future work. Recombination at grain boundaries is also not considered in these simulations, although it may play a role in the performance of real devices.

The contacts were not considered in detail and were instead modeled as covering the whole back surface as if a the whole back surface was metallized and a covering the whole front surface as if a high-conductivity transparent window layer (*e.g.*, indium tin oxide) were covering the front surface. The point of extraction is taken to be the semiconductor surface itself, so no contact materials were specified. Present devices are limited by bulk material properties and defects at the heterojunction interface, not contact effects. Note that lifetimes of 1 – 10 μs have been achieved on Cu_2O films from oxidized copper foils [38], but higher lifetimes did not improve the performance of the simulated devices, which were limited by the voltage achievable with the Cu_2O-ZnO heterojunction. To give a sense of the ultimate performance limit of this tandem structure, a 1-D simulation of an ideal Cu_2O homojunction device under perfect spectral splitting was also performed using SCAPS-1D [39]. The parameters for all simulations are listed in Table 2.2.

The widths of the 2-D devices were varied in order to determine if the length-scale of the spatial variation of light had any impact on the results. As mentioned above, the unit cell of the Si devices was the smallest distance between two lines of symmetry, either half the width of a contact or halfway between two contacts. For wider simulations, unit cells were reflected and replicated. Widths of 0.6, 1.8, and 4.8 mm were simulated for both standard diffused junction and PERT architectures. Since the Cu_2O devices were completely uniform in the lateral direction, any widths were possible. Widths of 1, 10, and 100 μm were simulated. It was hypothesized that the relevant length scale for spatial variation of light intensity was the length over which carriers could diffuse to redistribute from the uneven generation, the minority carrier diffusion length. As the simulated Cu_2O had much shorter minority-carrier diffusion lengths (0.8 μm for the low-efficiency and 12.5 μm for the high-efficiency Cu_2O devices *vs.* ~1600 μm for the Si devices), the device widths simulated were significantly smaller.

Table 2.2 Parameters for simulated Cu_2O device architectures

	Lower Efficiency	Higher Efficiency	Homojunction
Cu_2O Thickness	3 µm	3 µm	7 µm
Cu_2O Doping	10^{14} cm^{-3}	10^{14} cm^{-3}	10^{15} cm^{-3}
Cu_2O Lifetime	8 ns	600 ns	∞
Cu_2O Mobility	30 $cm^2/V{\cdot}s$	100 $cm^2/V{\cdot}s$	60 $cm^2/V{\cdot}s$
Emitter Thickness	100 nm (ZnO)	100 nm (ZnO)	100 nm (Cu_2O)
Emitter Doping	10^{20} cm^{-3} (ZnO)	10^{20} cm^{-3} (ZnO)	10^{19} cm^{-3} (Cu_2O)
Front Surface Recombination Velocity	10^4 cm/s	10 cm/s	0 cm/s
AM 1.5G Efficiency	11.6%	13.7%	17.1%
AM 1.5G Short-Circuit Current (J_{SC})	11.9 mA/cm^2	12.3 mA/cm^2	12.3 mA/cm^2
AM 1.5G Open-Circuit Voltage (V_{OC})	1.28 V	1.30 V	1.51 V
AM 1.5G Fill Factor (FF)	76.1%	85.7%	91.3%

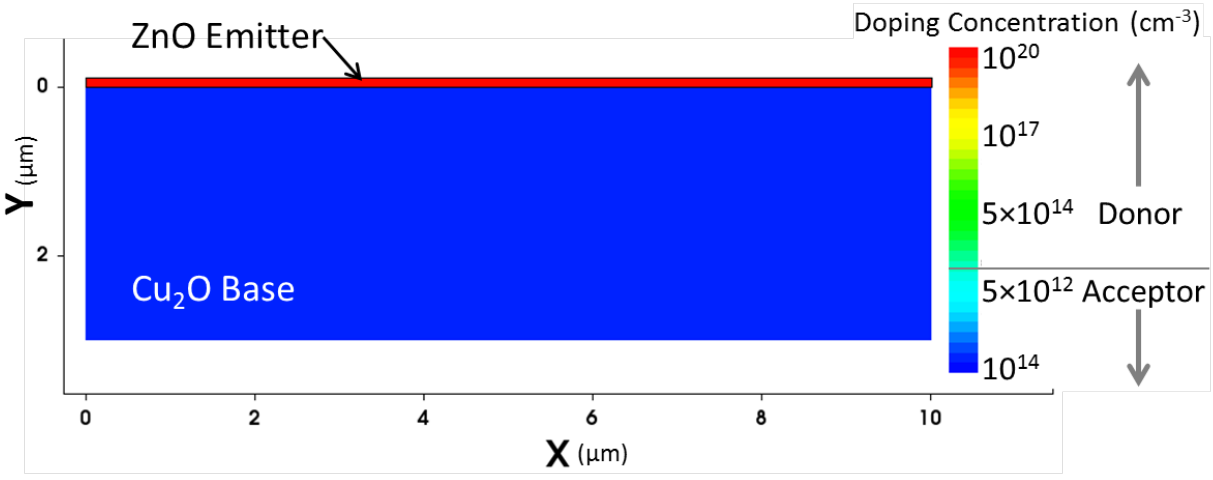

Figure 2.3: Simulated Cu_2O device architecture

2.1.2 Materials

Si is non-toxic and the second-most abundant element in the Earth's crust [40]. Solar cells using Si absorbers are high-efficiency, low-cost, have a proven track-record in the field [5], and comprise more than 90% of the PV market [31]. Cu_2O is also non-toxic and sufficiently abundant to provide more than 10 TW of power from PV [41]. A calculation like the one described in Chapter 1.2.3 was performed to determine the best absorber band gaps for MJ solar cells, assuming one of the absorbers had the band gap of Si (1.1 eV). Cu_2O, with a band gap of 2.0 eV, was found to be almost ideal. Furthermore, high carrier lifetimes [38], long carrier transport lengths [42], high carrier mobilities [43], controllable doping [44], and good contact formation [45] have all been demonstrated on Cu_2O films.

Table 2.3 Calculated maximum efficiency and ideal band gaps for MJ PV devices including Si

Number of absorbers	Absorber band gaps (eV)	Maximum efficiency
# Absorbers	Bandgaps (eV)	Efficiency
1	1.1	34%
2	1.9, 1.1	44%
3	2.3, 1.6, 1.1	49%
4	2.5, 1.9, 1.5, 1.1	52%

Most material parameters for Si were taken from the material database in Sentaurus version H-2013.03. Defect-assisted, or Shockley-Read-Hall (SRH), and multiple carrier, or Auger, recombination were included in the simulation. The Si parameter file, which contains select properties for certain models used, is included in Appendix B.1 Si parameter file. The properties of SiN_x were taken from the Sentaurus material database, except for the complex refractive index, which was input separately. The complex refractive index of SiN_x was only relevant for the spatially uniform simulation for which Sentaurus was used to model the optical generation. Recombination at the Si-SiN_x interface was also included in the model.

Sentaurus did not include material properties for either Cu_2O or ZnO. These files had to be created and added to the database. The full files are available in Appendix B.2 Cu_2O parameter file and Appendix B.3 ZnO parameter file. Note that parameters such as SRH lifetime and carrier mobilities for Cu_2O and electron affinity for ZnO were idealized to simulate devices with significantly higher efficiencies than present world record devices.

2.1.3 TCAD/Sentaurus

There are two key processes that need to be accounted for in the simulation of semiconductor devices: carrier transport and carrier generation and recombination. These phenomena are described by a set of couple differential equations. The first of these is Poisson's Equation, which describes the relationship between the electric field and the charge distribution:

$$\nabla \bullet \boldsymbol{E} = \frac{\rho}{\varepsilon} = \frac{q}{\varepsilon}(p(\boldsymbol{x}) - n(\boldsymbol{x}) + N_D^+(\boldsymbol{x}) - N_A^-(\boldsymbol{x})) \tag{2.1}$$

Where $\boldsymbol{E}$ is the electric field vector as a function of position, ρ is the total charge as a function, ε is the permittivity of the material, q is the fundamental charge, p is the number of free holes as a function of position, n is the number of free electrons as a function of position, N_D^+ is the ionized donor density as a function of position and N_A^- is the ionized acceptor density as a function of position and $\boldsymbol{x}$ is the position vector.

The transport equations describe the movement of free carriers in response to concentration gradients (diffusion) and electric potential gradients (drift). For electrons, denoted by subscript n:

$$\boldsymbol{J}_n(\boldsymbol{x}) = q\,\mu_n \boldsymbol{E}(\boldsymbol{x}) + q\,D_n \nabla n(\boldsymbol{x}) \tag{2.2}$$

and for holes, denoted by subscript p:

$$\boldsymbol{J}_p(\boldsymbol{x}) = q\,\mu_p \boldsymbol{E}(\boldsymbol{x}) + q\,D_p \nabla p(\boldsymbol{x}) \tag{2.3}$$

Where $\boldsymbol{J}$ is the current density vector, μ is the carrier mobility, D is the carrier diffusivity, and μ and D are related through the Einstein relation:

$$D = \mu \frac{kT}{q} \tag{2.4}$$

Finally, the continuity equations account for charge generation, recombination, and conservation. For electrons:

$$\nabla \bullet \boldsymbol{J}_n(\boldsymbol{x}) = q(G - U) \tag{2.5}$$

And for holes:

$$\nabla \bullet \boldsymbol{J}_p(\boldsymbol{x}) = -q(G - U) \tag{2.6}$$

Where U is the net recombination rate of electrons and holes and G is the net generation rate of electron-hole pairs.

These five equations (Poisson's equation, the transport equations, and the continuity equations) are a set of coupled non-linear differential equations that fully describe the electrostatics and electrodynamics of semiconductor devices, including solar cells. As with most

sets of coupled non-linear differential equations, for all but the simplest cases, they must be solved numerically.

For the simulations in this thesis, a technology computer aided design (TCAD) software package, Synopsys Sentaurus (Sentaurus) was used to solve the set of equations. The full package is broken in several "tools." The one that actually solves the semiconductor equations is Sentaurus Device (SDevice). Sentaurus Structure Editor (SDE) was used to design device structures with appropriate materials and create a finite element mesh (set of connected nodes) at which SDevice then solved the semiconductor equations simultaneously and consistently. Inspect and Sentaurus Visual (SVisual) were used to plot and visualize results.

Sentaurus is a particularly powerful package for several reasons. First, all of the tools are integrated. For example, a device combining any materials (materials not already included in Sentaurus's material database can be defined based on their properties as described in Chapter 2.1.2) in any geometric configuration can be created in SDE and then solved in SDevice. Sentaurus also includes a process simulator that will modify a device created in SDE based on a simulated process, like annealing or deposition, and the kinetic properties of the materials involved. Second, Sentaurus is designed to accurately simulate 1-D, 2-D, and 3-D problems. This flexibility allows the user to develop models in a low-dimensional system and then import them to a higher dimensional system. Finally, the meshing algorithm used by SDE (SDE actually calls a separate tool, Sentaurus Mesh) allows a great deal of flexibility as well as built-in optimization for convergence and speed.

The simulations described in this thesis were carried out in 2-D. While some spectral splitting schemes create spatial variation in light intensity in two dimensions across the surface of a solar cell, which would require 3-D simulation (two dimensions across the surface and one through the thickness), there are schemes, such as diffraction gratings that only create spatial variation in one dimension [46]. Many of the physical mechanisms that could cause spatial variation to impact device performance can be captured by 2-D simulation (1-D spatial variation). Additionally, 2-D simulations run exponentially faster than 3-D simulations since they require geometrically fewer nodes, and once implemented, the model can easily be extended to an extra spatial dimension to model the performance of systems that vary the intensity of light across two spatial dimensions. 2-D simulations were used even for the spatially uniform illumination profiles to decouple

optical effects from lateral carrier transport effects like current crowding at contacts, heterogeneous electric fields, etc.

2.2 Optical Modeling

2.2.1 Parameters Considered

This thesis considers the sensitivity of device performance to two optical parameters. The first, which will be called **spectral fidelity,** is defined for each spectral band and is related to the precision with which the solar spectrum is split between the spectral bands. An ideal split (perfect fidelity) would send all of the photons with energy greater than the band gap of the wide-gap material (Cu_2O for these simulations) to the high-energy spectral band and direct that band to the wide-gap device. All photons with less energy would be sent to the low-energy spectral band and directed to the narrow-gap device. Spectral fidelity measures the fraction of photons that are split into the correct spectral band (the inverse of the fraction that leak into the wrong spectral band). It is defined as the ratio of the number of photons in a given spectral band to the number of photons in that spectral band under a perfect split.

The second parameter relates to the spatial uniformity of illumination intensity across the surface of the cell. Intensity is measured in W/m^2, so the integral of intensity over a spatial dimension is either W, if it is integrated over an area or in the case of the 2-D simulations described here, W/m, or power per unit length in the dimension that is not explicitly simulated. A generic parameter that can be applied to any intensity distribution is the minimum fraction of the total width that can be integrated to get power (per unit length) equal to half the total incident power. The width of a distribution where its value is half of the peak value, or full width half maximum intensity, is often used to describe the spatial variation of light intensity. However, this parameter requires the distribution of intensity over space to be both symmetrical and have only a single peak. Some spectral splitting optics, like diffraction gratings, are likely to create asymmetrical distributions with multiple peaks, therefore the new optical metric is proposed. This metric, which will be referred to as **normalized minimum width for half total power (*NMWHT*)**, can perhaps be best understood through a method for calculating it:

For any function of power *vs*. position $p(x)$, numerical integration can be performed by discretizing x into N equal segments, Δx_i, with i = 1,2,...,N. Each of these segments has an

associated integrated power, P_i, which is the average value of $p(x)$ on the interval multiplied by Δx. If the list of ordered pairs (Δx_i, P_i) is sorted from largest to smallest values of P_i, giving a new set of ordered pairs (Δx_j, P_j), and the summation $S = \frac{1}{2}\sum_{i=1}^{N} P_i = \sum_{j=1}^{m} P_j$ is performed, then MWHT = $m \times \Delta x$. This value should be normalized to the total spatial extent, so devices of different widths can be easily compared. This gives $NMWHT = \frac{m}{\mathrm{N}}$. For an intensity distribution that varies over two spatial dimensions, minimum width can be replaced with a minimum area. In the example above, Δx would be replaced with ΔA.

NMWHT is further clarified by Figure 2.4. On the left, full width half maximum (green line) and *NMWHT* (filled area) are shown for a Gaussian distribution with a mean of 0 and standard deviation of 1. On the right, the *NMWHT* (shaded area, orange line) is shown for a distribution with the same integrated power as the figure on the left, but multiple peaks. The full width half maximum cannot be calculated for this distribution. The *NMWHT* for the left distribution is 0.13 and the full width half maximum is 0.24. For the right distribution, the *NMWHT* is 0.46.

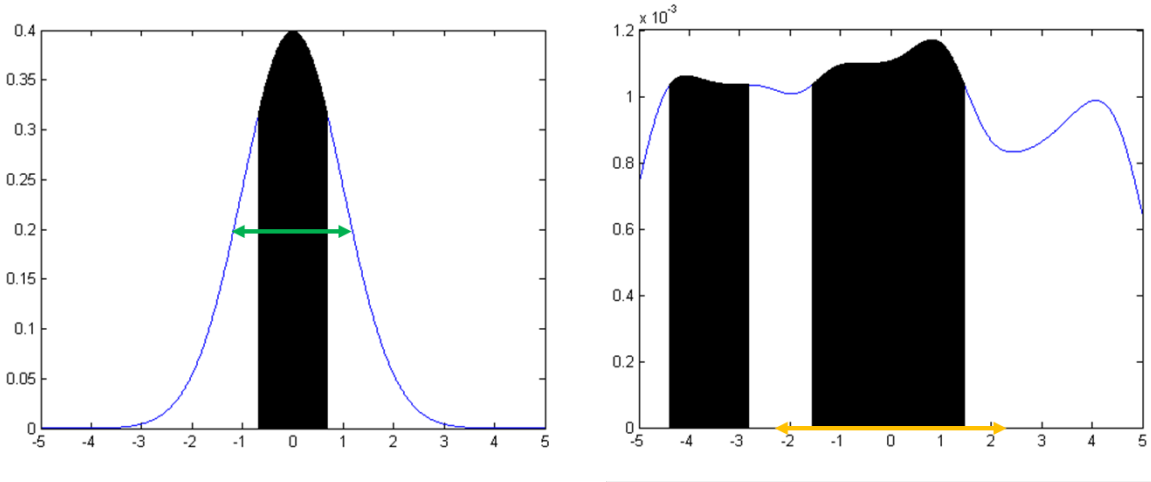

Figure 2.4: Normalized minimum width half total (NMWHT) illustrated
Left: *NMWHT* (filled area) and full width half maximum (green line) for a Gaussian distribution (μ = 0, σ = 1). Right: *NMWHT* (filled area, orange line) for a pseudo-random distribution with equal integrated power to the Gaussian on the left and multiple peaks.

2.2.2 Splitting the Solar Spectrum

Simulations were performed over a range of spectral fidelity and *NMWHT* values. The first step in this process was to split the solar spectrum into spectral bands. The ASTM G173-03 AM 1.5G spectrum was used [47]. A script was written in Matlab to split the spectrum into spectral

bands with a prescribed fidelity value. For this splitting, it was assumed first that there were no optical losses in the system, that is, that all incident photons ended up in one spectral band or another. It was further supposed that leakage from one spectral band to the other would be most pronounced near the cutoff wavelength. To accomplish this, the following method was used (for full code, see Appendix A.1 Matlab Spectrum Splitting Script: Uniform):

- The spectrum was split perfectly.
- A Gaussian decay function (solid blue lines in Figure 2.5) was applied to the high-energy spectral band and the complement to that function (solid red lines in Figure 2.5) applied to the low-energy spectral band.
    - The decay constants and center of the function were fit using a least squares method to achieve the desired fidelity of each spectral band.
    - By using complementary functions, it was ensured that all photons were accounted for.

Combinations of fidelity were fit with values: 55%, 65%, 75%, 85%, 90%. Fidelity values below 50% are less effective at directing light to appropriate materials than not splitting at all, and so were not considered. Since only complementary functions with Gaussian decay profiles were allowed, achieving nearly perfect fidelity in both bands was not possible. Pairing 95% fidelity in both spectral bands with the Gaussian profile resulted in 84.87% fidelity in the high-energy spectral band and 93.84% fidelity in the low-energy spectral band. This precision was deemed inadequate, so 90% fidelity was the highest value simulated. A perfect split in both spectral bands was also considered. The combined difference between nominal fidelity and actual fidelity was less than 10^{-13} for all combination except 90% in both spectral bands, for which the high-energy spectral band fidelity was 89.44% and the low energy spectral band fidelity was 89.96%.

The decay functions and resulting spectra are illustrated in Figure 2.5 for a perfect split (top), 90% fidelity in both bands (middle), and 70% fidelity in both bands (bottom).

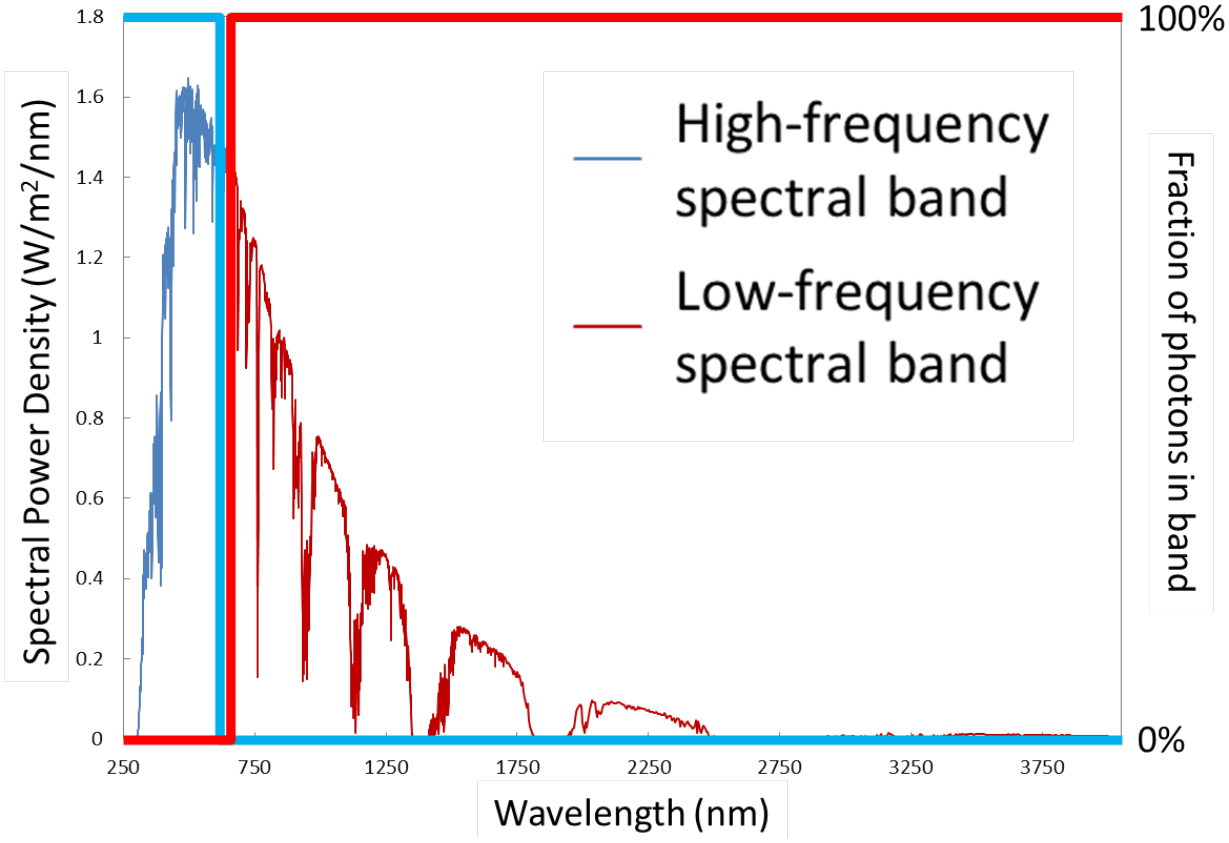
Spectral Power Density (W/m²/nm)
1.8
1.6
1.4
1.2
1
0.8
0.6
0.4
0.2
0
250
750
1250
1750
2250
2750
3250
3750
Wavelength (nm)
High-frequency spectral band
Low-frequency spectral band
100%
0%
Fraction of photons in band

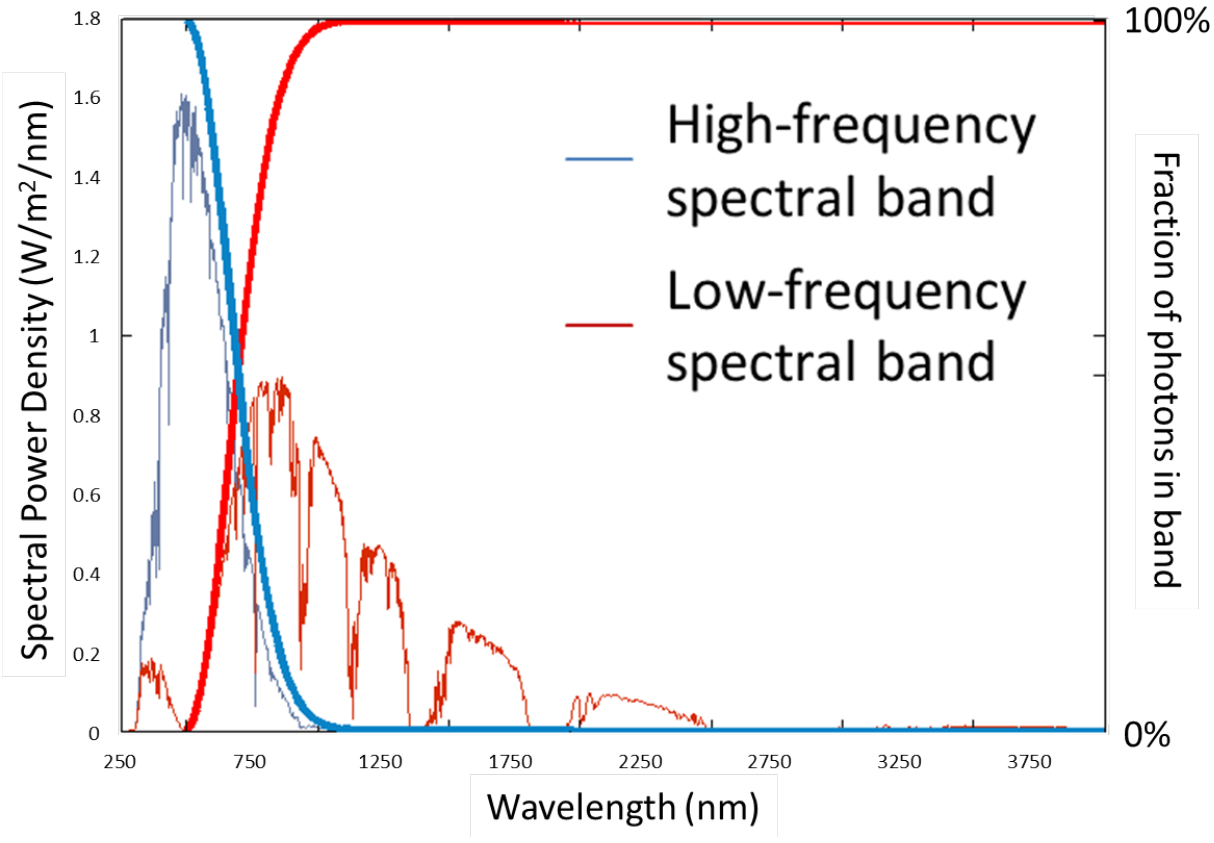
Spectral Power Density (W/m²/nm)
1.8
1.6
1.4
1.2
1
0.8
0.6
0.4
0.2
0
250
750
1250
1750
2250
2750
3250
3750
Wavelength (nm)
High-frequency spectral band
Low-frequency spectral band
100%
0%
Fraction of photons in band

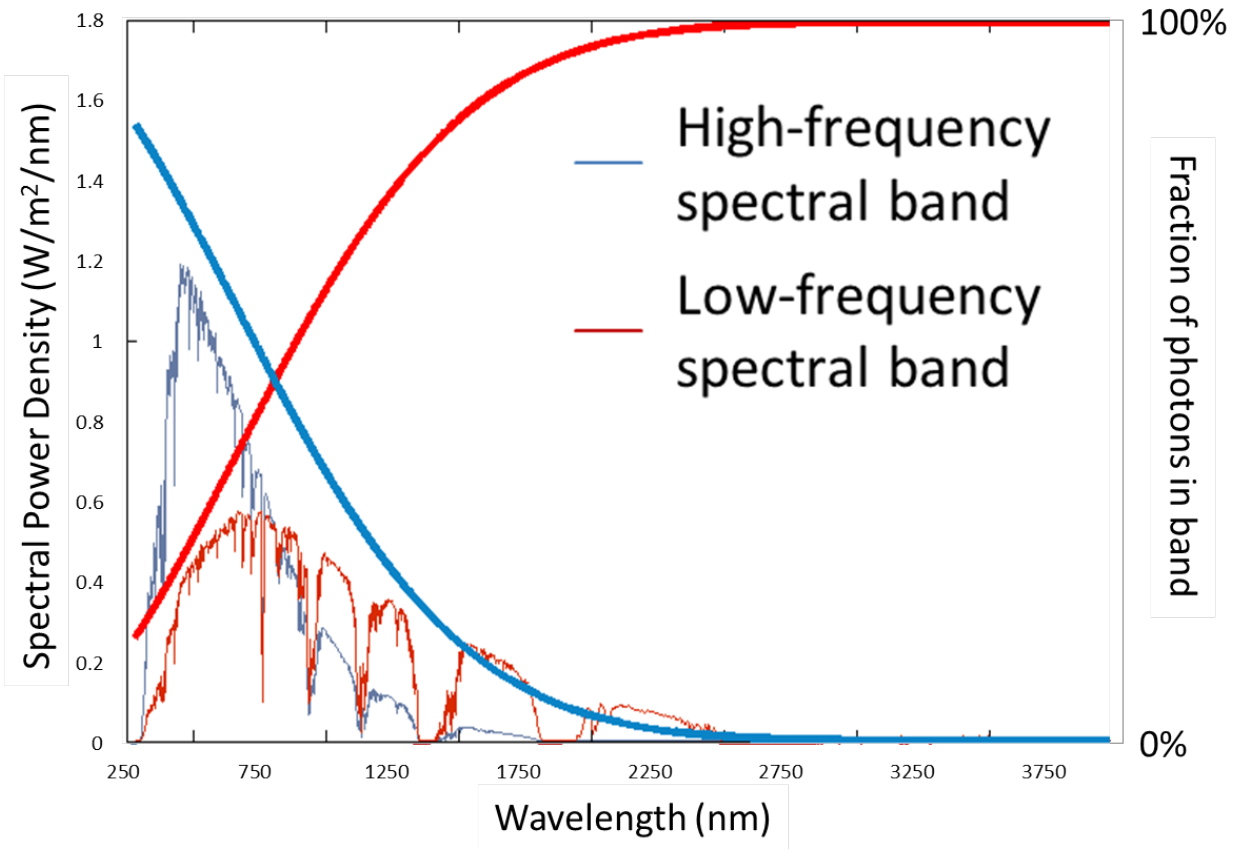

Figure 2.5: Example splitting functions and resulting spectra

Splitting functions with Gaussian decay and its complement (right axis) and spectral power density *vs.* wavelength for a perfect split (top), 90% fidelity in both spectral bands (middle) and 70% fidelity in both spectral bands (bottom).

The spatial variation in intensity considered in this thesis was also Gaussian. Gaussian variation is a reasonable approximation for random losses. Also, many lenses and mirrors are known to produce beams with Gaussian decays in intensity. However, the simulated variation is meant to be illustrative. There are certainly many optical systems, like diffraction gratings, that will produce very different variations in intensity. Spatial variation was only considered in one dimension, which significantly simplified and sped up the simulations. Spectral splitting schemes exist that result in spatial variation in intensity in a single dimension; for example, using diffractive optics [46]. Furthermore, adapting the approach and lessons to variations in two dimensions is straightforward. Spatially varying spectra were also generated with a Matlab script. The method was as follows (for full code, see Appendix A.2 Matlab Splitting Script: Spatially Varying):

- The spectrum was first split as above into spectral bands with the desired fidelity.
- A normal distribution was generated with the "normpdf" function on a vector x consisting of the integers from 1 to 21. The variance of this distribution determined the extent of the spatial variation (see below for details).
- The distribution was normalized so that the total photon flux remained constant at an intensity of one sun.
- The values of the normal distribution were multiplied by the split spectra.

Since the simulation unit cell can be taken between any two lines of symmetry, only half the distribution (the first 11 points) was needed. The *NMWHT* was calculated separately for each distribution.

2.2.3 Optical Models

To keep models consistent for the spatially varying and spatially uniform spectra, Sentaurus was used to model devices under all spectra. Sentaurus contains a built-in transfer-matrix-method (TMM) algorithm for calculating the generation rate as a function of wavelength and position based a wavelength-dependent absorption coefficient [48]. For uniform spectra, the Sentaurus TMM algorithm was used to calculate the generation rate as a function of position in the simulated silicon devices.

Since the thickness and the width of the silicon device simulated was much greater than all wavelengths of incoming light, for non-uniform spectra, the silicon device was modeled using geometrical optics (J.P. Mailoa, MIT). Monocrystalline silicon devices are typically textured into pyramids with a facet angle to the horizontal of 54.4^{O}. The light was all assumed to be normally incident and to strike one of these facets and be refracted based on a constant index of refraction. Any photons that reached the back surface were assumed to be perfectly reflected, and any photons that subsequently reached the front surface were assumed to escape. A wavelength-dependent absorption coefficient was convoluted with the path vector to determine absorption as a function of position.

As illustrated in Figure 2.6, for spatial non-uniform illumination profiles, the generation rate for a spectrum of each intensity described in Chapter 2.2.2 was simulated by treating it as incident on a fraction of the top surface of the device from $\frac{(x-1)\times w}{10.5}$ to $\frac{x\times w}{10.5}$ where w is the full width of the simulated device, and x is an integer from 1 to 10 corresponding to both the position

across the device and the vector used to generate the Gaussian as described in Chapter 2.2.2. Since the full width is 21 segments, in order to split the spectrum at a true line of symmetry and avoid overcounting the highest intensity, the eleventh segment of the device had only half the width of the first ten and corresponded to the spectrum for $x = 11$. Note that while each spectrum was only incident on a fraction of the device surface for each simulation, the generation rate was simulated for the full device with periodic boundary conditions. The generation rates for each of these spectra were then superposed to give the full generation rate as a function of position.

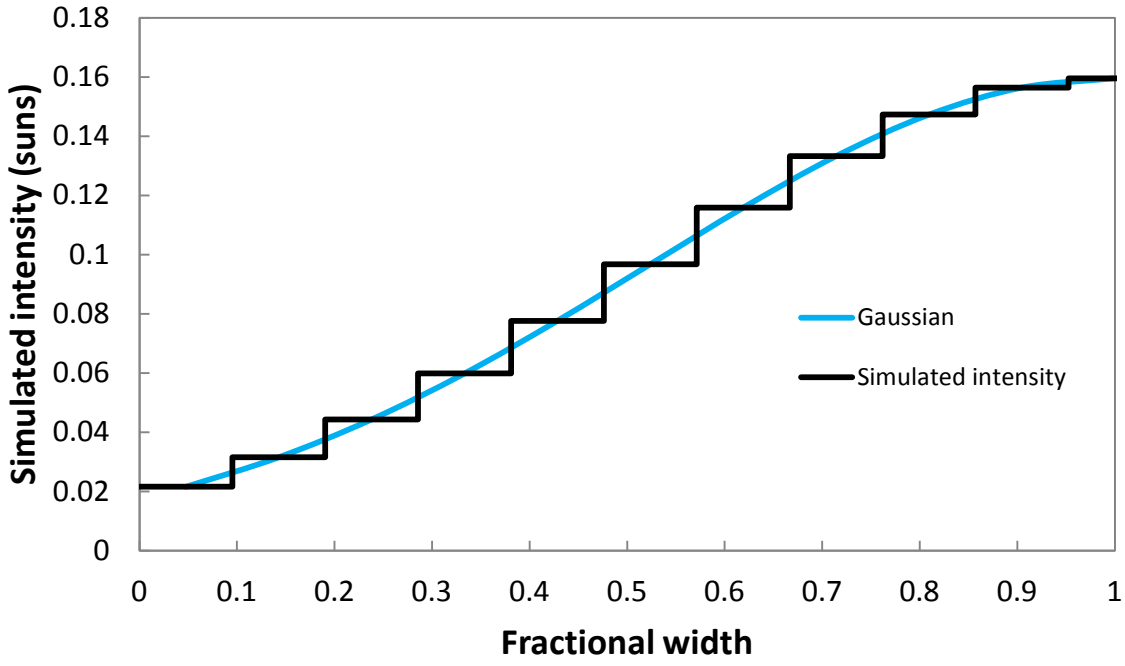

Figure 2.6: Simulated illumination intensity and Gaussian from which it is derived
Plotted *vs.* position as a fraction of total device width *w*.

For the Cu_2O devices, a similar approach was taken. However, the thickness (and in some cases the width) of the Cu_2O devices simulated were on the order of the wavelength of solar illumination. Therefore, simulations for both the uniform and spatially varying illumination were performed using the finite-difference time-domain (FDTD) method (J.P. Mailoa, MIT) with a repeating surface texture taken from a representative atomic force micrograph of a real Cu_2O device. More details on the FDTD simulations can be found in Ref. [49].

2.3 Integration of Optical and Device Models

2.3.1 Spatially Uniform, Varying Fidelity

For the Si simulations, the TMM simulation is part of SDevice, so changing the spectrum was all that was needed to incorporate it into the device model. For the Cu_2O simulations, since the simulated device had a planar surface while the FDTD simulation had a textured surface (Figure 2.7, top), the optical generation profile from the FDTD simulation was first rearranged so that the top surface was at a constant level and height variations appeared at the bottom of the generation profile (Figure 2.7, middle). To account for these variations since these generation profiles were supposed to be uniform, the generation rate was averaged over the lateral spatial dimension to give a 1-D (Figure 2.7, bottom). To reduce the number of nodes required for meshing in Sentaurus, depth values were removed from these profiles for which the instantaneous change in generation rate was less than 10% of the total change. The script for these manipulations can be found in Appendix A.3 **Matlab FDTD Generation Rate Conversion**. The modified generation rate file was then input as a 1-D generation profile into SDE.

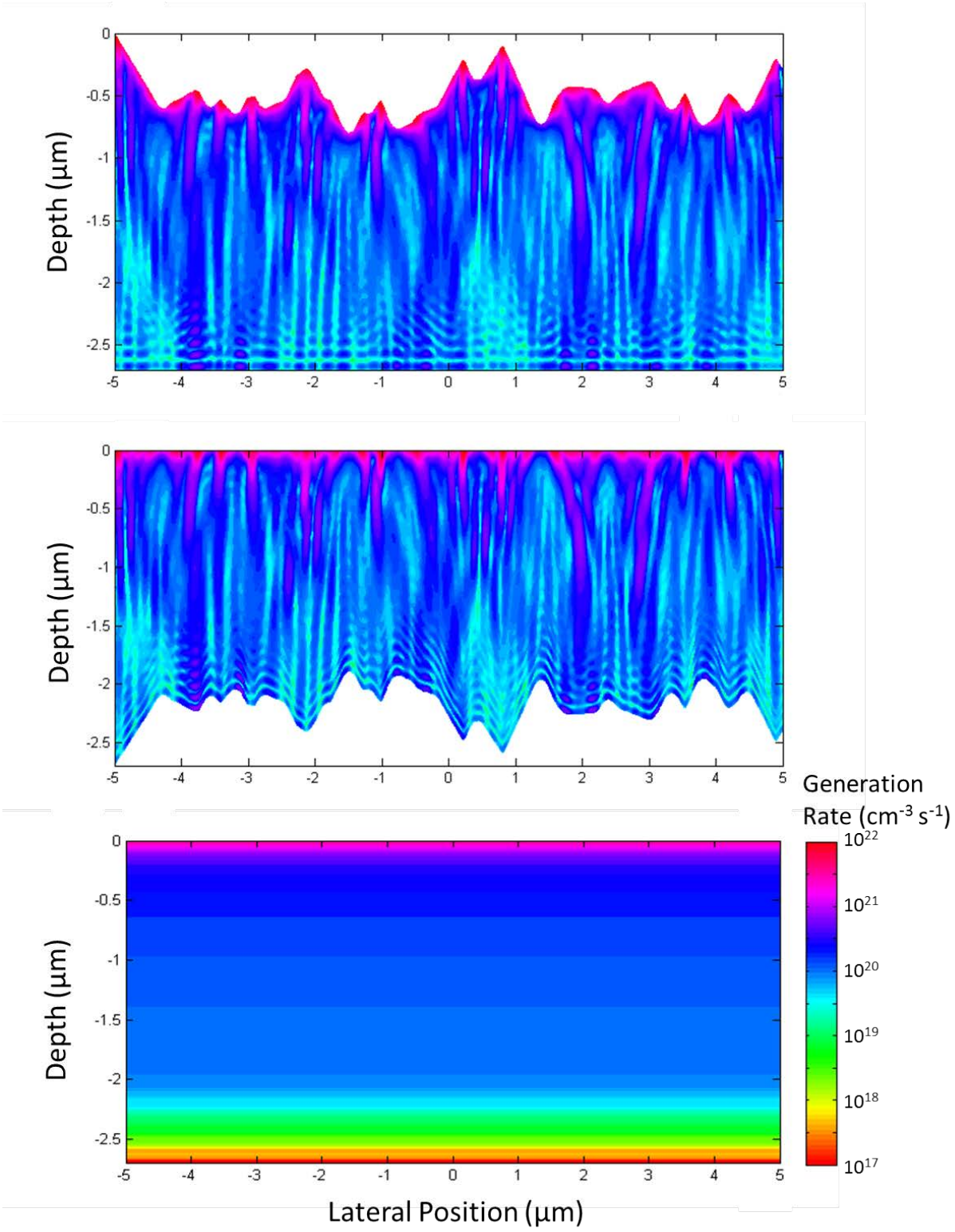

Figure 2.7: Manipulation of FDTD optical generation profile for spatially uniform simulation
2-D optical generation profile is obtained by FDTD (top), effects of surface texture are moved to the back of the cell (middle), and generation rate is averaged over lateral position to obtain a 1-D profile (bottom).

2.3.2 Spatially Varying

In order to implement spatially varying generation rates, 11 different regions of each device, corresponding to the 11 different illumination intensities, were created in SDE. These regions, whose boundaries are indicated by the vertical black lines in Figure 2.8, all had the same material properties, only the generation profile was changed. For the Cu_2O simulations, the procedure described in Chapter 2.3.1 was followed for each region. For the Si simulations, the superposed generation profile of the whole device was split back into 11 segments, and the generation rate was averaged over lateral position for each segment. Each of these generation profiles was input into the corresponding region in SDE. The generation rate at the mesh points closest to the boundary of each region is the average of the generation rate in the regions on either side. Generation rates were input as a discrete set of 1-D profiles because Sentaurus allows region-wise definition of 1-D generation profiles on an arbitrary grid and requires a pre-defined grid that is the same for 2-D generation profiles and the rest of the simulation.

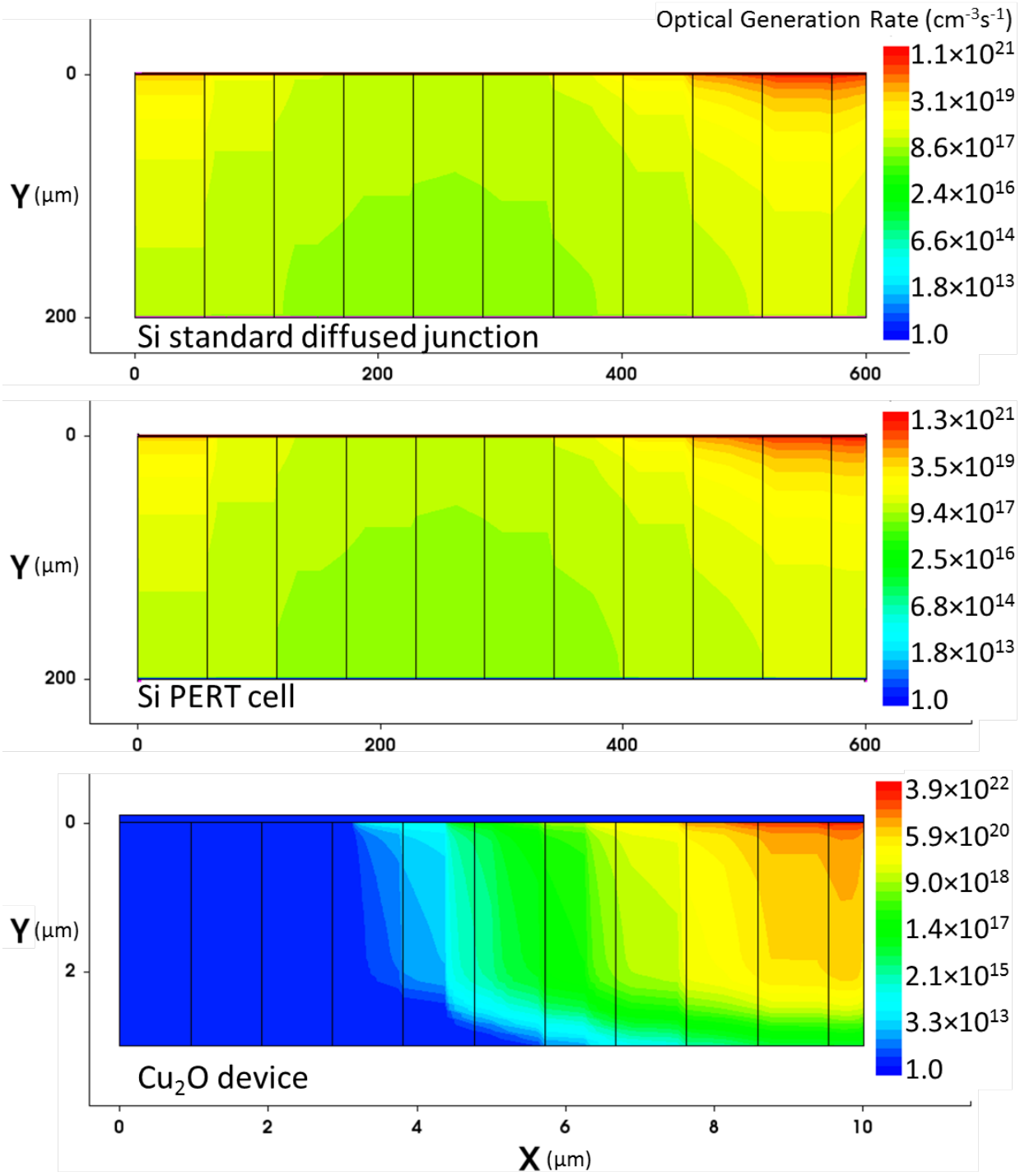

Figure 2.8: Implementation of spatially varying illumination profiles in SDevice

Optical generation rates as a function of position for standard diffused junction Si device (top), PERT device (middle), and Cu_2O device (bottom) with fidelity=100% in both spectral bands and *NMWHT*=0.068. Discrete 1-D profiles are input into each region (region boundaries indicated by vertical black lines). Generation rate at the mesh points closest to the boundaries are the average of generation rates in the adjacent regions. Differences between the two Si simulations are due to slight differences in the meshes.

CHAPTER

3

IMPACT OF SPECTRAL FIDELITY

3.1 Fidelity Results

Fidelity, as defined in Chapter 2.2.1, is the ratio of the number of photons in a given spectral band to the number of photons in that spectral band in a perfect split. As shown in Figure 3.1, the importance of fidelity was first measured generally by comparing the combined system efficiency for all combinations of high-efficiency (in blue) and low-efficiency (in orange) Si devices with high-efficiency (diamonds) and low-efficiency (squares) Cu_2O devices when the fidelity of both the high- and low-energy spectral bands were varied together. For example, if the fidelity is 90%, 90% of photons with energy greater than the band gap of Cu_2O (2.0 eV) go to the Cu_2O device and 10% go to the Si device. Likewise, 90% of photons with energy less than 2.0 eV go to the Si device and 10% go to the Cu_2O device. It is clear that fidelity has a strong impact on system performance, with efficiency falling off rapidly as fidelity decreases from 100%. To help give a sense of the scale, the solid blue and orange lines in Figure 3.1 indicate the efficiency under the full solar spectrum of the high-efficiency and low-efficiency Si devices respectively. The red circle shows the efficiency of a high-efficiency Si device with an ideal Cu_2O homojunction device.

It can be shown that the importance of the fidelity of the low-energy spectral band (*i.e.*, the light incident on the narrower-band gap Si device) far outweighs the importance of the fidelity of the high-energy spectral band (*i.e.*, the light incident on the wider-band gap Cu_2O device). Figure 3.2 – Figure 3.5 show the system efficiency as a function of the fidelities of each spectral band varied independently. The data is plotted in two ways in each figure to highlight the difference in the importance of each band.

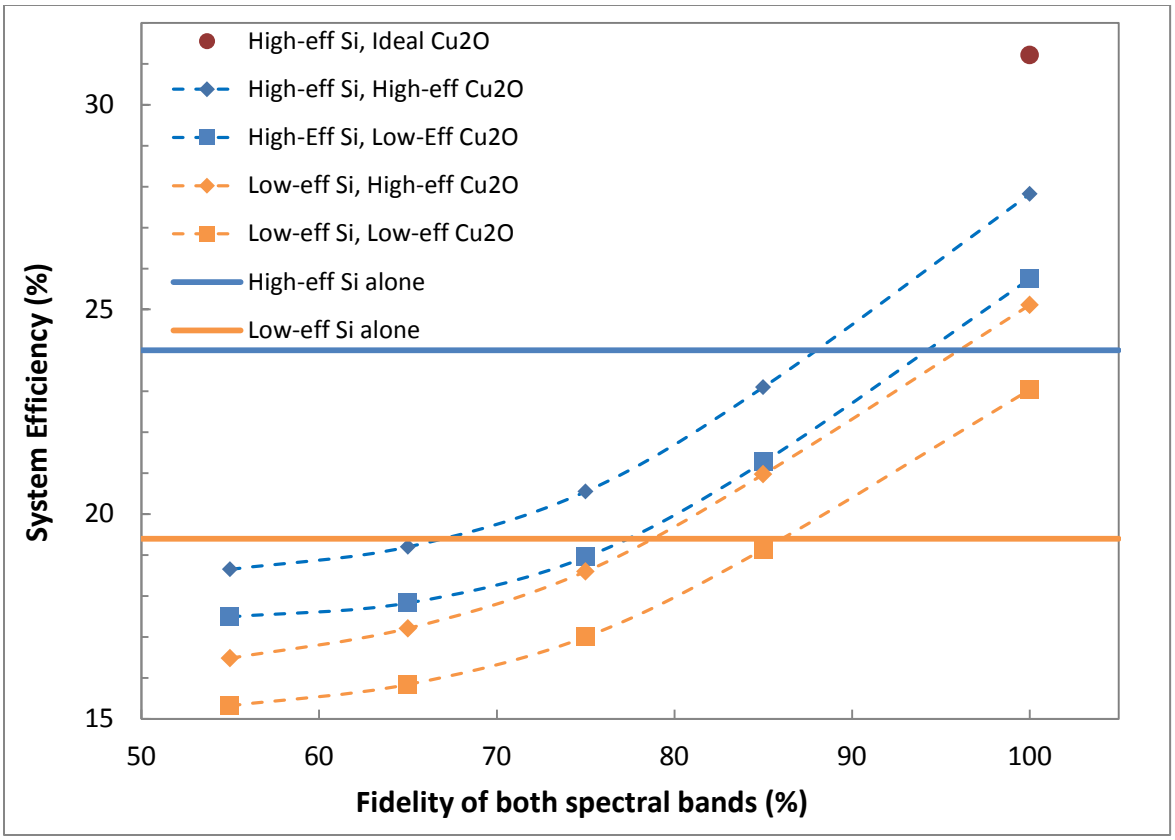

Figure 3.1: System efficiency shows a strong sensitivity to fidelity

System efficiency plotted *vs.* fidelity with fidelity of both spectral bands varied together. Solid lines indicate the efficiency of high- and low-effiiciency Si by itself under the AM 1.5G spectrum. Red circle indicates efficiency of a combination of high-efficiency Si and a nearly ideal Cu_2O homojunction under perfect splitting.

As can be seen from the top plot in each figure where the data is plotted with the fidelity of the low-energy spectral band on the *x*-axis and data series for the fidelity of the high-energy spectral band, the fidelity of the low-energy spectral band has a strong impact on system efficiency (slope of the curves), while the fidelity of the high-energy spectral band has little impact (clustering of the data series). The bottom plot in each figure where the fidelity of the high-energy spectral band is plotted on the *x*-axis with the data series for the fidelity of the low-energy spectral band, further highlights the lack of importance of the fidelity of the high-energy spectral band.

In fact, it can be seen that for a system where the device with the narrower-band gap absorber (Si in this case) has a significantly higher efficiency than the wider band-gap absorber (high-efficiency Si with either high- or low-efficiency Cu_2O and low-efficiency Si with low-efficiency

Cu_2O), it can be deleterious to increase the fidelity of the high-energy spectral band in certain situations, even though 100% fidelity in both spectral bands is always the maximum efficiency. It is important to note that it is not primarily because, for the device simulated here, the narrower-gap absorber (Si) has a higher efficiency than the wider-gap absorber (Cu_2O) that the fidelity of the low-energy spectral band is more important. The main drivers of these trends will be discussed in Chapter 3.2.

Since relative efficiency of the devices was found to significantly affect the impact of fidelity on system efficiency, whether lower-efficiency devices responded differently to spectra of different fidelity than higher-efficiency devices was investigated. The relative efficiency (efficiency of the device under a spectra of a given fidelity divided by the efficiency of the device under perfect splitting—100% fidelity) was compared for the lower-efficiency simulations and the higher-efficiency simulations. Little difference was observed for either Si or Cu_2O devices (Figure 3.6).

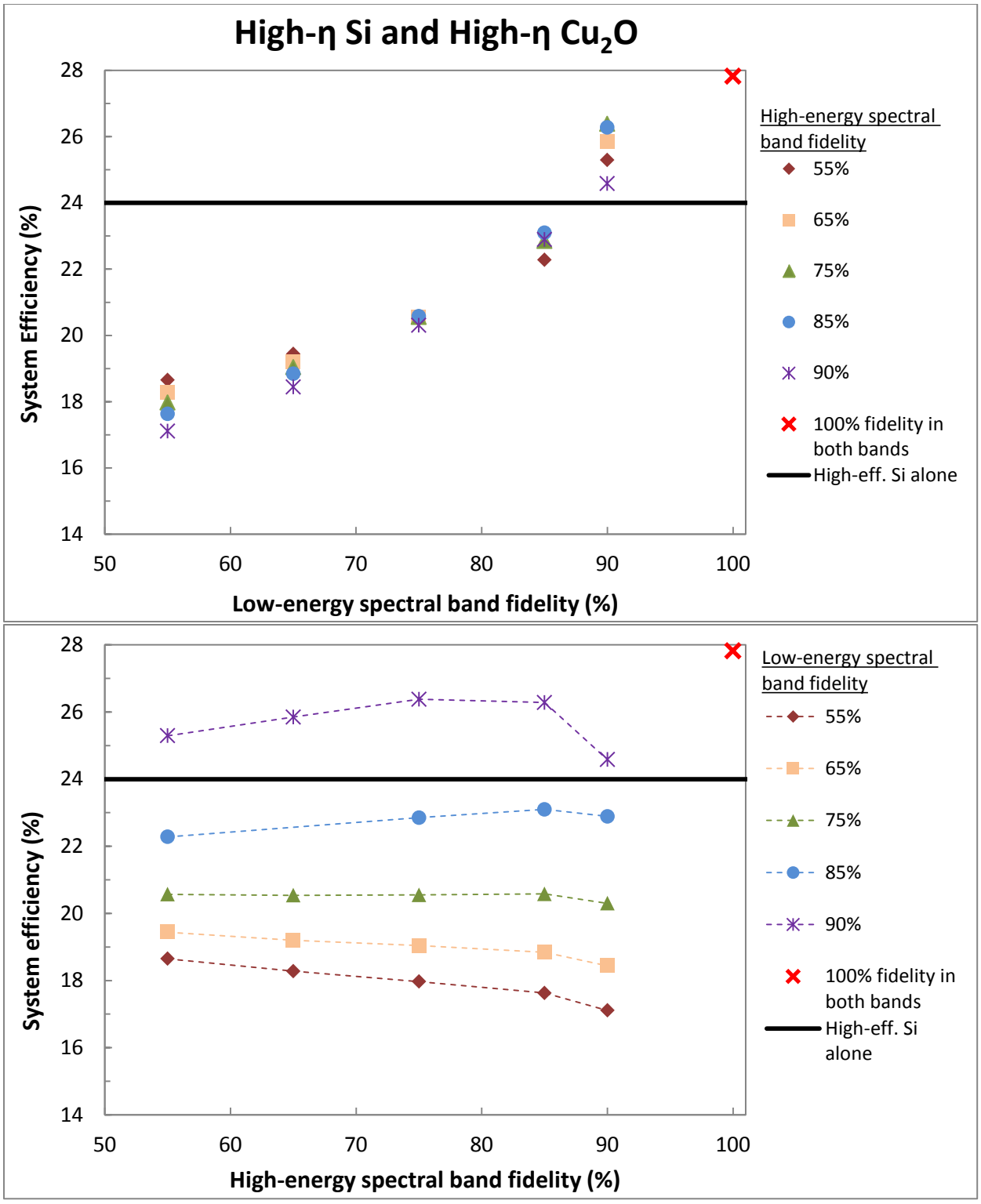

Figure 3.2: System efficiency sensitive mostly to fidelity of low-energy spectral band (high-η Si and Cu_2O) System efficiency plotted *vs.* fidelity of low-energy spectral band with data series for fidelity of high-energy spectral band (top) and system efficiency plotted *vs.* fidelity of high-energy spectral band with data series for fidelity of low-energy spectral band (bottom).

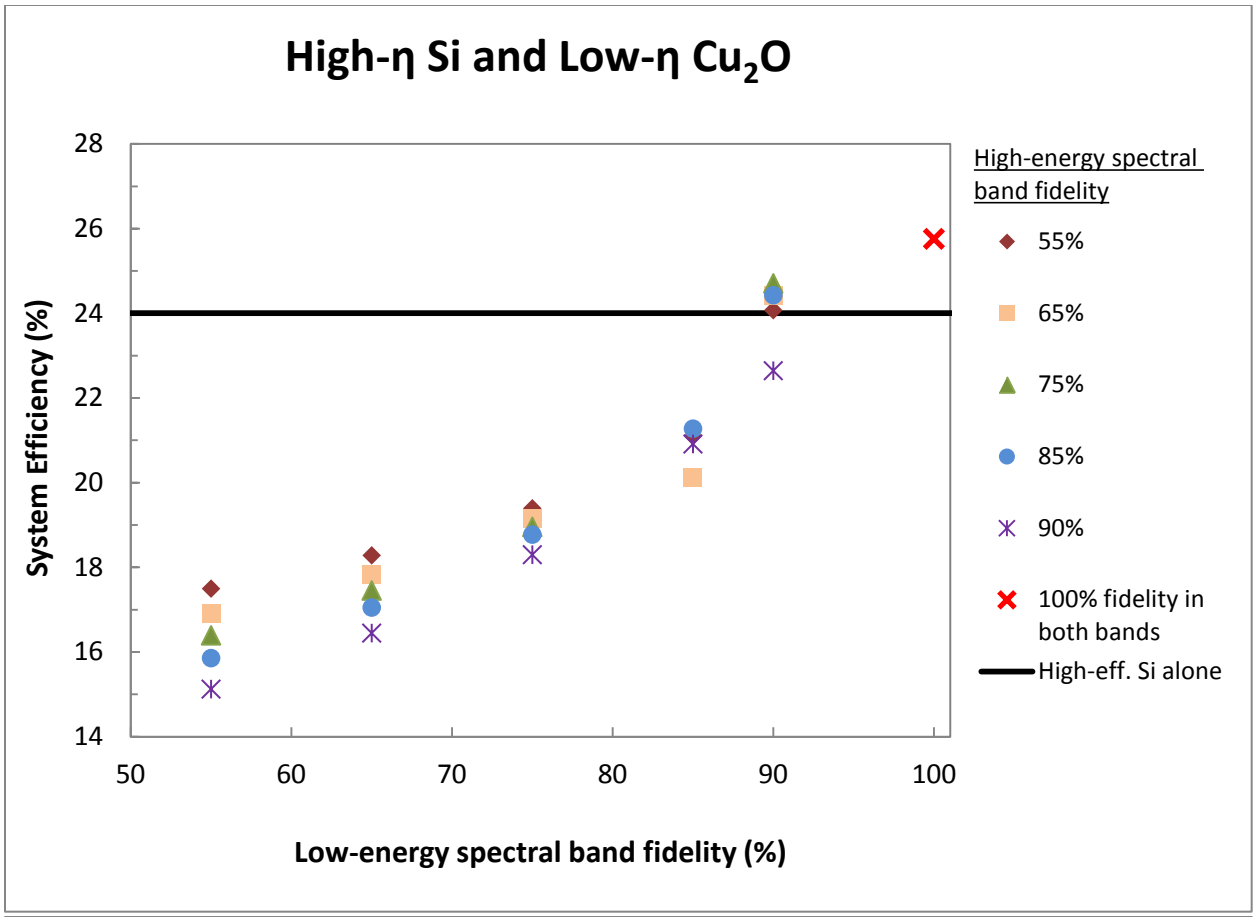

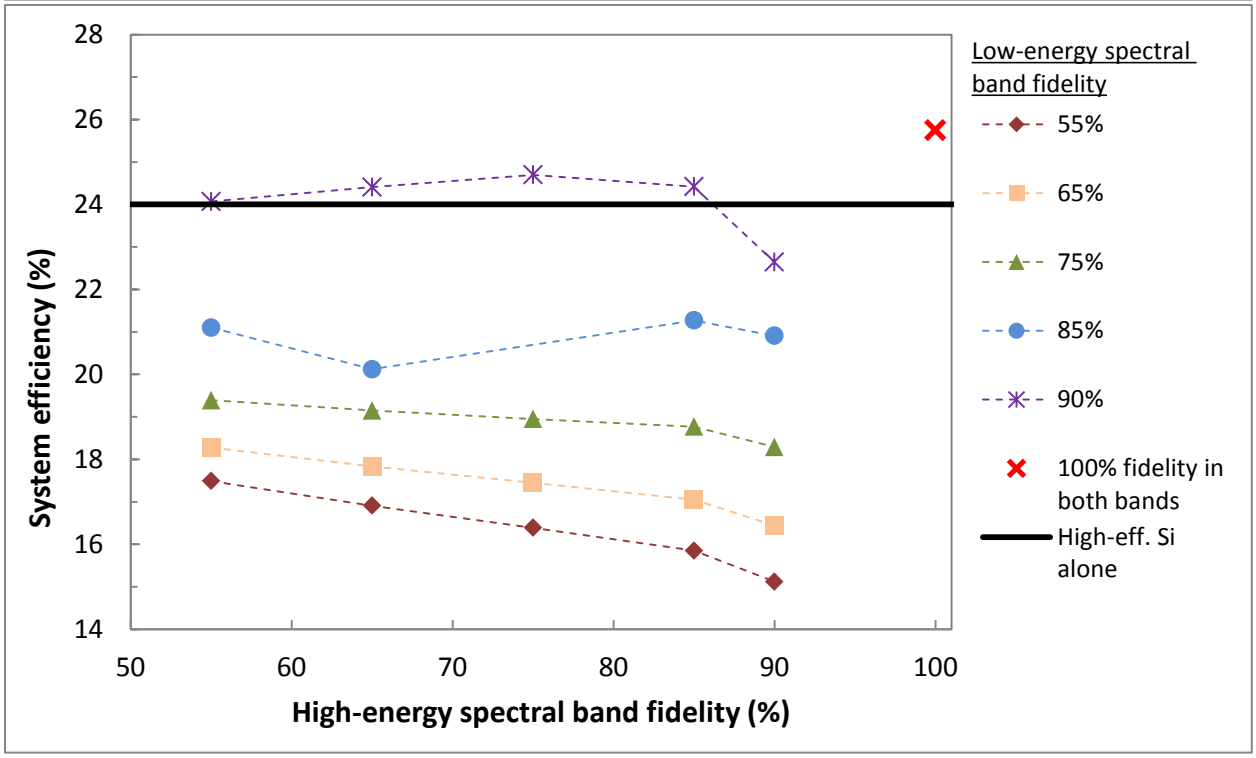

Figure 3.3: High-η Si and low-η Cu_2O

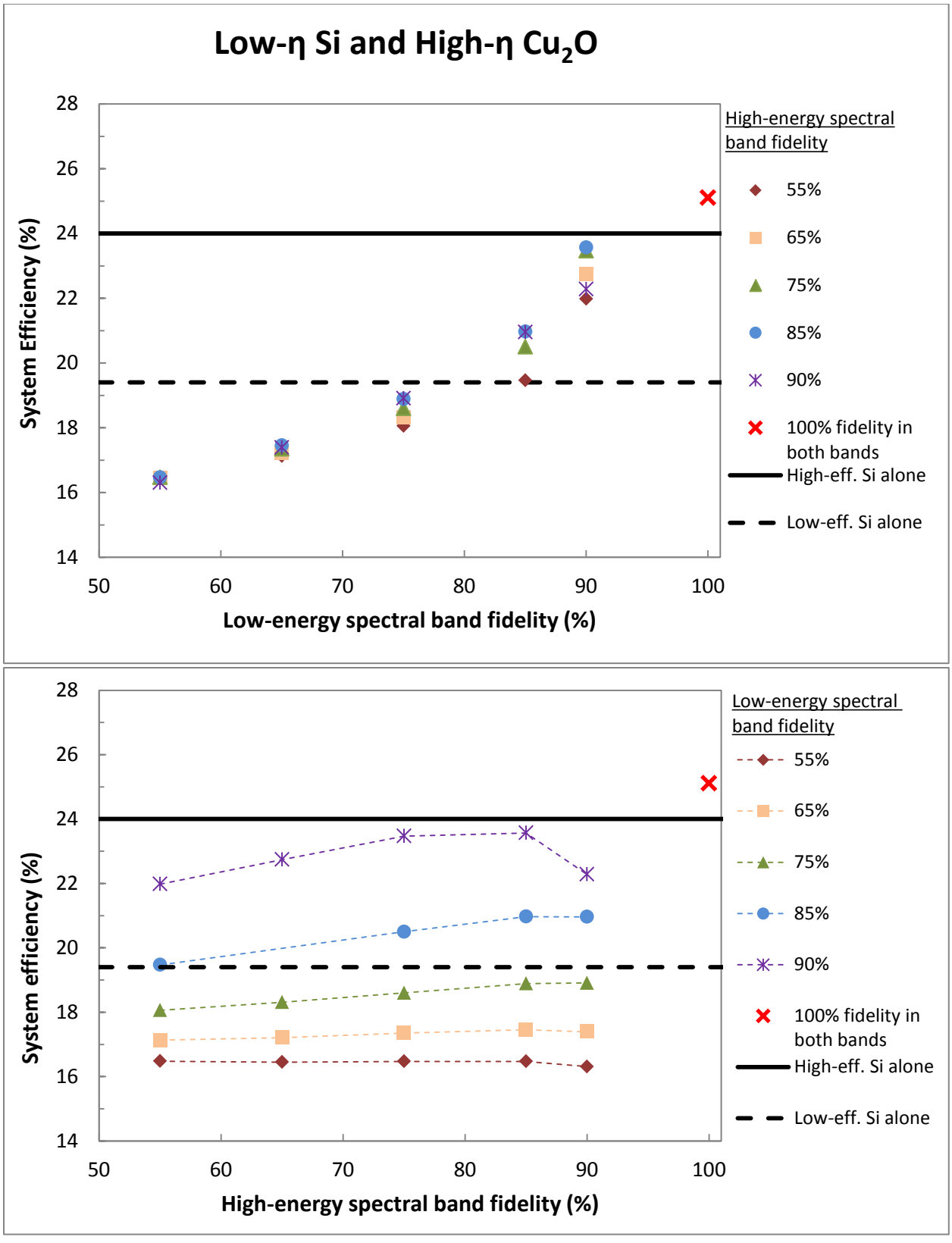

Figure 3.4: Low-η Si and high-η Cu_2O

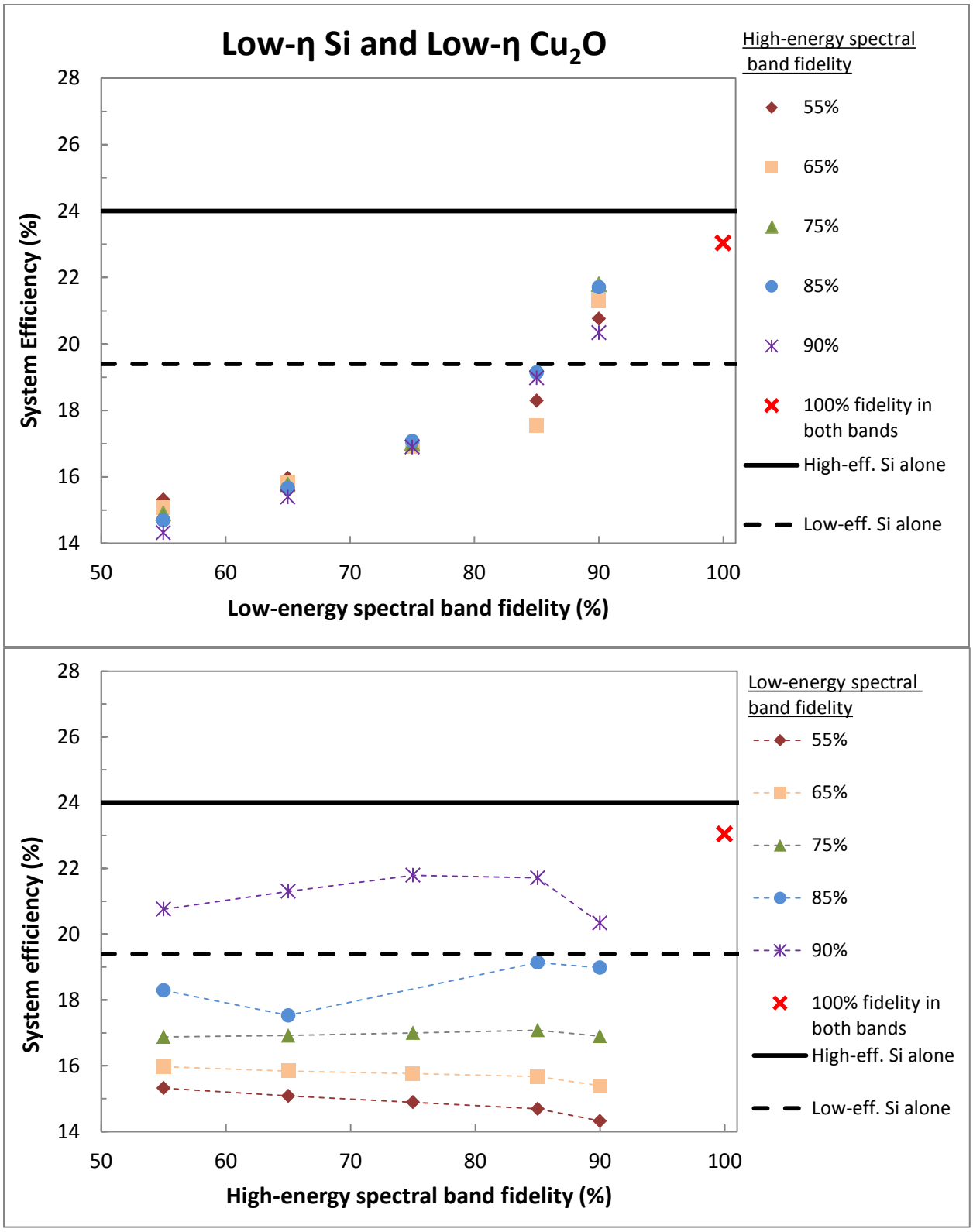

Figure 3.5: Low-η Si and Cu_2O

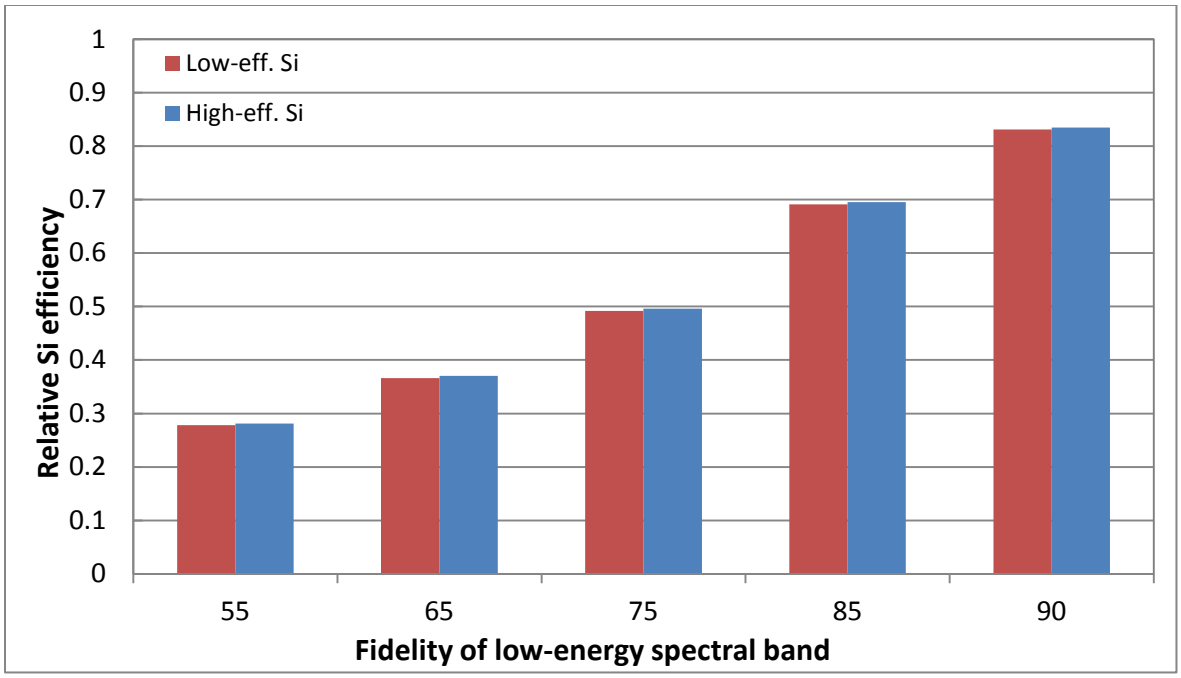

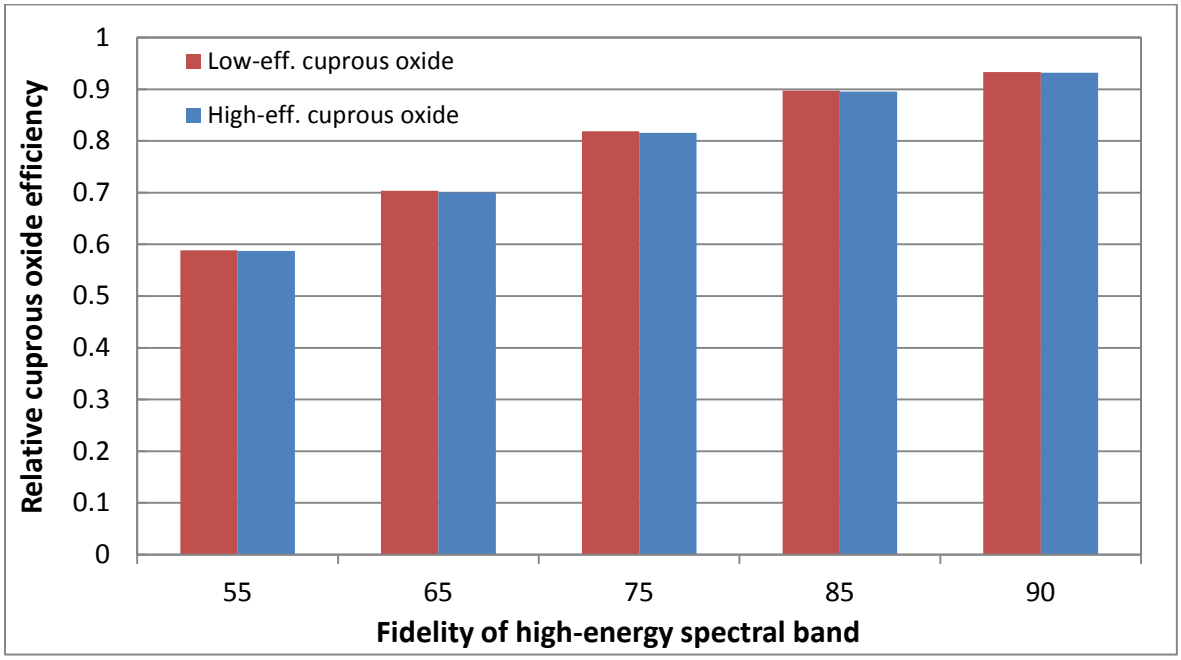

Figure 3.6: No difference between response of high-η and low-η devices to varying fidelity

Top: Si device efficiencies of higher and lower-efficiency Si devices, normalized to the efficiency of the respective device under a perfectly split spectra, were compared under spectra with varying low-energy spectral band fidelities. The high-energy spectral band fidelity was kept constant at 90%.

Bottom: Cu_2O device efficiencies of higher and lower-efficiency Cu_2O devices, normalized to the efficiency of the respective device under a perfectly split spectra, were compared under spectra with varying high-energy spectral band fidelities. The low-energy spectral band fidelity was kept constant at 90%.

3.2 Fidelity Discussion

The importance of the fidelity of the low-energy spectral band is due to the fact that high-energy photons that are "incorrectly" directed to the narrower band gap material are still absorbed while low-energy photons that are directed to the wider band gap material are not absorbed. This results in a one-to-one correlation fidelity losses in the low-energy spectral band and photocurrent losses. A one-to-one loss in current must result in at least a one-to-one loss in efficiency, as can be seen by the following definition of the efficiency, η:

$$\eta = \frac{J_{SC} \times V_{OC} \times FF}{P_{solar}} \tag{3.1}$$

If the common approximation that the short-circuit current equals the photocurrent is used, the loss of absorption is directly proportional to the loss in efficiency. Since V_{OC} also usually decreases (logarithmically) with the photocurrent (approximated as J_{SC}) and fill factor (FF) can also be negatively affected, a trend that is superlinear is also possible. In contrast, losses in fidelity in the high-energy spectral band only result in greater thermalization losses as discussed in Chapter 1.2.2.

Figure 3.7 shows that nearly all of the losses in the system for any fidelity values are current losses and therefore due to reduced absorption. When the efficiency, normalized to the efficiency of a perfect split, is plotted against $J_{SC,}$ normalized to J_{SC} of a perfect split, the data falls very close to the 1:1 line for all pairs of fidelities and all pairs of devices. This trend demonstrates the nearly 1:1 correlation between current losses and efficiency losses.

The low sensitivity of system performance to fidelity of the high-frequency spectral band has some implications for device design. It suggests that strong spectral response for a wide range of photon energies is not necessary as long as the carrier collection and voltage output are high for the strongly absorbing range. Photons outside this range can be directed to narrower-gap materials that absorb them more efficiently with little effect on system efficiency.

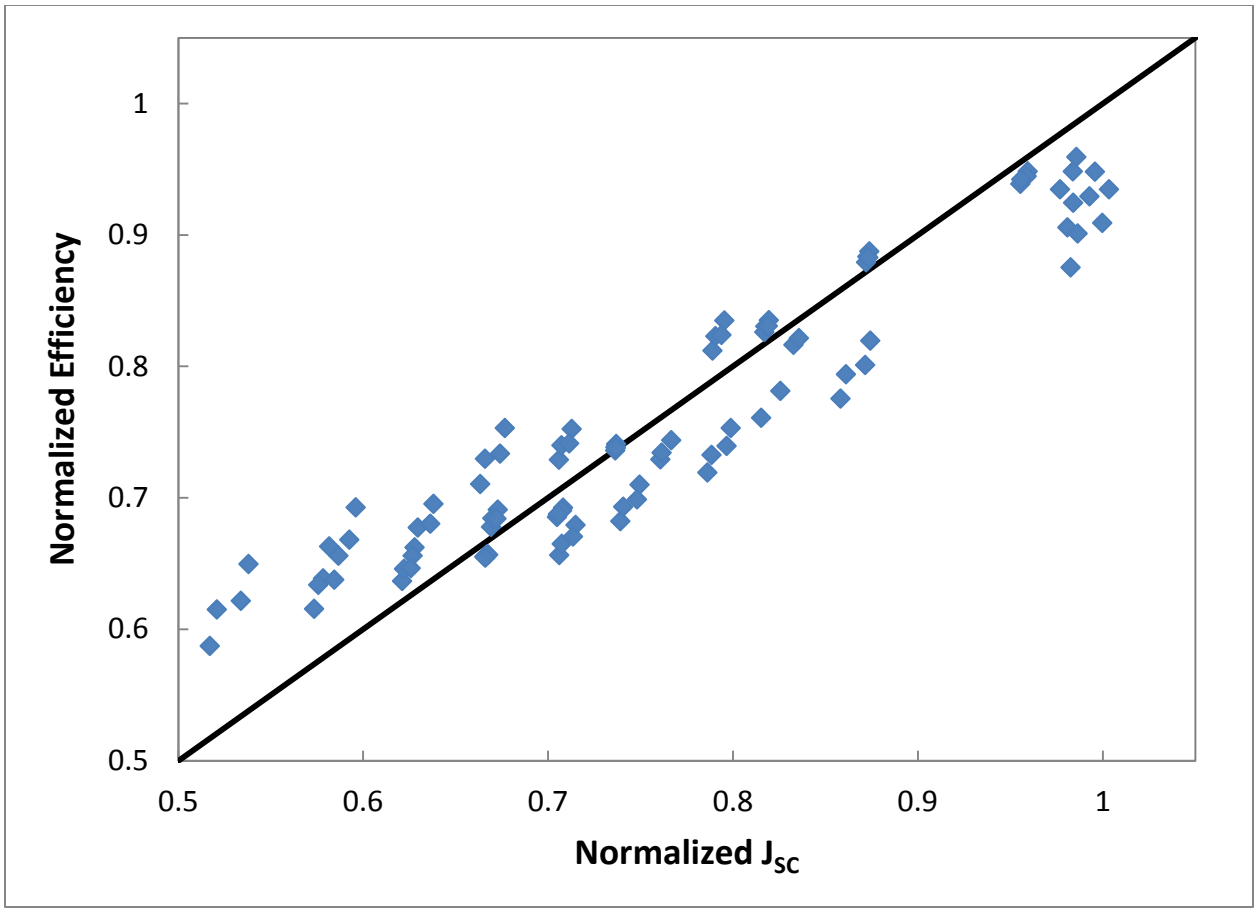

Figure 3.7: Nearly 1:1 correlation between normalized efficiency and normalized J_{SC}

Data includes every combination of fidelities and every combination of high- and low-efficiency devices. Efficiency and J_{SC} are normalized for each point to the efficiency and J_{SC} of the same pair of devices under illumination by a perfectly split spectrum (100% fidelity in both spectral bands). Line shows a 1:1 correlation between current losses and efficiency losses.

CHAPTER

4

IMPACT OF SPATIAL UNIFORMITY

4.1 Spatial Uniformity Results

Spatial uniformity of the incident light intensity was found to have virtually no effect on any of the standard set of device parameters used to evaluate the performance of PV devices: Efficiency, internal quantum efficiency (*IQE*, ratio of electrons extracted to absorbed photons with no voltage applied), open-circuit voltage (V_{OC}, the voltage at which no current flows), and fill factor (*FF*, the ratio of the maximum power produced at any voltage to the product of the current at zero applied bias—J_{SC}—and V_{OC}). So the parameters of interest could be compared across fidelities and spatial uniformities, each was normalized to the value for uniform illumination under the same illumination spectrum.

Because of the way SDE handles external profiles at interfaces between regions, the total illumination intensity varied slightly from simulation to simulation. This variation was controlled to the extent possible, but the error in illumination was measured and from it the errors in the parameters of interest were calculated to see if the small variations in performance were significant. The error in illumination was taken to be $\frac{\mathrm{Range}(J_{\mathrm{ph}})}{\mathrm{Max}(J_{\mathrm{ph}})}$ where the photocurrent, J_{ph}, was the optical carrier generation rate times the electron charge over the whole device integrated over the full device. This error in current, E_J was used directly for the error in *IQE*. V_{OC} goes as the natural logarithm of photocurrent, so the error in voltage, E_V, was taken to be $\frac{\mathrm{Range}[\ln(J_{\mathrm{ph}})]}{\mathrm{Max}[\ln(J_{\mathrm{ph}})]}$. The error in fill factor was treated as propagating from a multiplication of current and voltage terms, so E_{FF} was taken to be $\sqrt{{E_J}^2 + {E_V}^2}$. Finally, the error in efficiency was treated as propagating

from a multiplication of current, voltage, and *FF* terms, so E_η was taken to be $\sqrt{{E_J}^2 + {E_V}^2 + {E_{FF}}^2}$. The errors were assumed to be symmetric about the simulated values.

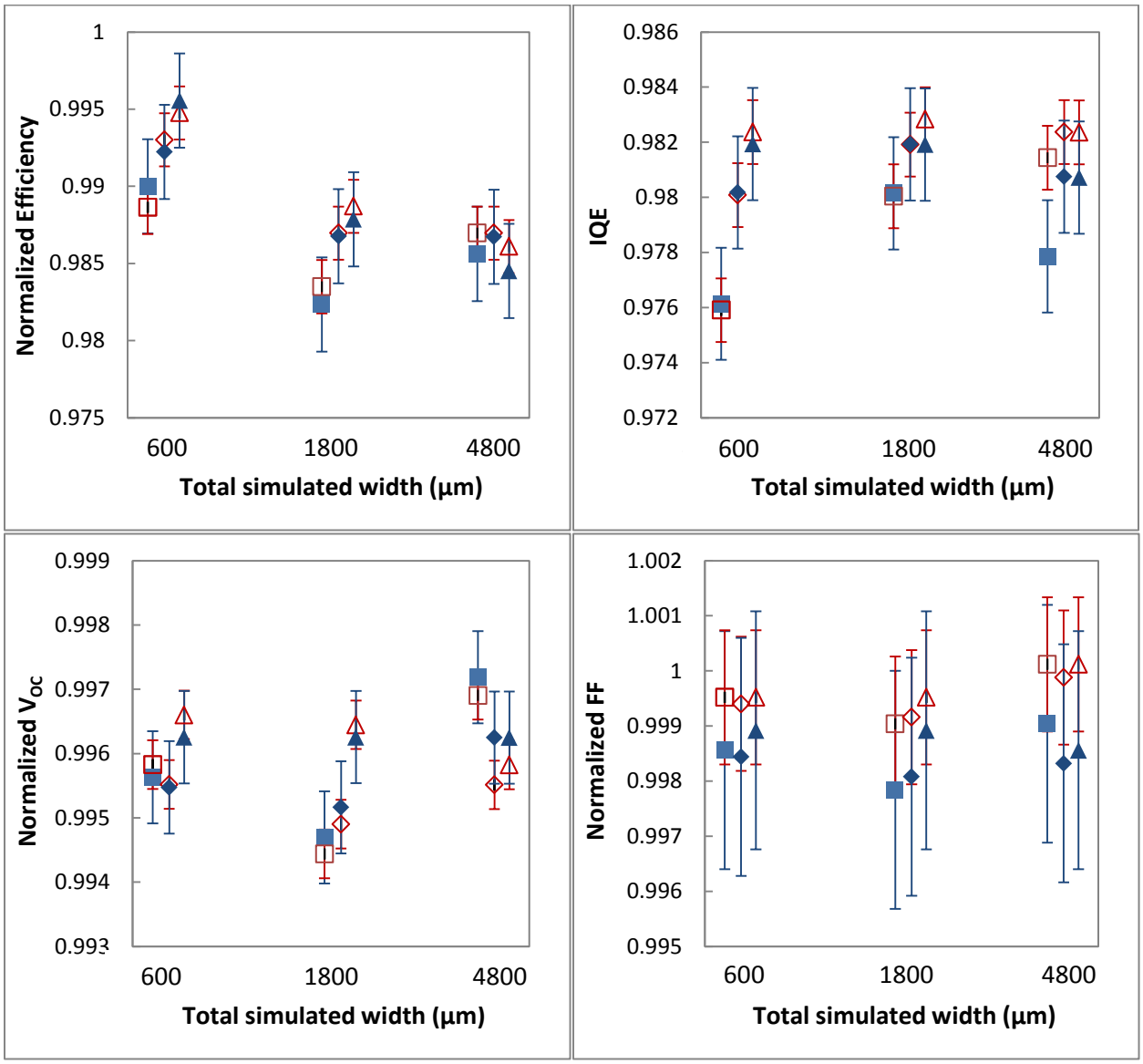

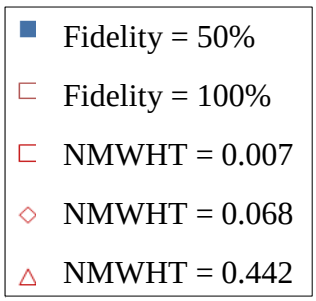

Figure 4.1: Spatial uniformity has little impact on Si diffused junction device performance

Simulated performance metrics, efficiency (top left), V_{OC} (top right), *IQE* (lower left), and *FF* (lower right) plotted *vs.* simulation width. The data series for each width is the *NMWHT*, varying from 0.007 to 0.442. Spectra with two fidelities, 50% and 100% were simulated.

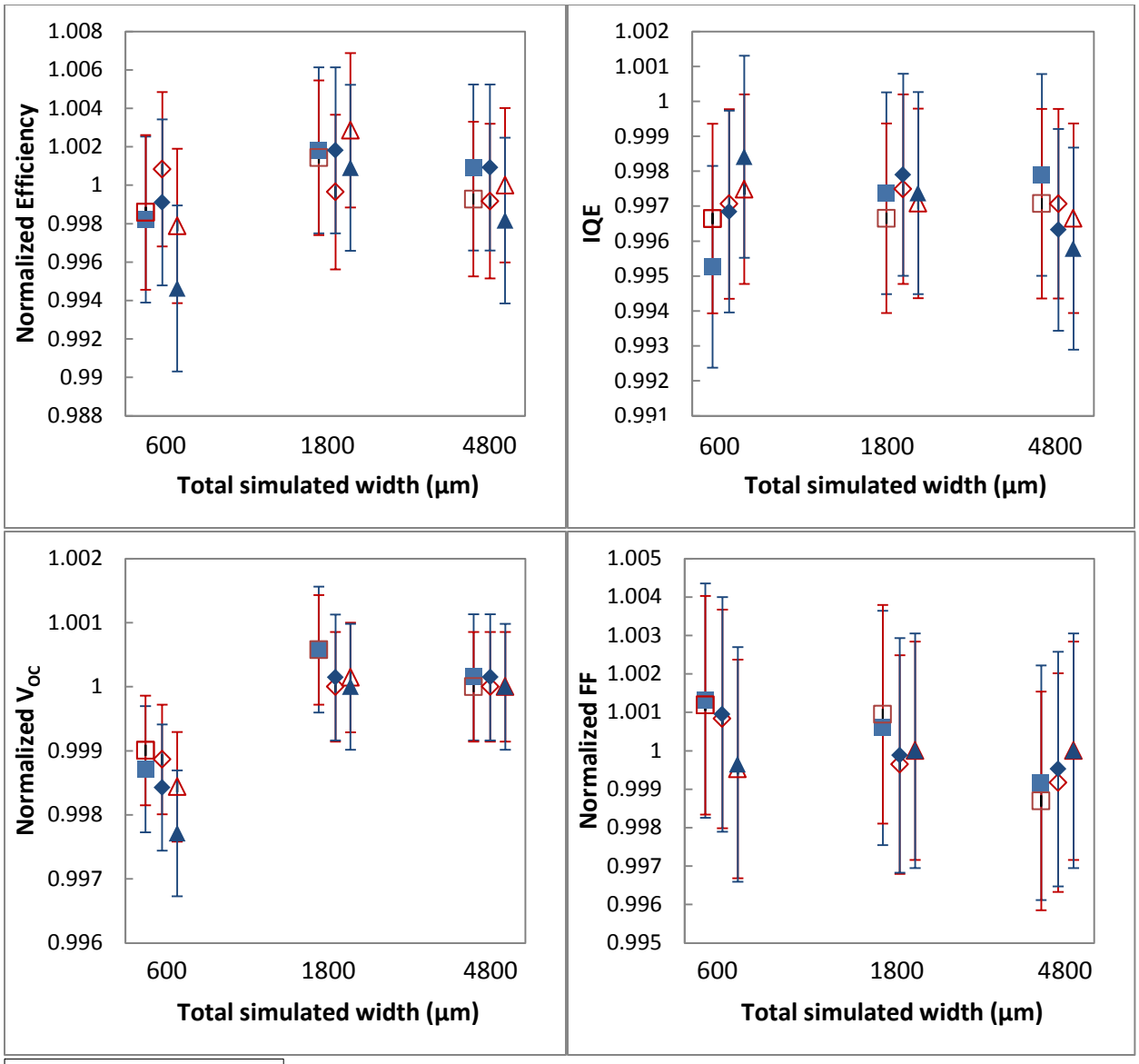

Figure 4.2: Spatial uniformity has little impact on Si PERT device performance Simulated performance metrics, efficiency (top left), V_{OC} (top right), *IQE* (lower left), and *FF* (lower right) plotted *vs.* simulation width. The data series for each width is the *NMWHT*, varying from 0.007 to 0.442. Spectra with two fidelities, 50% and 100% were simulated.

4.2 Spatial Uniformity Discussion

While the lack of impact of spatial variation may seem counter-intuitive, it does not contradict the existing literature. To begin with, most studies of non-uniform light intensity have been carried out for concentrating systems (systems where the light intensity is greater than 1 sun) and often for stacked MJ devices [50]–[53]. This thesis deals with non-concentrating optics and two-terminal tandem cells, so many of the loss mechanisms described in the literature, like resistive effects, will be lessened, and some, like local current mismatches and increased resistivity of tunnel junctions, will be totally absent. Furthermore, local temperature differences due to varying intensity were neglected, so the known deleterious effects of increased temperature were also neglected. Some of the losses described in the literature are due to current flow through the contact. That is, voltage is increased toward open-circuit conditions, current actually flows through the contact metallization grid from areas of higher illumination intensity to areas of lower illumination intensity. In the 2-D structures modeled in this thesis, regions of high and low intensity were not connected by low-resistivity metals, so the barrier to this type of current flow was significantly higher.

While it might be expected that carriers would have trouble redistributing themselves beyond the bulk minority-carrier diffusion length (~1600 μm in the Si devices simulated), it has been observed that provided the emitter is fairly conductive, it offers a much more efficient conduction path enabling transport over much longer distances [52]. As shown in Figure 4.3, lateral current flow near open circuit conditions that redistributes carriers from regions of high illumination intensity to regions of low illumination intensity was concentrated in the emitter, where, as mentioned above, transport lengths much longer than the bulk minority carrier diffusion length are possible. This redistribution current requires a lateral voltage drop in the device, which will have a negative impact on device performance (for example, by locally lowering V_{OC}). However, since relatively little current redistribution is required for a non-concentrating cell, it is logical that the power loss due to this redistribution would also be small. The importance of low sheet resistance to allow lateral current flow in situations with non-uniform illumination has long been established, even for non-concentrating solar cells [54], [55].

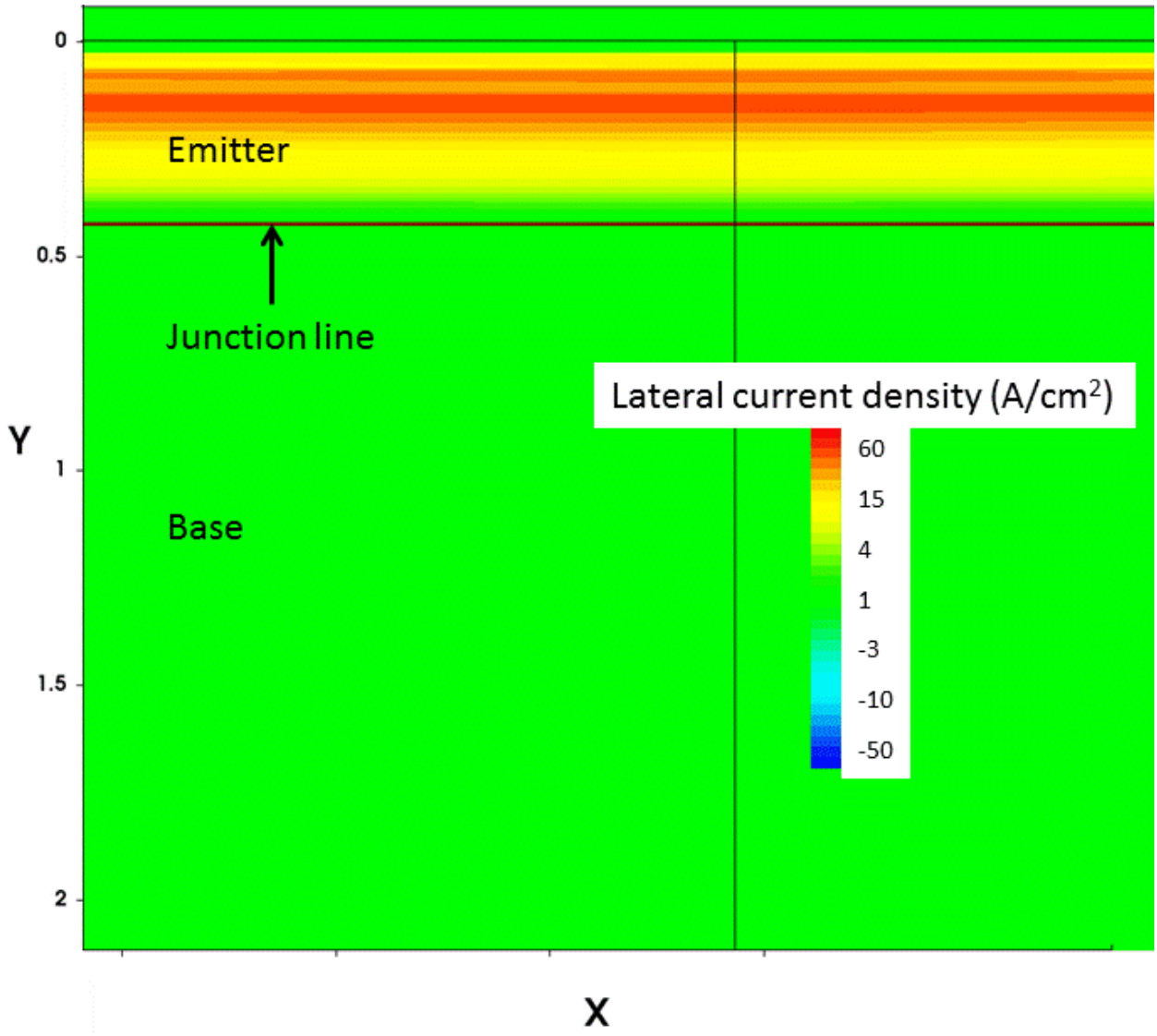

Figure 4.3: Lateral current flow concentrated in the emitter of an unevenly illuminated device

Lateral current flow is one to two orders of magnitude higher in the emitter of a standard diffused junction solar cell under an illumination profile with 100% low-energy spectral band fidelity and a *NMWHT* of 0.007. This region is representative of the majority of the device. The junction line indicates the transition from net *n*-type to net *p*-type doping.

The hypothesis that high emitter conductivity was eliminating effects of spatial inhomogeneity was tested by increasing the emitter sheet resistance in the 600 μm-wide standard diffused junction Si device simulation. In order to see the effect, the emitter doping concentration had to be reduced by several orders of magnitude. The peak emitter doping concentration in the original simulation was 6×10^{19} cm^{-3}. For the high sheet resistance simulations, it was varied from

5×10^{16} to 1×10^{19} cm^{-3}. The depth of the emitter doping, was also reduced. A Gaussian profile was used in both cases. For the original simulation the characteristic length of the Gaussian was 150 nm, while for the high sheet resistance simulations, it was 100 nm. To maintain a reasonable V_{OC}, the base doping concentration was reduced from 2×10^{16} to 5×10^{15} cm^{-3}. For a peak doping concentration of 1×10^{19} cm^{-3}, this device had a simulated efficiency under uniform illumination of 11.5% with a J_{SC} of 21.43 mA/cm^2, V_{OC} of 0.651 V, and *FF* of 82.1%.

The effect of sheet resistance on efficiency, *IQE*, V_{OC}, and *FF* for the modified device under illumination by a perfectly split spectrum (fidelity = 100% in both spectral bands) with a *NMWHT* of 0.007 are shown in Figure 4.4. These results are qualitatively similar to those observed under concentrated light by García *et al.* [52]. As they noted, the spike in *FF* is an artifact of the sudden decrease in *IQE* at low sheet resistance, since J_{SC} appears in the denominator of the definition of *FF*. A reduction in efficiency of about 1% (relative) was observed for an emitter doping concentration of 1×10^{19} cm^{-3}. This corresponds to a sheet resistance of 494 Ω/sq, compared with 87 Ω/sq for the original simulation. Thus, the lack of sensitivity in the more realistic devices is considered the more important result.

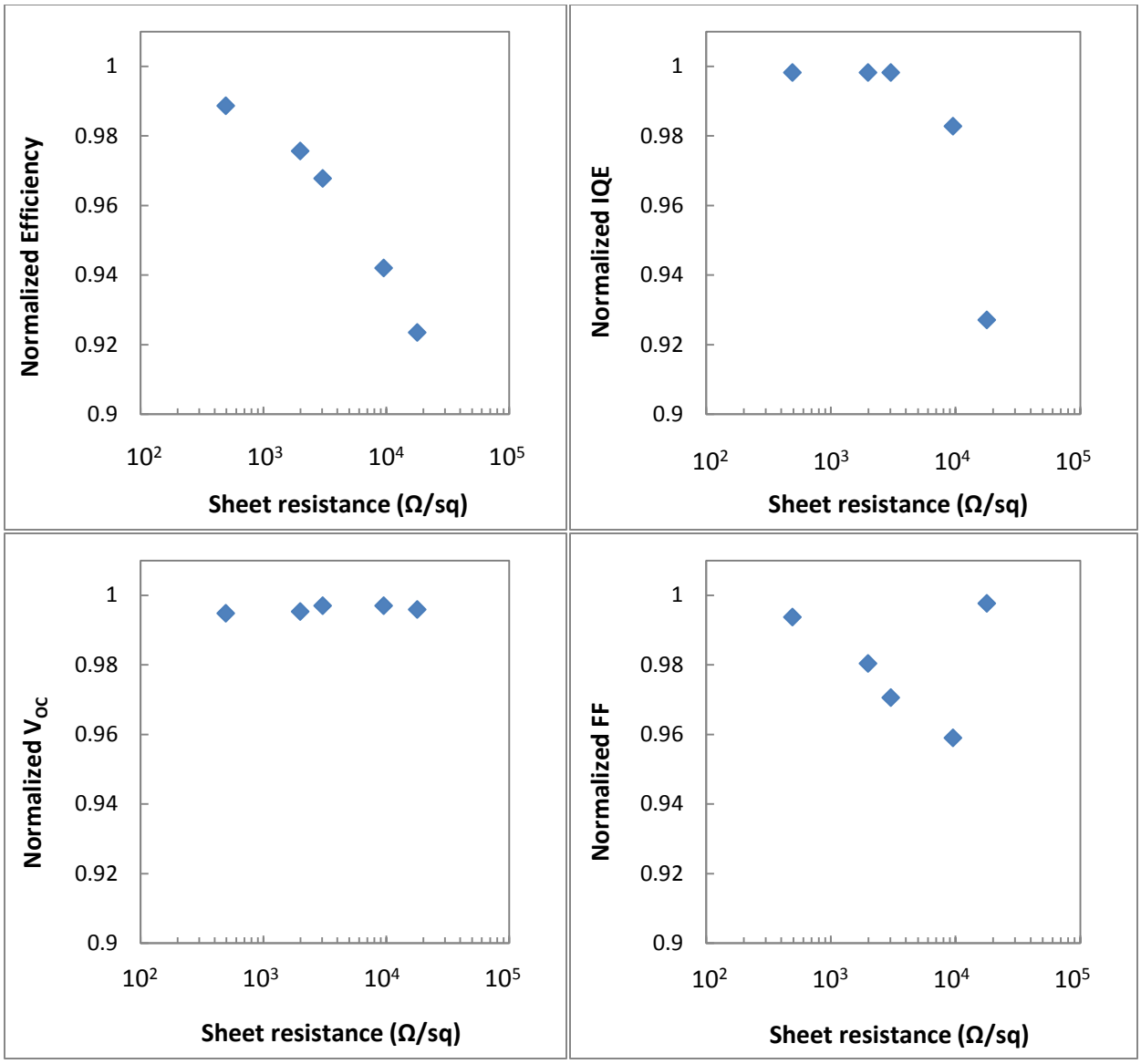

Figure 4.4: Devices with high-resistance emitters are sensitive to spatial variation of light intensity

Device performance for a 600 μm-wide diffused junction Si cell with modified doping profiles under illumination with a split solar spectrum with fidelity=100% in both spectral bands and *NMWHT* of 0.007 plotted *vs.* emitter sheet resistance. Values of the performance metrics for the *NMWHT* = 0.007 are normalized to the values for the same device architecture under uniform illumination with the same perfectly split solar spectrum.

CHAPTER

5

CONCLUSIONS

A sensitivity-analysis approach to identifying important optical parameters for spectral splitting PV systems was presented. A tandem structure employing 1-D light manipulation and a combination of Si and Cu_2O absorbers was presented. Two optical parameters were considered: the fidelity, or fraction of photons that arrived at the desired material, and the spatial uniformity of the incident light intensity as characterized by the normalized minimum width half total, which was the minimum width over which intensity could be integrated to yield half the total incident power.

Variation in fidelity was found to have a significant impact on device performance, particularly the fidelity of the low-energy spectral band. The dominance of the low-energy spectral band fidelity was increased when the wide-gap material had higher efficiency than the narrow-gap material but was primarily due to the fact that high-energy photons directed to the narrow-gap material were still absorbed, while low-energy photons directed toward the wide-gap material were lost entirely.

Spatial uniformity was found to have little effect on device performance. While somewhat counter-intuitive, this result is explained by the low concentration of light in the simulations and the high emitter conductivity, which allowed carrier redistribution through lateral current flow with minimal voltage losses. However, several potential loss mechanisms, including increased heating of highly illuminated areas and front metallization grid resistance effects were neglected. Future work could examine these effects as well as considering system performance under concentration.

This type of analysis can be applied to any spectral splitting scheme, incorporating any optics and any combination of absorber materials. Determining the important optical properties through simulation can improve the rate of progress for spectral splitting PV systems by focusing efforts on the most important areas. Additionally, as the spatial uniformity analysis demonstrated, the

important relationships between optical properties and device properties must also be understood and can be established through simulation as well. Using simulations to make these determinations can improve the speed of research progress, allow access to parts of the parameter-space not yet experimentally accessible, and decouple the properties of interest from experimental error and fabrication issues.

REFERENCES

[1] O. Morton, "Solar energy: A new day dawning?: Silicon Valley sunrise," *Nature*, vol. 443, no. 7107, pp. 19–22, Sep. 2006.

[2] M. D. Kempe, "Ultraviolet light test and evaluation methods for encapsulants of photovoltaic modules," *Solar Energy Materials and Solar Cells*, vol. 94, no. 2, pp. 246–253, Feb. 2010.

[3] W. Hoffmann, "PV solar electricity industry: Market growth and perspective," *Solar Energy Materials and Solar Cells*, vol. 90, no. 18–19, pp. 3285–3311, Nov. 2006.

[4] P. Mints, "Solar PV Profit's Last Stand," *Renewable Energy World*, 20-Mar-2013. [Online]. Available: http://www.renewableenergyworld.com/rea/news/article/2013/03/solar-pv-profits-last-stand. [Accessed: 25-Mar-2014].

[5] D. M. Powell, M. T. Winkler, H. J. Choi, C. B. Simmons, D. B. Needleman, and T. Buonassisi, "Crystalline silicon photovoltaics: a cost analysis framework for determining technology pathways to reach baseload electricity costs," *Energy Environ. Sci.*, vol. 5, no. 3, pp. 5874–5883, Mar. 2012.

[6] W. Shockley and H. J. Queisser, "Detailed Balance Limit of Efficiency of p-n Junction Solar Cells," *Journal of Applied Physics*, vol. 32, no. 3, p. 510, 1961.

[7] M. A. Green, "Limiting photovoltaic efficiency under new ASTM International G173-based reference spectra: Efficiency limits under ASTM G173," *Progress in Photovoltaics: Research and Applications*, vol. 20, no. 8, pp. 954–959, 2011.

[8] C. H. Henry, "Limiting efficiencies of ideal single and multiple energy gap terrestrial solar cells," *Journal of Applied Physics*, vol. 51, no. 8, p. 4494, 1980.

[9] S. Kurtz and J. Geisz, "Multijunction solar cells for conversion of concentrated sunlight to electricity," *Opt. Express*, vol. 18, no. S1, pp. A73–A78, Apr. 2010.

[10] R. R. King, D. Bhusari, D. Larrabee, X.-Q. Liu, E. Rehder, K. Edmondson, H. Cotal, R. K. Jones, J. H. Ermer, C. M. Fetzer, D. C. Law, and N. H. Karam, "Solar cell generations over 40% efficiency," *Prog. Photovolt: Res. Appl.*, vol. 20, no. 6, pp. 801–815, Sep. 2012.

[11] A. Feltrin and A. Freundlich, "Material considerations for terawatt level deployment of photovoltaics," *Renewable Energy*, vol. 33, no. 2, pp. 180–185, Feb. 2008.

[12] M. A. Green, K. Emery, Y. Hishikawa, W. Warta, and E. D. Dunlop, "Solar cell efficiency tables (version 43)," *Prog. Photovolt: Res. Appl.*, vol. 22, no. 1, pp. 1–9, Jan. 2014.

[13] A. Mojiri, R. Taylor, E. Thomsen, and G. Rosengarten, "Spectral beam splitting for efficient conversion of solar energy—A review," *Renewable and Sustainable Energy Reviews*, vol. 28, pp. 654–663, Dec. 2013.

[14] H. A. Atwater, M. D. Escarra, C. N. Eisler, E. D. Kosten, E. C. Warmann, S. Darbe, J. Lloyd, and C. Flowers, "Full spectrum ultrahigh efficiency photovoltaics," in *Photovoltaic Specialists Conference (PVSC), 2013 IEEE 39th*, 2013, pp. 1631–1634.

[15] B. Mitchell, G. Peharz, G. Siefer, M. Peters, T. Gandy, J. C. Goldschmidt, J. Benick, S. W. Glunz, A. W. Bett, and F. Dimroth, "Four-junction spectral beam-splitting photovoltaic receiver with high optical efficiency," *Progress in Photovoltaics: Research and Applications*, vol. 19, no. 1, pp. 61–72, Jan. 2011.

[16] A. G. Imenes and D. R. Mills, "Spectral beam splitting technology for increased conversion efficiency in solar concentrating systems: a review," *Solar Energy Materials and Solar Cells*, vol. 84, no. 1–4, pp. 19–69, Oct. 2004.

[17] Trivich, D. and Flinn, P.A., "Maximum efficiency of solar energy conversion by quantum processes," in *Solar Energy Research*, Daniels, F. and Duffie, J., Eds. Madison: University of Wisconsin Press, 1955, p. 143.
[18] Jackson, E.D., in *Transaction of Conference on use of Solar Energy*, Tuscon, AZ, 1958, vol. 5, pp. 122–126.
[19] N. S. Alvi, C. E. Backus, and G. W. Masden, "The potential for increasing the efficiency of photovoltaic systems by using multiple cell concepts," in *Proceedings of the 12th IEEE Photovoltaic Specialists Conference*, Baton Rouge, LA, 1976, pp. 948–956.
[20] G. W. Masden and C. E. Backus, "Increased photovoltaic conversion efficiency through use of spectrum splitting and multiple cells," in *Proceedings of the 13th IEEE Photovoltaic Specialists Conference*, Washington, DC, 1978, pp. 853–858.
[21] R. L. Moon, L. W. James, H. A. Vander Plas, T. O. Yep, G. A. Antypas, and Y. Chai, "Multigap solar cell requirements and the performance of AlGaAs and Si cells in concentrated sunlight," in *Proceedings of the 13th IEEE Photovoltaic Specialists Conference*, Washington, DC, 1978, pp. 859–867.
[22] J. A. Cape, J. S. Harris, and R. Sahai, "Spectrally split tandem cell converter studies," in *Proceedings of the 13th IEEE Photovoltaic Specialists Conference*, Washington, DC, 1978, pp. 881–885.
[23] P. G. Borden, P. E. Gregory, O. E. Moore, H. Vander Plas, and L. W. James, "A 10-unit dichroic filter spectral splitter module," in *Proceedings of the 15th IEEE Photovoltaic Specialists Conference*, Kissimmee, FL, 1981, pp. 311–316.
[24] L. Fraas, J. Avery, H. Huang, L. Minkin, and E. Shifman, "Demonstration of a 33% Efficient Cassegrainian Solar Module," in *Conference Record of the 2006 IEEE 4th World Conference on Photovoltaic Energy Conversion*, 2006, vol. 1, pp. 679–682.
[25] J. H. Karp and J. E. Ford, "Multiband solar concentrator using transmissive dichroic beamsplitting," 2008, vol. 7043, p. 70430F–70430F–8.
[26] A. Barnett, D. Kirkpatrick, C. Honsberg, D. Moore, M. Wanlass, K. Emery, R. Schwartz, D. Carlson, S. Bowden, D. Aiken, A. Gray, S. Kurtz, L. Kazmerski, M. Steiner, J. Gray, T. Davenport, R. Buelow, L. Takacs, N. Shatz, J. Bortz, O. Jani, K. Goossen, F. Kiamilev, A. Doolittle, I. Ferguson, B. Unger, G. Schmidt, E. Christensen, and D. Salzman, "Very high efficiency solar cell modules," *Progress in Photovoltaics: Research and Applications*, vol. 17, no. 1, pp. 75–83, Jan. 2009.
[27] M. A. Green and A. Ho-Baillie, "Forty three per cent composite split-spectrum concentrator solar cell efficiency," *Progress in Photovoltaics: Research and Applications*, vol. 18, no. 1, pp. 42–47, Jan. 2010.
[28] J. C. Goldschmidt, C. Do, M. Peters, and A. Goetzberger, "Spectral splitting module geometry that utilizes light trapping," *Solar Energy Materials and Solar Cells*, vol. 108, pp. 57–64, Jan. 2013.
[29] R. Zekun, "Private communication," 2014.
[30] J. M. Russo, D. Zhang, M. Gordon, S. Vorndran, Y. Wu, and R. K. Kostuk, "Spectrum splitting metrics and effect of filter characteristics on photovoltaic system performance," *Optics Express*, vol. 22, no. S2, p. A528, Mar. 2014.
[31] ITRPV Working Group, "International Technology Roadmap for Photovoltaic (ITRPV): 2013 Results, Revision 1," SEMI PV Group, Mar. 2014.
[32] D. D. Smith, P. J. Cousins, A. Masad, S. Westerberg, M. Defensor, R. Ilaw, T. Dennis, R. Daquin, N. Bergstrom, A. Leygo, X. Zhu, B. Meyers, B. Bourne, M. Shields, and D. Rose,

"SunPower's Maxeon Gen III solar cell: High efficiency and energy yield," in *Photovoltaic Specialists Conference (PVSC), 2013 IEEE 39th*, 2013, pp. 0908–0913.

[33] M. Taguchi, A. Yano, S. Tohoda, K. Matsuyama, Y. Nakamura, T. Nishiwaki, K. Fujita, and E. Maruyama, "24.7% Record Efficiency HIT Solar Cell on Thin Silicon Wafer," *IEEE Journal of Photovoltaics*, vol. 4, no. 1, pp. 96–99, Jan. 2014.

[34] T. Minami, Y. Nishi, and T. Miyata, "High-Efficiency Cu_2O-Based Heterojunction Solar Cells Fabricated Using a Ga_2O_3 Thin Film as N-Type Layer," *Applied Physics Express*, vol. 6, no. 4, p. 044101, Apr. 2013.

[35] J. Zhao, A. Wang, and M. A. Green, "24·5% Efficiency silicon PERT cells on MCZ substrates and 24·7% efficiency PERL cells on FZ substrates," *Prog. Photovolt: Res. Appl.*, vol. 7, no. 6, pp. 471–474, Nov. 1999.

[36] J. Zhao, A. Wang, and M. A. Green, "24.5% efficiency PERT silicon solar cells on SEH MCZ substrates and cell performance on other SEH CZ and FZ substrates," *Solar Energy Materials and Solar Cells*, vol. 66, no. 1–4, pp. 27–36, Feb. 2001.

[37] J. Zhao, A. Wang, and M. A. Green, "High-efficiency PERL and PERT silicon solar cells on FZ and MCZ substrates," *Solar Energy Materials and Solar Cells*, vol. 65, no. 1–4, pp. 429–435, Jan. 2001.

[38] Siah, Sin Cheng, Lloyd, Michael, Johnston, Steven, Brandt, Riley, Lee, Yun Seog, and Buonassisi, Tonio, "Achieving a High 10 μs μ-PCD Carrier Lifetime in Cuprous Oxide (Cu2O) by Bulk Defect Engineering," presented at the MRS Spring Meeting, San Francisco, CA, 2014.

[39] M. Burgelman, P. Nollet, and S. Degrave, "Modelling polycrystalline semiconductor solar cells," *Thin Solid Films*, vol. 361–362, pp. 527–532, Feb. 2000.

[40] C. Wadia, A. P. Alivisatos, and D. M. Kammen, "Materials Availability Expands the Opportunity for Large-Scale Photovoltaics Deployment," *Environ. Sci. Technol.*, vol. 43, no. 6, pp. 2072–2077, Mar. 2009.

[41] Y. S. Lee, M. Bertoni, M. K. Chan, G. Ceder, and T. Buonassisi, "Earth abundant materials for high efficiency heterojunction thin film solar cells," in *2009 34th IEEE Photovoltaic Specialists Conference (PVSC)*, 2009, pp. 002375–002377.

[42] K. P. Musselman, Y. Ievskaya, and J. L. MacManus-Driscoll, "Modelling charge transport lengths in heterojunction solar cells," *Applied Physics Letters*, vol. 101, no. 25, p. 253503, 2012.

[43] Y. S. Lee, M. T. Winkler, S. Cheng Siah, R. Brandt, and T. Buonassisi, "High-mobility copper (I) oxide thin films prepared by reactive dc magnetron sputtering for photovoltaic applications," in *2011 37th IEEE Photovoltaic Specialists Conference (PVSC)*, 2011, pp. 000250–000251.

[44] Y. S. Lee, M. T. Winkler, S. Cheng Siah, R. Brandt, and T. Buonassisi, "Growth and p-type doping of cuprous oxide thin-films for photovoltaic applications," in *2012 38th IEEE Photovoltaic Specialists Conference (PVSC)*, 2012, pp. 002557–002558.

[45] S. C. Siah, Y. S. Lee, Y. Segal, and T. Buonassisi, "Low contact resistivity of metals on nitrogen-doped cuprous oxide (Cu2O) thin-films," *Journal of Applied Physics*, vol. 112, no. 8, p. 084508, Oct. 2012.

[46] G. Kim, J. A. Dominguez-Caballero, H. Lee, D. J. Friedman, and R. Menon, "Increased Photovoltaic Power Output via Diffractive Spectrum Separation," *Phys. Rev. Lett.*, vol. 110, no. 12, p. 123901, Mar. 2013.

[47] “Solar Spectral Irradiance: Air Mass 1.5.” [Online]. Available: http://rredc.nrel.gov/solar/spectra/am1.5/. [Accessed: 28-Mar-2014].
[48] “Sentaurus Device User Guide,” Synopsys, Version H-2013.03, Mar. 2013.
[49] Y. S. Lee, J. Heo, S. C. Siah, J. P. Mailoa, R. E. Brandt, S. B. Kim, R. G. Gordon, and T. Buonassisi, “Ultrathin amorphous zinc-tin-oxide buffer layer for enhancing heterojunction interface quality in metal-oxide solar cells,” *Energy Environ. Sci.*, vol. 6, no. 7, pp. 2112–2118, Jun. 2013.
[50] E. Franklin and J. Coventry, “Effects of highly non-uniform illumination distribution on electrical performance of solar cells,” 2004.
[51] A. Luque and V. M. Andreev, *Concentrator photovoltaics*. Berlin: Springer, 2007.
[52] I. García, P. Espinet-González, I. Rey-Stolle, and C. Algora, “Analysis of Chromatic Aberration Effects in Triple-Junction Solar Cells Using Advanced Distributed Models,” *IEEE Journal of Photovoltaics*, vol. 1, no. 2, pp. 219–224, Oct. 2011.
[53] H. Baig, K. C. Heasman, and T. K. Mallick, “Non-uniform illumination in concentrating solar cells,” *Renewable and Sustainable Energy Reviews*, vol. 16, no. 8, pp. 5890–5909, Oct. 2012.
[54] A. Cuevas and S. López-Romero, “The combined effect of non-uniform illumination and series resistance on the open-circuit voltage of solar cells,” *Solar Cells*, vol. 11, no. 2, pp. 163–173, Mar. 1984.
[55] A. Vishnoi, R. Gopal, R. Dwivedi, and S. K. Srivastava, “Combined effect of non-uniform illumination and surface resistance on the performance of a solar cell,” *International Journal of Electronics*, vol. 66, no. 5, pp. 755–774, 1989.

APPENDICES

Appendix A.1 Matlab Spectrum Splitting Script: Uniform

```
% Create split spectrum files for tandem devices in Sentaurus
clear all;close all;

% Define constants and spectrum properties
c = 2.998e8;   % [m/s] speed of light
h = 6.626e-34;   % [J s] Planck's constant
highGap = 2.0;  % [eV] Bandgap of wide-gap material (target energy of split)

% Initialize Fidelity output matrices
fidelityHighReal=zeros(6);
fidelityLowReal=zeros(6);
fidelityError=zeros(6);

for i=5:9
    for j=5:9

fidelityHigh = .1 .* i + 0.05;  % Fraction of high-energy photons that go to
wide-gap material
fidelityLow = .1 .* j + 0.05;   % Fraction of low-energy photons that go to
narrow-gap material

% Import solar spectrum and split between high and low BG materials
am15gFull = xlsread('SolarSpectra','Sheet3'); % import AM1.5G spectrum
[wavelength(nm), SpecPowDensity(W/m^2/nm)]
splitnm = zeros(size(am15gFull,1),3); % initialize matrix of split spectrum
splitnm(:,1) = am15gFull(:,1);    % [nm] assign wavelength values to first
column
splitnm(:,2) = (am15gFull(:,1)<=(1240./highGap)).*am15gFull(:,2).*1e-4; %
[W/cm^2/um] spectral power density above wide gap in column 2
splitnm(:,3) = (am15gFull(:,1)>(1240./highGap)).*am15gFull(:,2).*1e-4; %
[W/cm^2/um] below gap photons

% generate power/area curves rather than power/area/nm curves for Sentaurus
lambda = transpose(280:1:4000);   % [nm] wavelength range with even spacing
(1nm increments)
split = zeros(length(lambda),3);
split(:,1) = lambda.*1e-3;    % [um]
am15g(:,1) = lambda.*1e-3;  % [um]
splitRespace(:,1) = lambda; % [nm]
splitRespace(:,2) = interp1(splitnm(:,1),splitnm(:,2),lambda);    %
interpolated to even 1nm spacing
splitRespace(:,3) = interp1(splitnm(:,1),splitnm(:,3),lambda);
am15gRespace(:,1) = lambda; % [nm]
am15gRespace(:,2) = interp1(am15gFull(:,1),am15gFull(:,2),lambda);
split(1,2) = splitRespace(1,2)*(splitRespace(2,1)-splitRespace(1,1));
split(1,3) = splitRespace(1,3)*(splitRespace(2,1)-splitRespace(1,1));
am15g(1,2) = am15gRespace(1,2)*(am15gRespace(2,1)-am15gRespace(1,1)).*1e-4;
```

```
for k = 2:length(splitRespace);
    split(k,2) = trapz(splitRespace((k-1):k,1),splitRespace((k-1):k,2));
    split(k,3) = trapz(splitRespace((k-1):k,1),splitRespace((k-1):k,3));
    am15g(k,2) = trapz(am15gRespace((k-1):k,1),am15gRespace((k-1):k,2)).*1e-
4;
end

% Send photons to the wrong place as specified by fidelity values using
% Gaussian dropoff from high and low ends of spectrum
splitPhotons = [split(:,1) split(:,2)./(c.*h./split(:,1))
split(:,3)./(c.*h./split(:,1))];  % split spectra in [photons/cm^2/s]
am15gPhotons = [am15g(:,1) am15g(:,2)./(c.*h./am15g(:,1))]; % solar spectrum
in photons/cm^2/s
% function for fitting with Gaussian dropoff from lamdba=0
gaussianFit = @(a) ...
    [trapz(splitPhotons(:,1),exp(-(splitPhotons(:,1)-
a(2)).^2./a(1)).*splitPhotons(:,2)) -
fidelityHigh.*trapz(splitPhotons(:,1),splitPhotons(:,2)),...
    trapz(splitPhotons(:,1),(1-exp(-(splitPhotons(:,1)-
a(2)).^2./a(1))).*splitPhotons(:,3)) -
fidelityLow.*trapz(splitPhotons(:,1),splitPhotons(:,3))];
a0 = [1 0.5];
fit = lsqnonlin(gaussianFit,a0,0,[],optimset('TolX',1e-7,'TolFun',1e-7));
correctHigh = splitPhotons(:,2).*exp(-(splitPhotons(:,1)-fit(2)).^2./fit(1));
correctLow = splitPhotons(:,3).*(1-exp(-(splitPhotons(:,1)-
fit(2)).^2./fit(1)));
splitPhotonsAdjusted = [splitPhotons(:,1) exp(-(splitPhotons(:,1)-
fit(2)).^2./fit(1)).*am15gPhotons(:,2) (1-exp(-(splitPhotons(:,1)-
fit(2)).^2./fit(1))).*am15gPhotons(:,2)];

% Check real fidelity
fidelityHighReal(i-4,j-4) =
trapz(splitPhotons(:,1),correctHigh)/trapz(splitPhotons(:,1),splitPhotons(:,2
));
fidelityLowReal(i-4,j-4) =
trapz(splitPhotons(:,1),correctLow)/trapz(splitPhotons(:,1),splitPhotons(:,3)
);
fidelityError(i-4,j-4) = abs(fidelityHighReal(i-4,j-4)-
fidelityHigh)+abs(fidelityLowReal(i-4,j-4)-fidelityLow);

% Convert spectra back into power from photons
splitAdjusted = [splitPhotonsAdjusted(:,1)
splitPhotonsAdjusted(:,2).*(c.*h./splitPhotonsAdjusted(:,1))
splitPhotonsAdjusted(:,3).*(c.*h./splitPhotonsAdjusted(:,1))];

% write Sentaurus spectrum files
fileHigh =
fopen(strcat('splitSpectrumSentaurus',num2str(i),num2str(j),'High','.txt'),'w
');
fprintf(fileHigh,strcat('# High Split: Fidelity=',num2str(fidelityHighReal(i-
4,j-4)),'\r\n','Optics/Excitation/Wavelength [um] intensity [W*cm^-2]\r\n'));
dlmwrite(strcat('splitSpectrumSentaurus',num2str(i),num2str(j),'High','.txt')
,[splitAdjusted(:,1) splitAdjusted(:,2)],'delimiter',' ','newline','pc','-
append');
fclose(fileHigh);
```

```
fileLow =
fopen(strcat('splitSpectrumSentaurus',num2str(i),num2str(j),'Low','.txt'),'w'
);
fprintf(fileLow,strcat('# Low Split: Fidelity=',num2str(fidelityLowReal(i-
4,j-4)),'\r\n','Optics/Excitation/Wavelength [um] intensity [W*cm^-2]\r\n'));
dlmwrite(strcat('splitSpectrumSentaurus',num2str(i),num2str(j),'Low','.txt'),
[splitAdjusted(:,1) splitAdjusted(:,3)],'delimiter',' ','newline','pc','-
append');
fclose(fileLow);

    end
end
```

Appendix A.2 Matlab Splitting Script: Spatially Varying

```
% Create split spectrum files for tandem devices in Sentaurus
clear all;close all;

% Define constants and spectrum properties
c = 2.998e8;   % [m/s] speed of light
h = 6.626e-34;   % [J s] Planck's constant
highGap = 1.9;  % [eV] Bandgap of wide-gap material (target energy of split)

% Initialize Fidelity output matrices
fidelityHighReal=zeros(6);
fidelityLowReal=zeros(6);
fidelityError=zeros(6);

for i=5:9
%     for j=5:9

fidelityHigh = .1 .* i;  % Fraction of high-energy photons that go to wide-
gap material
fidelityLow = .1 .* i;   % Fraction of low-energy photons that go to narrow-
gap material

% Import solar spectrum and split between high and low BG materials
am15gFull = xlsread('SolarSpectra','Sheet3'); % import AM1.5G spectrum
[wavelength(nm), SpecPowDensity(W/m^2/nm)]
splitnm = zeros(size(am15gFull,1),3); % initialize matrix of split spectrum
splitnm(:,1) = am15gFull(:,1);    % [nm] assign wavelength values to first
column
splitnm(:,2) = (am15gFull(:,1)<=(1240./highGap)).*am15gFull(:,2).*1e-4; %
[W/cm^2/um] spectral power density above wide gap in column 2
splitnm(:,3) = (am15gFull(:,1)>(1240./highGap)).*am15gFull(:,2).*1e-4; %
[W/cm^2/um] below gap photons

% generate power/area curves rather than power/area/nm curves for Sentaurus
lambda = transpose(280:1:4000);   % [nm] wavelength range with even spacing
(1nm increments)
split = zeros(length(lambda),3);
split(:,1) = lambda.*1e-3;    % [um]
am15g(:,1) = lambda.*1e-3;  % [um]
splitRespace(:,1) = lambda; % [nm]
splitRespace(:,2) = interp1(splitnm(:,1),splitnm(:,2),lambda);    %
interpolated to even 1nm spacing
splitRespace(:,3) = interp1(splitnm(:,1),splitnm(:,3),lambda);
am15gRespace(:,1) = lambda; % [nm]
am15gRespace(:,2) = interp1(am15gFull(:,1),am15gFull(:,2),lambda);
split(1,2) = splitRespace(1,2)*(splitRespace(2,1)-splitRespace(1,1));
split(1,3) = splitRespace(1,3)*(splitRespace(2,1)-splitRespace(1,1));
am15g(1,2) = am15gRespace(1,2)*(am15gRespace(2,1)-am15gRespace(1,1)).*1e-4;
for k = 2:length(splitRespace);
    split(k,2) = trapz(splitRespace((k-1):k,1),splitRespace((k-1):k,2));
    split(k,3) = trapz(splitRespace((k-1):k,1),splitRespace((k-1):k,3));
    am15g(k,2) = trapz(am15gRespace((k-1):k,1),am15gRespace((k-1):k,2)).*1e-
4;
```

```
end

% Send photons to the wrong place as specified by fidelity values using
% Gaussian dropoff from high and low ends of spectrum
splitPhotons = [split(:,1) split(:,2)./(c.*h./split(:,1))
split(:,3)./(c.*h./split(:,1))];  % split spectra in [photons/cm^2/s]
am15gPhotons = [am15g(:,1) am15g(:,2)./(c.*h./am15g(:,1))]; % solar spectrum
in photons/cm^2/s
% function for fitting with Gaussian dropoff from lamdba=0
gaussianFit = @(a) ...
    [trapz(splitPhotons(:,1),exp(-(splitPhotons(:,1)-
a(2)).^2./a(1)).*splitPhotons(:,2)) -
fidelityHigh.*trapz(splitPhotons(:,1),splitPhotons(:,2)),...
    trapz(splitPhotons(:,1),(1-exp(-(splitPhotons(:,1)-
a(2)).^2./a(1))).*splitPhotons(:,3)) -
fidelityLow.*trapz(splitPhotons(:,1),splitPhotons(:,3))];
a0 = [1 0.5];
fit = lsqnonlin(gaussianFit,a0,0,[],optimset('TolX',1e-7,'TolFun',1e-7));
correctHigh = splitPhotons(:,2).*exp(-(splitPhotons(:,1)-fit(2)).^2./fit(1));
correctLow = splitPhotons(:,3).*(1-exp(-(splitPhotons(:,1)-
fit(2)).^2./fit(1)));
splitPhotonsAdjusted = [splitPhotons(:,1) exp(-(splitPhotons(:,1)-
fit(2)).^2./fit(1)).*am15gPhotons(:,2) (1-exp(-(splitPhotons(:,1)-
fit(2)).^2./fit(1))).*am15gPhotons(:,2)];

% Check real fidelity
fidelityHighReal(i-4) =
trapz(splitPhotons(:,1),correctHigh)/trapz(splitPhotons(:,1),splitPhotons(:,2
));
fidelityLowReal(i-4) =
trapz(splitPhotons(:,1),correctLow)/trapz(splitPhotons(:,1),splitPhotons(:,3)
);
fidelityError(i-4) = abs(fidelityHighReal(i-4)-
fidelityHigh)+abs(fidelityLowReal(i-4)-fidelityLow);

% Convert spectra back into power from photons
splitAdjusted = [splitPhotonsAdjusted(:,1)
splitPhotonsAdjusted(:,2).*(c.*h./splitPhotonsAdjusted(:,1))
splitPhotonsAdjusted(:,3).*(c.*h./splitPhotonsAdjusted(:,1))];

% split spectrum spatially using a Gaussian profile
sigma = 70; % sigma of Gaussian profile
gaussian = normpdf(1:21,11,sigma);   % create Gaussian profile
gaussianNorm = length(gaussian)/sum(gaussian).*gaussian;    % Normalize
Gaussian profile, so total intensity is the same as flat spectrum
splitSpatialHigh = zeros(size(splitAdjusted,1),length(gaussianNorm)+1); %
initialize output spectra
splitSpatialLow = zeros(size(splitAdjusted,1),length(gaussianNorm)+1);
splitSpatialHigh(:,1) = splitAdjusted(:,1); % make first column of output
spectra wavelengths
splitSpatialLow(:,1) = splitAdjusted(:,1);
% create spatially varying spectra
for k=1:length(gaussianNorm)
    splitSpatialHigh(:,k+1) = gaussianNorm(k).*splitAdjusted(:,2);
    splitSpatialLow(:,k+1) = gaussianNorm(k).*splitAdjusted(:,3);
```

```
    % write Sentaurus spectrum files
    fileHigh =
fopen(strcat('splitSpectrumSentaurus',num2str(i),'HighSigma',num2str(sigma),'
Position',num2str(k),'.txt'),'w');
    fprintf(fileHigh,strcat('# High Split:
Fidelity=',num2str(fidelityHighReal(i-4)),',
Position=',num2str(k),'/',num2str(length(gaussian)),',
Sigma=',num2str(sigma),'\r\n','Optics/Excitation/Wavelength [um] intensity
[W*cm^-2]\r\n'));

dlmwrite(strcat('splitSpectrumSentaurus',num2str(i),'HighSigma',num2str(sigma
),'Position',num2str(k),'.txt'),[splitSpatialHigh(:,1)
splitSpatialHigh(:,k+1)],'delimiter',' ','newline','pc','-append');
    fclose(fileHigh);
    fileLow =
fopen(strcat('splitSpectrumSentaurus',num2str(i),'LowSigma',num2str(sigma),'P
osition',num2str(k),'.txt'),'w');
    fprintf(fileLow,strcat('# Low Split:
Fidelity=',num2str(fidelityLowReal(i-4)),',
Position=',num2str(k),'/',num2str(length(gaussian)),',
Sigma=',num2str(sigma),'\r\n','Optics/Excitation/Wavelength [um] intensity
[W*cm^-2]\r\n'));

dlmwrite(strcat('splitSpectrumSentaurus',num2str(i),'LowSigma',num2str(sigma)
,'Position',num2str(k),'.txt'),[splitSpatialLow(:,1)
splitSpatialLow(:,k+1)],'delimiter',' ','newline','pc','-append');
    fclose(fileLow);
end
%     end
end
```

Appendix A.3 Matlab FDTD Generation Rate Conversion

```
% Create split spectrum optical generation input files for Sentaurus from
optical
% modeling data
clear all; close all;

for fidelityHigh=5:9
    for fidelityLow=5:9
        clear gen x y
% Open file
load(strcat('C:\Users\David\Desktop\MIT\Synopsys Sentaurus\Cu2O\Cu2O
generation\Uniform
intensity\splitSpectrumSentaurus',num2str(fidelityHigh),num2str(fidelityLow),
'High.mat'));

% Flip generation and y-position data
genFlip=flipud(gen);
yflip=abs(flipud(y).*1e6);   % make y-positions positive to match SDE and
convert from [m] to [um]

% Flatten top surface by moving effects of texture to bottom
genFlat=zeros(size(genFlip));
for i=1:size(genFlip,2)

genFlat(1:length(genFlip(genFlip(:,i)~=0,i)),i)=genFlip(genFlip(:,i)~=0,i);
end

% Average over x-position
for i=1:size(genFlat,1)
    genFlatPrime(i)=mean(genFlat(i,:));
end

% Remove data points according to gradient of generation
genFlatPrimeSparse=genFlatPrime(1);     % assign value of first data point
ySparse=yflip(1);
count=0;                                % initialize counting variable

for i=2:length(genFlatPrime)
    dgen=genFlatPrime(i)-genFlatPrimeSparse(length(genFlatPrimeSparse));    %
difference of generation and last used generation
    dy=yflip(i)-ySparse(length(ySparse));                                   %
difference of y-position and last used y-position
    dgendy=abs(dgen./dy);                                                   %
slope from current position to last used position
    count=count+1;                                                          %
# points since last used position
    % add data point to vector if slope since last data point is > 10% of
    % total slope across absorber
    if dgendy>0.1.*abs((genFlatPrime(1)-
genFlatPrime(length(genFlatPrime))./(yflip(1)-
yflip(length(genFlatPrime))))||count==100;
        genFlatPrimeSparse=[genFlatPrimeSparse;genFlatPrime(i)];
        ySparse=[ySparse;yflip(i)];
```

```
        count=0;    % reset counter
    end
end

if abs(ySparse(length(ySparse))-3)>.0001
    genLast=genFlatPrimeSparse(length(genFlatPrimeSparse));
    gen2nd=genFlatPrimeSparse(length(genFlatPrimeSparse)-1);
    yLast=ySparse(length(ySparse));
    y2nd=ySparse(length(ySparse)-1);
    genFlatPrimeSparse=[genFlatPrimeSparse;genLast./exp((yLast-
3)*(log(gen2nd/genLast)/(y2nd-yLast)))];
    ySparse=[ySparse;3.000];
end

% Write OpticalGeneration.dat file
opticalFile =
fopen(strcat('OpticalGeneration',num2str(fidelityHigh),num2str(fidelityLow),'
.dat'),'w');
fprintf(opticalFile,'"OpticalGeneration"\r\n');
dlmwrite(strcat('OpticalGeneration',num2str(fidelityHigh),num2str(fidelityLow
),'.dat'),[ySparse genFlatPrimeSparse],'delimiter',' ','newline','pc','-
append');
fclose(opticalFile);

    end
end
```

Appendix B.1 Si parameter file

```
Bandgap {
    Eg0 = +1.1752165e+00  # n_i = 9.65e9 at 300 K (Altermatt PVSC Sapporo 1999)
    alpha = +4.73e-04
    beta = +6.36e+02
}

* Schenk model for band gap narrowing
TableBGN {
Acceptor  +1.0000000e+10  +000000000e+00      Acceptor  +3.1622777e+18  +4.0292000e-02
Acceptor  +1.0000000e+15  +1.4051583e-03      Acceptor  +3.7153523e+18  +4.2161341e-02
Acceptor  +1.1748976e+15  +1.5206727e-03      Acceptor  +4.3651583e+18  +4.4086607e-02
Acceptor  +1.3803843e+15  +1.6454732e-03      Acceptor  +5.1286138e+18  +4.6064873e-02
Acceptor  +1.6218101e+15  +1.7802713e-03      Acceptor  +6.0255959e+18  +4.8093417e-02
Acceptor  +1.9054607e+15  +1.9258276e-03      Acceptor  +7.0794578e+18  +5.0169411e-02
Acceptor  +2.2387211e+15  +2.0829536e-03      Acceptor  +8.3176377e+18  +5.2289550e-02
Acceptor  +2.6302680e+15  +2.2525147e-03      Acceptor  +9.7723722e+18  +5.4449713e-02
Acceptor  +3.0902954e+15  +2.4354322e-03      Acceptor  +1.1481536e+19  +5.6644789e-02
Acceptor  +3.6307805e+15  +2.6326857e-03      Acceptor  +1.3489629e+19  +5.8868845e-02
Acceptor  +4.2657952e+15  +2.8453154e-03      Acceptor  +1.5848932e+19  +6.1115840e-02
Acceptor  +5.0118723e+15  +3.0744238e-03      Acceptor  +1.8620871e+19  +6.3381069e-02
Acceptor  +5.8884366e+15  +3.3211775e-03      Acceptor  +2.1877616e+19  +6.5663281e-02
Acceptor  +6.9183097e+15  +3.5868093e-03      Acceptor  +2.5703958e+19  +6.7967054e-02
Acceptor  +8.1283052e+15  +3.8726185e-03      Acceptor  +3.0199517e+19  +7.0304467e-02
Acceptor  +9.5499259e+15  +4.1799729e-03      Acceptor  +3.5481339e+19  +7.2695032e-02
Acceptor  +1.1220185e+16  +4.5103084e-03      Acceptor  +4.1686938e+19  +7.5163362e-02
Acceptor  +1.3182567e+16  +4.8651296e-03      Acceptor  +4.8977882e+19  +7.7735212e-02
Acceptor  +1.5488166e+16  +5.2460092e-03      Acceptor  +5.7543994e+19  +8.0433422e-02
Acceptor  +1.8197009e+16  +5.6545873e-03      Acceptor  +6.7608298e+19  +8.3275258e-02
Acceptor  +2.1379621e+16  +6.0925695e-03      Acceptor  +7.9432823e+19  +8.6271728e-02
Acceptor  +2.5118864e+16  +6.5617248e-03      Acceptor  +9.3325430e+19  +8.9428500e-02
Acceptor  +2.9512092e+16  +7.0638822e-03      Acceptor  +1.0964782e+20  +9.2747564e-02
Acceptor  +3.4673685e+16  +7.6009265e-03      Acceptor  +1.2882496e+20  +9.6228912e-02
Acceptor  +4.0738028e+16  +8.1747919e-03      Acceptor  +1.5135612e+20  +9.9871838e-02
Acceptor  +4.7863009e+16  +8.7874538e-03      Acceptor  +1.7782794e+20  +1.0367577e-01
Acceptor  +5.6234133e+16  +9.4409168e-03      Acceptor  +2.0892961e+20  +1.0764072e-01
Acceptor  +6.6069345e+16  +1.0137196e-02      Acceptor  +2.4547089e+20  +1.1176740e-01
Acceptor  +7.7624712e+16  +1.0878292e-02      Acceptor  +2.8840315e+20  +1.1605729e-01
Acceptor  +9.1201084e+16  +1.1666151e-02      Acceptor  +3.3884416e+20  +1.2051250e-01
Acceptor  +1.0715193e+17  +1.2502602e-02      Acceptor  +3.9810717e+20  +1.2513568e-01
Acceptor  +1.2589254e+17  +1.3389274e-02      Acceptor  +4.6773514e+20  +1.2992990e-01
Acceptor  +1.4791084e+17  +1.4327467e-02      Acceptor  +5.4954087e+20  +1.3489856e-01
Acceptor  +1.7378008e+17  +1.5317973e-02      Acceptor  +6.4565423e+20  +1.4004528e-01
Acceptor  +2.0417379e+17  +1.6360844e-02      Acceptor  +7.5857758e+20  +1.4537385e-01
Acceptor  +2.3988329e+17  +1.7455116e-02      Acceptor  +8.9125094e+20  +1.5088819e-01
Acceptor  +2.8183829e+17  +1.8598517e-02      Acceptor  +1.0471285e+21  +1.5659232e-01
Acceptor  +3.3113112e+17  +1.9787260e-02      Acceptor  +1.2302688e+21  +1.6249042e-01
Acceptor  +3.8904514e+17  +2.1016072e-02      Acceptor  +1.4454398e+21  +1.6858680e-01
Acceptor  +4.5708819e+17  +2.2278648e-02      Acceptor  +1.6982437e+21  +1.7488602e-01
Acceptor  +5.3703180e+17  +2.3568704e-02      Acceptor  +1.9952623e+21  +1.8139296e-01
Acceptor  +6.3095734e+17  +2.4881569e-02      Acceptor  +2.3442288e+21  +1.8811299e-01
Acceptor  +7.4131024e+17  +2.6215946e-02      Acceptor  +2.7542287e+21  +1.9505213e-01
Acceptor  +8.7096359e+17  +2.7575083e-02      Acceptor  +3.2359366e+21  +2.0221722e-01
Acceptor  +1.0232930e+18  +2.8966616e-02      Acceptor  +3.8018940e+21  +2.0961622e-01
Acceptor  +1.2022644e+18  +3.0400895e-02      Acceptor  +4.4668359e+21  +2.1725839e-01
Acceptor  +1.4125375e+18  +3.1888388e-02      Acceptor  +5.2480746e+21  +2.2515463e-01
Acceptor  +1.6595869e+18  +3.3437288e-02      Acceptor  +6.1659500e+21  +2.3331769e-01
Acceptor  +1.9498446e+18  +3.5052217e-02      Acceptor  +7.2443596e+21  +2.4176248e-01
Acceptor  +2.2908677e+18  +3.6734250e-02      Acceptor  +8.5113804e+21  +2.5050626e-01
Acceptor  +2.6915348e+18  +3.8481835e-02      Acceptor  +1.0000000e+22  +2.5956885e-01
```

```
Donor     +1.0000000e+10  +000000000e+00      Donor     +3.7153523e+18  +4.6885363e-02
Donor     +1.0000000e+15  +1.4062347e-03      Donor     +4.3651583e+18  +4.8993682e-02
Donor     +1.1748976e+15  +1.5219386e-03      Donor     +5.1286138e+18  +5.1170056e-02
Donor     +1.3803843e+15  +1.6469623e-03      Donor     +6.0255959e+18  +5.3416736e-02
Donor     +1.6218101e+15  +1.7820231e-03      Donor     +7.0794578e+18  +5.5734777e-02
Donor     +1.9054607e+15  +1.9278886e-03      Donor     +8.3176377e+18  +5.8124085e-02
Donor     +2.2387211e+15  +2.0853788e-03      Donor     +9.7723722e+18  +6.0583432e-02
Donor     +2.6302680e+15  +2.2553687e-03      Donor     +1.1481536e+19  +6.3110525e-02
Donor     +3.0902954e+15  +2.4387915e-03      Donor     +1.3489629e+19  +6.5702249e-02
Donor     +3.6307805e+15  +2.6366404e-03      Donor     +1.5848932e+19  +6.8355268e-02
Donor     +4.2657952e+15  +2.8499720e-03      Donor     +1.8620871e+19  +7.1067129e-02
Donor     +5.0118723e+15  +3.0799081e-03      Donor     +2.1877616e+19  +7.3837903e-02
Donor     +5.8884366e+15  +3.3276384e-03      Donor     +2.5703958e+19  +7.6672069e-02
Donor     +6.9183097e+15  +3.5944230e-03      Donor     +3.0199517e+19  +7.9579985e-02
Donor     +8.1283052e+15  +3.8815942e-03      Donor     +3.5481339e+19  +8.2578090e-02
Donor     +9.5499259e+15  +4.1905585e-03      Donor     +4.1686938e+19  +8.5687344e-02
Donor     +1.1220185e+16  +4.5227991e-03      Donor     +4.8977882e+19  +8.8930252e-02
Donor     +1.3182567e+16  +4.8798772e-03      Donor     +5.7543994e+19  +9.2327600e-02
Donor     +1.5488166e+16  +5.2634341e-03      Donor     +6.7608298e+19  +9.5896151e-02
Donor     +1.8197009e+16  +5.6751936e-03      Donor     +7.9432823e+19  +9.9647875e-02
Donor     +2.1379621e+16  +6.1169637e-03      Donor     +9.3325430e+19  +1.0359053e-01
Donor     +2.5118864e+16  +6.5906400e-03      Donor     +1.0964782e+20  +1.0772892e-01
Donor     +2.9512092e+16  +7.0982093e-03      Donor     +1.2882496e+20  +1.1206626e-01
Donor     +3.4673685e+16  +7.6417546e-03      Donor     +1.5135612e+20  +1.1660522e-01
Donor     +4.0738028e+16  +8.2234619e-03      Donor     +1.7782794e+20  +1.2134866e-01
Donor     +4.7863009e+16  +8.8456296e-03      Donor     +2.0892961e+20  +1.2630001e-01
Donor     +5.6234133e+16  +9.5106804e-03      Donor     +2.4547089e+20  +1.3146340e-01
Donor     +6.6069345e+16  +1.0221177e-02      Donor     +2.8840315e+20  +1.3684371e-01
Donor     +7.7624712e+16  +1.0979842e-02      Donor     +3.3884416e+20  +1.4244647e-01
Donor     +9.1201084e+16  +1.1789578e-02      Donor     +3.9810717e+20  +1.4827781e-01
Donor     +1.0715193e+17  +1.2653491e-02      Donor     +4.6773514e+20  +1.5434434e-01
Donor     +1.2589254e+17  +1.3574911e-02      Donor     +5.4954087e+20  +1.6065310e-01
Donor     +1.4791084e+17  +1.4557386e-02      Donor     +6.4565423e+20  +1.6721147e-01
Donor     +1.7378008e+17  +1.5604661e-02      Donor     +7.5857758e+20  +1.7402714e-01
Donor     +2.0417379e+17  +1.6720575e-02      Donor     +8.9125094e+20  +1.8110807e-01
Donor     +2.3988329e+17  +1.7908875e-02      Donor     +1.0471285e+21  +1.8846250e-01
Donor     +2.8183829e+17  +1.9172870e-02      Donor     +1.2302688e+21  +1.9609897e-01
Donor     +3.3113112e+17  +2.0514899e-02      Donor     +1.4454398e+21  +2.0402636e-01
Donor     +3.8904514e+17  +2.1935611e-02      Donor     +1.6982437e+21  +2.1225397e-01
Donor     +4.5708819e+17  +2.3433144e-02      Donor     +1.9952623e+21  +2.2079164e-01
Donor     +5.3703180e+17  +2.5002439e-02      Donor     +2.3442288e+21  +2.2964992e-01
Donor     +6.3095734e+17  +2.6635059e-02      Donor     +2.7542287e+21  +2.3884018e-01
Donor     +7.4131024e+17  +2.8319882e-02      Donor     +3.2359366e+21  +2.4837493e-01
Donor     +8.7096359e+17  +3.0044811e-02      Donor     +3.8018940e+21  +2.5826799e-01
Donor     +1.0232930e+18  +3.1799142e-02      Donor     +4.4668359e+21  +2.6853482e-01
Donor     +1.2022644e+18  +3.3575801e-02      Donor     +5.2480746e+21  +2.7919283e-01
Donor     +1.4125375e+18  +3.5372605e-02      Donor     +6.1659500e+21  +2.9026166e-01
Donor     +1.6595869e+18  +3.7192170e-02      Donor     +7.2443596e+21  +3.0176349e-01
Donor     +1.9498446e+18  +3.9040695e-02      Donor     +8.5113804e+21  +3.1372335e-01
Donor     +2.2908677e+18  +4.0926272e-02      Donor     +1.0000000e+22  +3.2616938e-01
Donor     +2.6915348e+18  +4.2857330e-02      }
Donor     +3.1622777e+18  +4.4841561e-02

eDOSMass {
    Formula = 1
    a = +1.905e-01
    ml = +9.163e-01
}

DopingDependence {
  formula=1,1 #[1]
  mumin1=68.5,44.9 #[cm^2/Vs]
  mumin2=68.5,0.0 #[cm^2/Vs]
```

```
  mu1=56.1,29 #[cm^2/Vs]
  Pc=0.0000e+00,9.2300e+16 #[cm^3]
  Cr=9.2000e+16,2.2300e+17 #[cm^3]
  Cs=3.4100e+20,6.1000e+20 #[cm^3]
  alpha=0.711,0.719 #[1]
  beta=1.98,2 #[1]
}

Scharfetter {
  * tau = taumin + ( taumax - taumin ) / ( 1 + ( N/Nref )^gamma)
  * tau(T) = tau * ( (T/300)^Talpha )          (TempDep)
  * tau(T) = tau * exp( Tcoeff * ((T/300)-1) ) (ExpTempDep)
       taumin = 0.0000e+00 ,       0.0000e+00    # [s]
       taumax = 1.057e3 ,   1.057e3       # [s]
       Nref   = 1.900e+16 , 1.900e+16     # [cm^(-3)]
       gamma  = 1.7 ,       1.7    # [1]
       Talpha = -1.5000e+00 ,      -1.5000e+00   # [1]
       Tcoeff = 2.55 ,      2.55   # [1]
       Etrap  = 0.0000e+00  # [eV]
}

Auger {
  * R_Auger = ( C_n n + C_p p ) ( n p - ni_eff^2)
  * with C_n,p = (A + B (T/T0) + C (T/T0)^2) (1 + H exp(-{n,p}/N0))
       A      = 2.8e-31 ,   7.9e-32       # [cm^6/s]
       B      = 0,   1.24e-32      # [cm^6/s]
       C      = 0 ,  3.231e-32     # [cm^6/s]
       H      = 8 ,  8 # [1]
       N0     = 2.5e+17 ,   2.5e+17       # [cm^(-3)]
}
```

Appendix B.2 Cu_2O parameter file

```
*************************** Dielectric Constant: ****************************
******************************************************************************
Epsilon
{ *  Ratio of the permittivities of material and vacuum

  * epsilon() = epsilon
      epsilon       = 7.11                     # [1]
}


Epsilon_aniso
{ *  Ratio of the permittivities of material and vacuum

  * epsilon() = epsilon
      epsilon       = 7.11 # [1]
}


RefractiveIndex
{ *  Optical Refractive Index

  * refractiveindex() = refractiveindex * (1 + alpha * (T-Tpar))
      Tpar   = 3.0000e+02  # [K]
      refractiveindex      = 3.0  # [1]
      alpha  = 0    # [1/K] * No T-depedence specified

  * Gain dependence of refractive index in active region:
  * a) Linear model: delta n = a0 * ( (n+p)/2 - N0 )
  * b) Logarithmic model: delta n = a0 * log ( (n+p)/(2 * N0) )
  * where n/p are the carrier densities in the active region.
      a0     = 0.0000e+00  # [cm^3 or 1]
      N0     = 1.0000e+18  # [1/cm^3]
}


ComplexRefractiveIndex
{ *  Complex refractive index model: n_complex = n + i*k (unitless)
  *
  *  with n = n_0 + delta_n_lambda + delta_n_T + delta_n_carr + delta_n_gain
  *       k = k_0 + delta_k_lambda             + delta_k_carr

  * Base refractive index and extinction coefficient:
  *    n_0, k_0
      n_0    = 3.0  # [1]
      k_0    = 0.0000e+00  # [1]

  * Wavelength dependence (real and imag):
  *    Formula 0: delta_n_lambda = Cn_lambda * lambda + Dn_lambda * lambda^2
  *               delta_k_lambda = Ck_lambda * lambda + Dk_lambda * lambda^2
  *    Formula 1: Read tabulated values
  *               NumericalTable (...)
  *    Formula 2: Read tabulated values from file
  *               NumericalTable = <string>
  *    Formula 3: Read tabulated values from ODB Table
      Formula = 1
        TableInterpolation = Spline
```

```
NumericalTable (
*wavelength [um] n[1]
k[1]
0.25   1.774  1.53783;
0.255  1.759  1.57772;
0.26   1.756  1.6401;
0.265  1.775  1.72078;
0.27   1.824  1.81169;
0.275  1.910  1.89951;
0.28   2.032  1.96502;
0.285  2.178  1.98831;
0.29   2.321  1.95996;
0.295  2.432  1.88929;
0.3    2.498  1.80266;
0.305  2.520  1.72664;
0.31   2.517  1.6765;
0.315  2.503  1.65717;
0.32   2.494  1.66565;
0.325  2.499  1.69633;
0.33   2.526  1.74107;
0.335  2.578  1.78958;
0.34   2.656  1.83198;
0.345  2.756  1.85755;
0.35   2.870  1.85857;
0.355  2.986  1.83088;
0.36   3.095  1.77617;
0.365  3.186  1.70063;
0.37   3.255  1.6138;
0.375  3.302  1.52371;
0.38   3.331  1.43728;
0.385  3.345  1.35815;
0.39   3.350  1.28858;
0.395  3.348  1.2284;
0.4    3.343  1.17743;
0.405  3.336  1.13445;
0.41   3.330  1.09821;
0.415  3.325  1.06801;
0.42   3.321  1.04278;
0.425  3.320  1.02239;
0.43   3.321  1.00602;
0.435  3.325  0.99452;
0.44   3.332  0.98985;
0.445  3.347  0.99684;
0.45   3.385  1.0195;
0.452  3.414  1.03231;
0.454  3.457  1.0423;
0.456  3.517  1.0389;
0.458  3.584  1.00774;
0.46   3.637  0.94882;
0.462  3.664  0.87794;
0.464  3.666  0.81196;
0.466  3.654  0.75872;
0.468  3.638  0.71952;
0.47   3.622  0.6923;
0.472  3.612  0.67383;
0.474  3.611  0.65934;
0.476  3.621  0.64242;
0.478  3.637  0.61431;
0.48   3.649  0.57334;
0.482  3.651  0.52433;
0.484  3.639  0.47481;
0.486  3.619  0.40878;
0.488  3.594  0.34678;
0.49   3.568  0.29052;
0.492  3.541  0.2413;
0.494  3.515  0.19973;
0.496  3.491  0.16573;
0.498  3.468  0.13865;
0.5    3.446  0.11749;
0.504  3.406  0.08858;
0.508  3.371  0.07112;
0.512  3.340  0.05985;
0.516  3.312  0.05189;
0.52   3.286  0.04586;
0.524  3.262  0.04109;
0.528  3.241  0.0372;
0.532  3.221  0.03396;
0.536  3.202  0.03121;
0.54   3.184  0.02883;
0.544  3.168  0.02673;
0.548  3.153  0.02484;
0.552  3.138  0.0231;
0.556  3.124  0.02148;
0.56   3.111  0.01993;
0.564  3.099  0.01843;
0.568  3.087  0.01696;
0.572  3.075  0.01548;
0.576  3.065  0.01396;
0.58   3.054  0.01236;
0.584  3.044  0.01065;
0.588  3.035  0.00885;
0.59   3.030  0.00794;
0.592  3.026  0.00705;
0.594  3.021  0.00618;
0.596  3.017  0.00536;
0.598  3.013  0.00457;
0.6    3.008  0.00391;
0.602  3.004  0.00336;
0.603  3.002  0.00312;
0.604  3.000  0.00288;
0.606  2.996  0.00251;
0.608  2.992  0.00224;
0.61   2.988  0.00195;
0.611  2.987  0.00182;
0.612  2.985  0.00173;
0.614  2.981  0.00156;
0.616  2.977  0.00143;
0.618  2.974  0.0013;
0.62   2.970  0.00116;
0.622  2.967  0.00103;
0.624  2.963  9.04E-04;
0.626  2.960  7.57E-04;
0.627  2.958  6.64E-04;
0.628  2.957  5.35E-04;
0.629  2.955  3.69E-04;
0.63   2.953  3.49E-04;
0.632  2.950  3.04E-04;
0.634  2.947  2.53E-04;
0.636  2.944  1.85E-04;
0.637  2.942  1.37E-04;
0.638  2.941  3.71E-04;
0.64   2.938  0;
0.65   2.924  0;
0.66   2.910  0;
0.67   2.898  0;
0.68   2.886  0;
0.69   2.875  0;
0.7    2.865  0;
0.71   2.855  0;
0.72   2.846  0;
0.74   2.829  0;
0.76   2.814  0;
0.78   2.8    0;
0.8    2.787  0;
0.82   2.776  0;
0.84   2.765  0;
0.86   2.756  0;
0.88   2.747  0;
0.9    2.739  0;
0.95   2.721  0;
1      2.705  0;
1.05   2.692  0;
1.1    2.681  0;
1.15   2.672  0;
1.2    2.663  0;
1.25   2.655  0;
1.3    2.649  0;
1.35   2.643  0;
1.4    2.637  0;
1.45   2.632  0;
1.5    2.628  0;
1.55   2.624  0;
1.6    2.62   0;
1.65   2.617  0;
1.7    2.613  0;
1.75   2.61   0;
1.8    2.608  0;
1.85   2.605  0;
1.9    2.603  0;
1.95   2.601  0;
2      2.599  0;
2.05   2.597  0;
2.1    2.595  0;
2.15   2.593  0;
2.2    2.592  0;
2.25   2.59   0;
2.3    2.589  0;
2.35   2.587  0;
2.4    2.586  0;
2.45   2.585  0;
2.5    2.584  0;
       )

  * Temperature dependence (real):
  *    delta_n_T = n_0 * ( Cn_temp * (T-Tpar))
       Cn_temp       = 0    # [K^-1]
       Tpar   = 3.0000e+02  # [K]
```

```
  * Carrier dependence (real)
  *    delta_n_carr = - Cn_carr * (const.) * (n/m_e + p/m_h)
       Cn_carr       = 0    # [1]

  * Carrier dependence (imag)
  *    delta_k_carr = wavelength / (4*PI) * (Ck_carr_n*n + Ck_carr_p*p)
       Ck_carr       = 0.0000e+00 ,       0.0000e+00    # [cm^2]

  * Gain dependence (real)
  *    lin: delta_n_gain = Cn_gain * ( (n+p)/2 - Npar )
  *    log: delta_n_gain = Cn_gain * log ( (n+p)/(2 - Npar ) )
       Cn_gain       = 0    # [cm^3]
       Npar   = 1.0000e+18  # [cm^-3]
}


SpectralConversion
{ * Spectral Conversion Model
  * No default model, user has to define.
  * All wavelength parameters should be in nanometers.
  * Choice of Analytic or NumericalTable selected in Physics section of region
  *
  * ConversionEfficiency = float     * ratio of absorbed photons that are reemitted.
  * AbsorptionScaling = float        * scale absorption
  * EmissionScaling = float          * scale emission
  * Analytic (
  *   AbsorptionProfile = (
  *      Gaussian(lambda0 sigma peakvalue dc_offset lambda_range0 lambda_range1)
  *      Lorentzian(lambda0 width peakvalue dc_offset lambda_range0 lambda_range1)
  *      ...
  *   )
  *   EmissionProfile = (
  *      Gaussian(lambda0 sigma peakvalue dc_offset lambda_range0 lambda_range1)
  *      Lorentzian(lambda0 width peakvalue dc_offset lambda_range0 lambda_range1)
  *      ...
  *   )
  * )
  * NumericalTable (
  *   AbsorptionProfile = (
  *      lambda0 value0
  *      lambda1 value1
  *      ...
  *   )
  *   EmissionProfile = (
  *      lambda0 value0
  *      lambda1 value1
  *      ...
  *   )

  ConversionEfficiency = 1.0
}

************************** Lattice Heat Capacity: **************************
*****************************************************************************
LatticeHeatCapacity
{ *  lumped electron-hole-lattice heat capacity
  * cv() = cv + cv_b * T + cv_c * T^2 + cv_d * T^3
       cv     = 2.52                          # [J/(K cm^3)]
       cv_b   = 0.0000e+00                    # [J/(K^2 cm^3)]
       cv_c   = 0.0000e+00                    # [J/(K^3 cm^3)]
       cv_d   = 0.0000e+00                    # [J/(K^4 cm^3)]
}
```

```
*************************** Thermal Conductivity: ***************************
*****************************************************************************
Kappa
{ *  Lattice thermal conductivity

  Formula = 1
  * Formula = 1:
  * kappa() = kappa + kappa_b * T + kappa_c * T^2
      kappa        = 2.2                                  # [W/(K cm)]
      kappa_b      = 0.0000e+00                       # [W/(K^2 cm)]
      kappa_c      = 0.0000e+00                       # [W/(K^3 cm)]
}     * just halfway between Si and GaN, not a measured value

*****************************  Hydro Parameters  ****************************
*****************************************************************************
EnergyRelaxationTime
{ *  Energy relaxation times in ps//Taken as equal to GaN values
       tau_w_ele    = 0.2                     # [ps]
       tau_w_hol    = 0.2                     # [ps]

 * Below is the example of energy relaxation time approximation
 * by the ratio of two irrational polynomials.
 * If Wmax(interval-1) < Wc < Wmax(interval), then:
 * tau_w = (tau_w)*(Numerator^Gn)/(Denominator^Gd),
 * where (Numerator or Denominator)=SIGMA[A(i)(Wc^P(i))],
 * Wc=1.5(k*Tcar)/q (in eV).
 * By default: Wmin(0)=Wmax(-1)=0; Wmax(0)=infinity.
 * The option can be activated by specifying appropriate Formula equal to 2.
 *      Formula(tau_w_ele) = 2
 *      Formula(tau_w_hol) = 2
 *      Wmax(interval)_ele =
 *      tau_w_ele(interval)     =
 *      Numerator(interval)_ele{
 *        A(0)  =
 *        P(0)  =
 *        A(1)  =
 *        P(1)  =
 *        G     =
 *      }
 *      Denominator(interval)_ele{
 *        A(0)  =
 *        P(0)  =
 *        G     =
 *      }

 * Note: Energy relaxation times can be either molefraction dependent
 *       or energy dependent, but not both!

 *      Wmax(interval)_hol =
 *      tau_w_hol(interval)     =
}

AvalancheFactors
{ *  Coefficientss for avalanche generation with hydro
  *  Factors n_l_f, p_l_f for energy relaxation length in the expressions
  *  for effective electric field for avalanche generation
  *  eEeff = eEeff / n_l_f  ( or b = b*n_l_f )
  *  hEeff = hEeff / p_l_f  ( or b = b*p_l_f )
  *  Additional coefficients n_gamma, p_gamma, n_delta, p_delta
  *  GaN values used
       n_l_f  = 0.8                          # [1]
       p_l_f  = 0.8                          # [1]
```

```
      n_gamma       = 0.0000e+00                    # [1]
      p_gamma       = 0.0000e+00                    # [1]
      n_delta       = 0.0000e+00                    # [1]
      p_delta       = 0.0000e+00                    # [1]
}

*************************** Bandgap  ***************************************
********************************************************************************
Bandgap
{ * Eg = Eg0 + alpha Tpar2 / (beta + Tpar) - alpha T2 / (beta + T)
  * Parameter 'Tpar' specifies the value of lattice
  * temperature, at which parameters below are defined
  * Chi0 is electron affinity.
      Chi0   = 3.2                              # [eV]
      Bgn2Chi       = 0.5                       # [1]
      Eg0    = 2.06                     # [eV]
      alpha  = 6.07e-04                         # [eV K^-1]
      beta   = 6.00e+02                         # [K]
      Tpar   = 0.0000e+00               # [K]
}


BandstructureParameters
{
  * Parameters for k.p bandstructure calculation:

  * Zincblende crystals:
  * Luttinger parameters gamma_1, gamma_2, gamma_3
  * Spin-orbit split-off energy so
  * Matrix element parameters for TE and TM modes ep_te and ep_tm

  * Wurtzite crystals:
  * Effective mass parameters A1, A2, A3, A4, A5, A6
  * Spin-orbit split-off energy so
  * Crystal-field split  energy cr
  * Matrix element parameters for TE and TM modes ep_te and ep_tm
  *
  * Not modified from GaN parameters

      gamma_1       = 6.85 # [1]
      gamma_2       = 2.1  # [1]
      gamma_3       = 2.9  # [1]
      so     = 0.014       # [eV]
      ep_te  = 18.8 # [eV]
      ep_tm  = 12.4 # [eV]
      cr     = 0.019       # [eV]
      A1     = -7.2400e+00 # [1]
      A2     = -5.1000e-01 # [1]
      A3     = 6.73 # [1]
      A4     = -3.3600e+00 # [1]
      A5     = -3.3500e+00 # [1]
      A6     = -4.7200e+00 # [1]
}

QWStrain
{
  * Zincblende crystals:
  *   Parameters: a_nu, a_c, b, C_12, C_11
  *   StrainConstant eps (formula = 1) or lattice constant
  *   a0 (formula = 2) for energy shift of quantum-well
  *   subbands.
  *   a0(T) = a0 + alpha (T-Tpar)
```

```
  * Wurtzite crystals:
  *   Parameters: a_c, D1, D2, D3, D4, C_13, C_33
  *   Lattice constants a0 and c0 (formula 2 must be used)
  *   a0(T) = a0 + alpha (T-Tpar)
  *   c0(T) = c0 + alpha (T-Tpar)

        * Default formula  = 1    # [1]
       eps    = 0.0000e+00  # [1]
       a0     = 3.1890e-10  # [cm]
       alpha  = 0.0000e+00  # [cm/K]
       Tpar   = 3.0000e+02  # [K]
       a_nu   = 0.19 # [eV]
       a_c    = -4.0800e+00 # [eV]
       b_shear       = 0.9163     # [eV]
       c_11   = 11.879      # [1e-2 GPa]
       c_12   = 5.376       # [1e-2 GPa]
       d1     = -8.9000e-01 # [eV]
       d2     = 4.27 # [eV]
       d3     = 5.18 # [eV]
       d4     = -2.5900e+00 # [eV]
       c_13   = 1    # [1e-2 GPa]
       c_33   = 3.92 # [1e-2 GPa]
       c0     = 5.1850e-10  # [cm]
}


eDOSMass
{
  * For effective mass specificatition Formula1 (me approximation):
  * or Formula2 (Nc300) can be used :
       Formula       = 2    # [1]
  * Formula2:
  * me/m0 = (Nc300/2.540e19)2/3
  * Nc(T) = Nc300 * (T/300)3/2
       Nc300  = 2.47e19                        # [cm-3]
  * mass=0.9895*mo
}

hDOSMass
{
  * For effective mass specificatition Formula1 (mh approximation):
  * or Formula2 (Nv300) can be used :
       Formula       = 2    # [1]
  * Formula2:
  * mh/m0 = (Nv300/2.540e19)2/3
  * Nv(T) = Nv300 * (T/300)3/2
       Nv300  = 1.1e19                         # [cm-3]
  *mass=.577*mo
}

****************************  Mobility Models: ******************************
* mu_lowfield^(-1) = mu_dop(mu_max)^(-1) + mu_Enorm^(-1) + mu_cc^(-1)
* Variable = electron value ,   hole value             # [units]
*****************************************************************************
ConstantMobility:
{ * mu_const = mumax (T/T0)^(-Exponent)
       mumax  = 1.000e+01 , 6.000         # [cm2/(Vs)]
       Exponent      = 1 ,  1                    # [1]
}

DopingDependence:
{
  * For doping dependent mobility model three formulas
```

```
  * can be used. Formula1 is based on Masetti et al. approximation.
  * Formula2 uses approximation, suggested by Arora.
      formula      = 1 ,  1                          # [1]
  * If formula=1, model suggested by Masetti et al. is used:
  * mu_dop = mumin1 exp(-Pc/N)
  *   + (mu_const - mumin2)/(1+(N/Cr)^alpha)
  *   - mu1/(1+(Cs/N)^beta)
  * with mu_const from ConstantMobility
      mumin1 = 85,  33                          # [cm2/Vs]
      mumin2 = 75,  0.00E+00                    # [cm2/Vs]
      mu1    = 50,  20                          # [cm2/Vs]
      Pc     = 6.50E+15,   5.00E+15             # [cm3]
      Cr     = 9.50E+16,   8.00E+16             # [cm3]
      Cs     = 7.20E+19,   8.00E+20             # [cm3]
      alpha  = 0.55,             0.55           # [1]
      beta   = 0.75,             0.7            # [1]


  * If formula=2, model suggested by Arora is used:
  ***** Not Callibrated  *****
  ***** Parameters Below are for InN  *****
  * mu_dop = muminA + mudA/(1.+(N/N00)^AA),
  * where muminA=Ar_mumin*(T/T0)^Ar_alm; mudA = Ar_mud*(T/T0)^Ar_ald
  * N is net doping
  * N00=Ar_N0*(T/T0)^Ar_alN; AA = Ar_a*(T/T0)^Ar_ala
####   Ar_mumin     = 88,  54.3               # [cm2/Vs]
####   Ar_alm       = -6.70E-01,  -5.70E-01    # [1]
####   Ar_mud       = 2.20E+03,   4.07E+02     # [cm2/Vs]
####   Ar_ald       = -4.00E+00,  -2.23E+00    # [1]
####   Ar_N0        = 1.25E+17,   2.35E+17     # [cm^(-3)]
####   Ar_alN       = 1.9, 2.4                 # [1]
####   Ar_a         = 0.98,       0.88         # [1]
####   Ar_ala       = -1.50E-01,  -1.46E-01    # [1]

}

HighFieldDependence:
{ * Caughey-Thomas model:
  * mu_highfield = mu_lowfield / ( 1 + (mu_lowfield E / vsat)^beta )1/beta
  * beta = beta0 (T/T0)^betaexp.
      beta0  = 1.7 ,       1.7                  # [1]
      betaexp      = 0.0000e+00 ,      0.0000e+00          # [1]

  * Smoothing parameter for HydroHighField Caughey-Thomas model:
  * if Tl < Tc < (1+K_dT)*Tl, then smoothing between low field mobility
  * and HydroHighField mobility is used.
      K_dT   = 0.2 ,       0.2                  # [1]
  * Transferred-Electron Effect:
  * mu_highfield = (mu_lowfield+(vsat/E)*(E/E0_TrEf)4)/(1+(E/E0_TrEf)4)
      E0_TrEf      = 1.5000e+05 ,      1.5000e+05          # [1]
      Ksmooth_TrEf  = 1 ,  1                    # [1]

 * For vsat either Formula1 or Formula2 can be used.
      Vsat_Formula  = 2 ,  2                    # [1]
 * Formula2 for saturation velocity:
 *            vsat = A_vsat - B_vsat*(T/T0)
 * (Parameter Vsat_Formula has to be equal to 2):
      A_vsat = 2.1000e+07 ,       2.1000e+07          # [1]
      B_vsat = 0 ,   0                          # [1]
      vsat_min     = 1.5000e+07 ,      1.5000e+07    # [1]
}
```

```
******************  Recombination/Generation Models: *************************
* Variable = electron value ,   hole value            # [unit]
*****************************************************************************
Scharfetter * relation and trap level for SRH recombination:
{ * tau = taumin + ( taumax - taumin ) / ( 1 + ( N/Nref )^gamma)
  * tau(T) = tau * ( (T/300)^Talpha )          (TempDep)
  * tau(T) = tau * exp( Tcoeff * ((T/300)-1) ) (ExpTempDep)
       taumin = 0.0000e+00 ,      0.0000e+00          # [s]
       taumax = .60000e-9 , .60000e-9           # [s]
       Nref   = 1.0000e+16 ,      1.0000e+16          # [cm^(-3)]
       gamma  = 1 ,  1                         # [1]
       Talpha = -1.5000e+00 ,     -1.5000e+00         # [1]
       Tcoeff = 2.55 ,      2.55               # [1]
       Etrap  = 0.0000e+00                     # [eV]
}

*****************************************************************
*  Parameters for the recombination models below were taken
*  from GaAs and require calibration for accurate simulations
*****************************************************************
Auger * coefficients:
{ * R_Auger = ( C_n n + C_p p ) ( n p - ni_eff^2)
  * with C_n,p = (A + B (T/T0) + C (T/T0)^2) (1 + H exp(-{n,p}/N0))
       A      = 1.0000e-30 ,      1.0000e-30   # [cm^6/s]
       B      = 0.0000e+00 ,      0.0000e+00   # [cm^6/s]
       C      = 0.0000e+00 ,      0.0000e+00   # [cm^6/s]
       H      = 0.0000e+00 ,      0.0000e+00   # [1]
       N0     = 1.0000e+18 ,      1.0000e+18   # [cm^(-3)]
}

RadiativeRecombination * coefficients:
{ * R_Radiative = C (n p - ni_eff^2)
       C      = 1.80000e-10 # [cm^3/s]
}
```

Appendix B.3 ZnO parameter file

```
*************************** Dielectric Constant: ****************************
*****************************************************************************
Epsilon
{ *  Ratio of the permittivities of material and vacuum

  * epsilon() = epsilon
      epsilon       = 6                                 # [1]
}


Epsilon_aniso
{ *  Ratio of the permittivities of material and vacuum

  * epsilon() = epsilon
      epsilon       = 6    # [1]
}


RefractiveIndex
{ *  Optical Refractive Index

  * refractiveindex() = refractiveindex * (1 + alpha * (T-Tpar))
      Tpar   = 3.0000e+02  # [K]
      refractiveindex      = 2.0  # [1]
      alpha  = 0    # [1/K] * No T-depedence specified

  * Gain dependence of refractive index in active region:
  * a) Linear model: delta n = a0 * ( (n+p)/2 - N0 )
  * b) Logarithmic model: delta n = a0 * log ( (n+p)/(2 * N0) )
  * where n/p are the carrier densities in the active region.
      a0     = 0.0000e+00  # [cm^3 or 1]
      N0     = 1.0000e+18  # [1/cm^3]
}


ComplexRefractiveIndex
{ *  Complex refractive index model: n_complex = n + i*k (unitless)
  *
  *  with n = n_0 + delta_n_lambda + delta_n_T + delta_n_carr + delta_n_gain
  *       k = k_0 + delta_k_lambda             + delta_k_carr

  * Base refractive index and extinction coefficient:
  *    n_0, k_0
      n_0    = 2.0  # [1]
      k_0    = 0.0000e+00  # [1]

  * Wavelength dependence (real and imag):
  *    Formula 0: delta_n_lambda = Cn_lambda * lambda + Dn_lambda * lambda^2
  *               delta_k_lambda = Ck_lambda * lambda + Dk_lambda * lambda^2
  *    Formula 1: Read tabulated values
  *               NumericalTable (...)
  *    Formula 2: Read tabulated values from file
  *               NumericalTable = <string>
  *    Formula 3: Read tabulated values from ODB Table
      Formula = 1
        TableInterpolation = Spline
```

```
NumericalTable (
*wavelength [um] n[1] k[1]
300    2.1026 0.42897       ;   361    2.2418 0.07845       ;   418    2.0403 1.00E-03      ;
301    2.1078 0.42728       ;   362    2.2326 0.06735       ;   419    2.0398 1.00E-03      ;
302    2.1157 0.42449       ;   363    2.2326 0.06735       ;   420    2.036  1.00E-03      ;
303    2.1237 0.42139       ;   364    2.2229 0.05725       ;   421    2.0326 1.00E-03      ;
304    2.1295 0.41895       ;   365    2.2215 0.05595       ;   422    2.0318 1.00E-03      ;
305    2.1318 0.41796       ;   366    2.2128 0.04818       ;   423    2.0278 1.00E-03      ;
306    2.14   0.41418       ;   367    2.2128 0.04818       ;   424    2.0259 1.00E-03      ;
307    2.14   0.41418       ;   368    2.2026 0.04013       ;   425    2.0238 1.00E-03      ;
308    2.1482 0.41003       ;   369    2.2026 0.04013       ;   426    2.02   1.00E-03      ;
309    2.1482 0.41003       ;   370    2.1981 0.03695       ;   427    2.0196 1.00E-03      ;
310    2.1566 0.40548       ;   371    2.1922 0.03307       ;   428    2.0162 1.00E-03      ;
311    2.1651 0.40051       ;   372    2.1818 0.02696       ;   429    2.0138 1.00E-03      ;
312    2.1651 0.40051       ;   373    2.1818 0.02696       ;   430    2.0126 1.00E-03      ;
313    2.1736 0.39509       ;   374    2.175  0.02339       ;   431    2.009  1.00E-03      ;
314    2.1821 0.38919       ;   375    2.175  0.02339       ;   432    2.0082 1.00E-03      ;
315    2.1836 0.3881 ;          376    2.1716 0.02175       ;   433    2.0055 1.00E-03      ;
316    2.1907 0.38277       ;   377    2.1666 0.01955       ;   434    2.003  1.00E-03      ;
317    2.1993 0.37579       ;   378    2.1616 0.01735       ;   435    2.0021 1.00E-03      ;
318    2.1993 0.37579       ;   379    2.15745                  436    1.9988 1.00E-03      ;
319    2.2078 0.36823       ;          0.01579       ;         437    1.998  1.00E-03      ;
320    2.2099 0.36624       ;   380    2.1533 0.01423       ;   438    1.9955 1.00E-03      ;
321    2.2162 0.36004       ;   381    2.1518 0.0137 ;          439    1.9933 1.00E-03      ;
322    2.2245 0.3512 ;          382    2.1471 0.0122 ;          440    1.9922 1.00E-03      ;
323    2.2245 0.3512 ;          383    2.1424 0.0107 ;          441    1.9891 1.00E-03      ;
324    2.2326 0.34166       ;   384    2.1381 0.00953       ;   442    1.9888 1.00E-03      ;
325    2.2345 0.33936       ;   385    2.1338 0.00836       ;   443    1.9859 1.00E-03      ;
326    2.2404 0.33142       ;   386    2.1334 0.00828       ;   444    1.9845 1.00E-03      ;
327    2.2404 0.33142       ;   387    2.1291 0.00731       ;   445    1.9829 1.00E-03      ;
328    2.2479 0.32044       ;   388    2.1248 0.00634       ;   446    1.9803 1.00E-03      ;
329    2.2549 0.30874       ;   389    2.1167 0.00482       ;   447    1.9798 1.00E-03      ;
330    2.2557 0.30727       ;   390    2.1165 0.00478       ;   448    1.9768 1.00E-03      ;
331    2.2614 0.29631       ;   391    2.1127 0.004205      ;   449    1.9763 1.00E-03      ;
332    2.2672 0.28318       ;   392    2.1089 0.00363       ;   450    1.9739 1.00E-03      ;
333    2.2672 0.28318       ;   393    2.1052 0.00318       ;   451    1.9725 1.00E-03      ;
334    2.2719 0.27045       ;   394    2.1015 0.00273       ;   452    1.971  1.00E-03      ;
335    2.2719 0.27045       ;   395    2.1012 0.0027 ;          453    1.9688 1.00E-03      ;
336    2.2722 0.26941       ;   396    2.09785                  454    1.9681 1.00E-03      ;
337    2.2764 0.25503       ;          0.002375      ;         455    1.9652 1.00E-03      ;
338    2.2797 0.24015       ;   397    2.0945 0.00205       ;   456    1.9624 1.00E-03      ;
339    2.2797 0.24015       ;   398    2.0945 0.00205       ;   457    1.9618 1.00E-03      ;
340    2.2813 0.23029       ;   399    2.0912 0.001795      ;   458    1.9596 1.00E-03      ;
341    2.2819 0.22485       ;   400    2.0879 0.00154       ;   459    1.9584 1.00E-03      ;
342    2.283  0.20925       ;   401    2.0879 0.00154       ;   460    1.9569 1.00E-03      ;
343    2.283  0.20925       ;   402    2.0816 0.00117       ;   461    1.9552 1.00E-03      ;
344    2.283  0.19349       ;   403    2.07885                  462    1.9541 1.00E-03      ;
345    2.2828 0.18891       ;          0.001046      ;         463    1.952  1.00E-03      ;
346    2.2818 0.17769       ;   404    2.077475                 464    1.9514 1.00E-03      ;
347    2.2818 0.17769       ;          0.000984      ;         465    1.949  1.00E-03      ;
348    2.2793 0.16202       ;   405    2.0761 9.22E-04      ;   466    1.9487 1.00E-03      ;
349    2.2793 0.16202       ;   406    2.0756 9.02E-04      ;   467    1.946  1.00E-03      ;
350    2.2763 0.14879       ;   407    2.073  1.00E-03      ;   468    1.946  1.00E-03      ;
351    2.2757 0.14661       ;   408    2.0699 1.00E-03      ;   469    1.9433 1.00E-03      ;
352    2.2709 0.13163       ;   409    2.066  1.00E-03      ;   470    1.943  1.00E-03      ;
353    2.265  0.1172 ;          410    2.0656 1.00E-03      ;   471    1.9407 1.00E-03      ;
354    2.265  0.1172 ;          411    2.0644 1.00E-03      ;   472    1.9402 1.00E-03      ;
355    2.2627 0.11227       ;   412    2.0592 1.00E-03      ;   473    1.938  1.00E-03      ;
356    2.2581 0.10345       ;   413    2.0562 1.00E-03      ;   474    1.9374 1.00E-03      ;
357    2.2581 0.10345       ;   414    2.0542 1.00E-03      ;   475    1.9354 1.00E-03      ;
358    2.2504 0.09051       ;   415    2.0494 1.00E-03      ;   476    1.9347 1.00E-03      ;
359    2.2504 0.09051       ;   416    2.0476 1.00E-03      ;   477    1.9327 1.00E-03      ;
360    2.2438 0.08105       ;   417    2.0448 1.00E-03      ;   478    1.932  1.00E-03      ;
```

479	1.9301	1.00E-03	;	542	1.9	1.00E-03	;	605	1.85	1.00E-03	;
480	1.9293	1.00E-03	;	543	1.9	1.00E-03	;	606	1.85	1.00E-03	;
481	1.9275	1.00E-03	;	544	1.9	1.00E-03	;	607	1.85	1.00E-03	;
482	1.9268	1.00E-03	;	545	1.9	1.00E-03	;	608	1.85	1.00E-03	;
483	1.9248	1.00E-03	;	546	1.9	1.00E-03	;	609	1.85	1.00E-03	;
484	1.9242	1.00E-03	;	547	1.9	1.00E-03	;	610	1.85	1.00E-03	;
485	1.9222	1.00E-03	;	548	1.9	1.00E-03	;	611	1.85	1.00E-03	;
486	1.9217	1.00E-03	;	549	1.9	1.00E-03	;	612	1.85	1.00E-03	;
487	1.9196	1.00E-03	;	550	1.9	1.00E-03	;	613	1.85	1.00E-03	;
488	1.9193	1.00E-03	;	551	1.9	1.00E-03	;	614	1.85	1.00E-03	;
489	1.9169	1.00E-03	;	552	1.9	1.00E-03	;	615	1.85	1.00E-03	;
490	1.9169	1.00E-03	;	553	1.9	1.00E-03	;	616	1.85	1.00E-03	;
491	1.9145	1.00E-03	;	554	1.9	1.00E-03	;	617	1.85	1.00E-03	;
492	1.9143	1.00E-03	;	555	1.9	1.00E-03	;	618	1.85	1.00E-03	;
493	1.9122	1.00E-03	;	556	1.9	1.00E-03	;	619	1.85	1.00E-03	;
494	1.9116	1.00E-03	;	557	1.9	1.00E-03	;	620	1.85	1.00E-03	;
495	1.9098	1.00E-03	;	558	1.9	1.00E-03	;	621	1.85	1.00E-03	;
496	1.909	1.00E-03	;	559	1.9	1.00E-03	;	622	1.85	1.00E-03	;
497	1.9076	1.00E-03	;	560	1.9	1.00E-03	;	623	1.85	1.00E-03	;
498	1.9063	1.00E-03	;	561	1.9	1.00E-03	;	624	1.85	1.00E-03	;
499	1.9053	1.00E-03	;	562	1.9	1.00E-03	;	625	1.85	1.00E-03	;
500	1.9	1.00E-03	;	563	1.9	1.00E-03	;	626	1.85	1.00E-03	;
501	1.9	1.00E-03	;	564	1.9	1.00E-03	;	627	1.85	1.00E-03	;
502	1.9	1.00E-03	;	565	1.9	1.00E-03	;	628	1.85	1.00E-03	;
503	1.9	1.00E-03	;	566	1.9	1.00E-03	;	629	1.85	1.00E-03	;
504	1.9	1.00E-03	;	567	1.9	1.00E-03	;	630	1.85	1.00E-03	;
505	1.9	1.00E-03	;	568	1.9	1.00E-03	;	631	1.85	1.00E-03	;
506	1.9	1.00E-03	;	569	1.9	1.00E-03	;	632	1.85	1.00E-03	;
507	1.9	1.00E-03	;	570	1.9	1.00E-03	;	633	1.85	1.00E-03	;
508	1.9	1.00E-03	;	571	1.9	1.00E-03	;	634	1.85	1.00E-03	;
509	1.9	1.00E-03	;	572	1.9	1.00E-03	;	635	1.85	1.00E-03	;
510	1.9	1.00E-03	;	573	1.9	1.00E-03	;	636	1.85	1.00E-03	;
511	1.9	1.00E-03	;	574	1.9	1.00E-03	;	637	1.85	1.00E-03	;
512	1.9	1.00E-03	;	575	1.9	1.00E-03	;	638	1.85	1.00E-03	;
513	1.9	1.00E-03	;	576	1.9	1.00E-03	;	639	1.85	1.00E-03	;
514	1.9	1.00E-03	;	577	1.9	1.00E-03	;	640	1.85	1.00E-03	;
515	1.9	1.00E-03	;	578	1.9	1.00E-03	;	641	1.85	1.00E-03	;
516	1.9	1.00E-03	;	579	1.9	1.00E-03	;	642	1.85	1.00E-03	;
517	1.9	1.00E-03	;	580	1.9	1.00E-03	;	643	1.85	1.00E-03	;
518	1.9	1.00E-03	;	581	1.9	1.00E-03	;	644	1.85	1.00E-03	;
519	1.9	1.00E-03	;	582	1.9	1.00E-03	;	645	1.85	1.00E-03	;
520	1.9	1.00E-03	;	583	1.9	1.00E-03	;	646	1.85	1.00E-03	;
521	1.9	1.00E-03	;	584	1.9	1.00E-03	;	647	1.85	1.00E-03	;
522	1.9	1.00E-03	;	585	1.9	1.00E-03	;	648	1.85	1.00E-03	;
523	1.9	1.00E-03	;	586	1.9	1.00E-03	;	649	1.85	1.00E-03	;
524	1.9	1.00E-03	;	587	1.9	1.00E-03	;	650	1.85	1.00E-03	;
525	1.9	1.00E-03	;	588	1.9	1.00E-03	;	651	1.85	1.00E-03	;
526	1.9	1.00E-03	;	589	1.9	1.00E-03	;	652	1.85	1.00E-03	;
527	1.9	1.00E-03	;	590	1.9	1.00E-03	;	653	1.85	1.00E-03	;
528	1.9	1.00E-03	;	591	1.9	1.00E-03	;	654	1.85	1.00E-03	;
529	1.9	1.00E-03	;	592	1.9	1.00E-03	;	655	1.85	1.00E-03	;
530	1.9	1.00E-03	;	593	1.9	1.00E-03	;	656	1.85	1.00E-03	;
531	1.9	1.00E-03	;	594	1.9	1.00E-03	;	657	1.85	1.00E-03	;
532	1.9	1.00E-03	;	595	1.9	1.00E-03	;	658	1.85	1.00E-03	;
533	1.9	1.00E-03	;	596	1.9	1.00E-03	;	659	1.85	1.00E-03	;
534	1.9	1.00E-03	;	597	1.9	1.00E-03	;	660	1.85	1.00E-03	;
535	1.9	1.00E-03	;	598	1.9	1.00E-03	;	661	1.85	1.00E-03	;
536	1.9	1.00E-03	;	599	1.9	1.00E-03	;	662	1.85	1.00E-03	;
537	1.9	1.00E-03	;	600	1.9	1.00E-03	;	663	1.85	1.00E-03	;
538	1.9	1.00E-03	;	601	1.85	1.00E-03	;	664	1.85	1.00E-03	;
539	1.9	1.00E-03	;	602	1.85	1.00E-03	;	665	1.85	1.00E-03	;
540	1.9	1.00E-03	;	603	1.85	1.00E-03	;	666	1.85	1.00E-03	;
541	1.9	1.00E-03	;	604	1.85	1.00E-03	;	667	1.85	1.00E-03	;

668	1.85	1.00E-03	;	731	1.8	1.00E-03	;	794	1.8	1.00E-03	;
669	1.85	1.00E-03	;	732	1.8	1.00E-03	;	795	1.8	1.00E-03	;
670	1.85	1.00E-03	;	733	1.8	1.00E-03	;	796	1.8	1.00E-03	;
671	1.85	1.00E-03	;	734	1.8	1.00E-03	;	797	1.8	1.00E-03	;
672	1.85	1.00E-03	;	735	1.8	1.00E-03	;	798	1.8	1.00E-03	;
673	1.85	1.00E-03	;	736	1.8	1.00E-03	;	799	1.8	1.00E-03	;
674	1.85	1.00E-03	;	737	1.8	1.00E-03	;	800	1.8	1.00E-03	;
675	1.85	1.00E-03	;	738	1.8	1.00E-03	;	801	1.75	1.00E-03	;
676	1.85	1.00E-03	;	739	1.8	1.00E-03	;	802	1.75	1.00E-03	;
677	1.85	1.00E-03	;	740	1.8	1.00E-03	;	803	1.75	1.00E-03	;
678	1.85	1.00E-03	;	741	1.8	1.00E-03	;	804	1.75	1.00E-03	;
679	1.85	1.00E-03	;	742	1.8	1.00E-03	;	805	1.75	1.00E-03	;
680	1.85	1.00E-03	;	743	1.8	1.00E-03	;	806	1.75	1.00E-03	;
681	1.85	1.00E-03	;	744	1.8	1.00E-03	;	807	1.75	1.00E-03	;
682	1.85	1.00E-03	;	745	1.8	1.00E-03	;	808	1.75	1.00E-03	;
683	1.85	1.00E-03	;	746	1.8	1.00E-03	;	809	1.75	1.00E-03	;
684	1.85	1.00E-03	;	747	1.8	1.00E-03	;	810	1.75	1.00E-03	;
685	1.85	1.00E-03	;	748	1.8	1.00E-03	;	811	1.75	1.00E-03	;
686	1.85	1.00E-03	;	749	1.8	1.00E-03	;	812	1.75	1.00E-03	;
687	1.85	1.00E-03	;	750	1.8	1.00E-03	;	813	1.75	1.00E-03	;
688	1.85	1.00E-03	;	751	1.8	1.00E-03	;	814	1.75	1.00E-03	;
689	1.85	1.00E-03	;	752	1.8	1.00E-03	;	815	1.75	1.00E-03	;
690	1.85	1.00E-03	;	753	1.8	1.00E-03	;	816	1.75	1.00E-03	;
691	1.85	1.00E-03	;	754	1.8	1.00E-03	;	817	1.75	1.00E-03	;
692	1.85	1.00E-03	;	755	1.8	1.00E-03	;	818	1.75	1.00E-03	;
693	1.85	1.00E-03	;	756	1.8	1.00E-03	;	819	1.75	1.00E-03	;
694	1.85	1.00E-03	;	757	1.8	1.00E-03	;	820	1.75	1.00E-03	;
695	1.85	1.00E-03	;	758	1.8	1.00E-03	;	821	1.75	1.00E-03	;
696	1.85	1.00E-03	;	759	1.8	1.00E-03	;	822	1.75	1.00E-03	;
697	1.85	1.00E-03	;	760	1.8	1.00E-03	;	823	1.75	1.00E-03	;
698	1.85	1.00E-03	;	761	1.8	1.00E-03	;	824	1.75	1.00E-03	;
699	1.85	1.00E-03	;	762	1.8	1.00E-03	;	825	1.75	1.00E-03	;
700	1.85	1.00E-03	;	763	1.8	1.00E-03	;	826	1.75	1.00E-03	;
701	1.8	1.00E-03	;	764	1.8	1.00E-03	;	827	1.75	1.00E-03	;
702	1.8	1.00E-03	;	765	1.8	1.00E-03	;	828	1.75	1.00E-03	;
703	1.8	1.00E-03	;	766	1.8	1.00E-03	;	829	1.75	1.00E-03	;
704	1.8	1.00E-03	;	767	1.8	1.00E-03	;	830	1.75	1.00E-03	;
705	1.8	1.00E-03	;	768	1.8	1.00E-03	;	831	1.75	1.00E-03	;
706	1.8	1.00E-03	;	769	1.8	1.00E-03	;	832	1.75	1.00E-03	;
707	1.8	1.00E-03	;	770	1.8	1.00E-03	;	833	1.75	1.00E-03	;
708	1.8	1.00E-03	;	771	1.8	1.00E-03	;	834	1.75	1.00E-03	;
709	1.8	1.00E-03	;	772	1.8	1.00E-03	;	835	1.75	1.00E-03	;
710	1.8	1.00E-03	;	773	1.8	1.00E-03	;	836	1.75	1.00E-03	;
711	1.8	1.00E-03	;	774	1.8	1.00E-03	;	837	1.75	1.00E-03	;
712	1.8	1.00E-03	;	775	1.8	1.00E-03	;	838	1.75	1.00E-03	;
713	1.8	1.00E-03	;	776	1.8	1.00E-03	;	839	1.75	1.00E-03	;
714	1.8	1.00E-03	;	777	1.8	1.00E-03	;	840	1.75	1.00E-03	;
715	1.8	1.00E-03	;	778	1.8	1.00E-03	;	841	1.75	1.00E-03	;
716	1.8	1.00E-03	;	779	1.8	1.00E-03	;	842	1.75	1.00E-03	;
717	1.8	1.00E-03	;	780	1.8	1.00E-03	;	843	1.75	1.00E-03	;
718	1.8	1.00E-03	;	781	1.8	1.00E-03	;	844	1.75	1.00E-03	;
719	1.8	1.00E-03	;	782	1.8	1.00E-03	;	845	1.75	1.00E-03	;
720	1.8	1.00E-03	;	783	1.8	1.00E-03	;	846	1.75	1.00E-03	;
721	1.8	1.00E-03	;	784	1.8	1.00E-03	;	847	1.75	1.00E-03	;
722	1.8	1.00E-03	;	785	1.8	1.00E-03	;	848	1.75	1.00E-03	;
723	1.8	1.00E-03	;	786	1.8	1.00E-03	;	849	1.75	1.00E-03	;
724	1.8	1.00E-03	;	787	1.8	1.00E-03	;	850	1.75	1.00E-03	;
725	1.8	1.00E-03	;	788	1.8	1.00E-03	;	851	1.75	1.00E-03	;
726	1.8	1.00E-03	;	789	1.8	1.00E-03	;	852	1.75	1.00E-03	;
727	1.8	1.00E-03	;	790	1.8	1.00E-03	;	853	1.75	1.00E-03	;
728	1.8	1.00E-03	;	791	1.8	1.00E-03	;	854	1.75	1.00E-03	;
729	1.8	1.00E-03	;	792	1.8	1.00E-03	;	855	1.75	1.00E-03	;
730	1.8	1.00E-03	;	793	1.8	1.00E-03	;	856	1.75	1.00E-03	;

```
857    1.75   1.00E-03      ;   906    1.7    1.00E-03      ;   955    1.7    1.00E-03      ;
858    1.75   1.00E-03      ;   907    1.7    1.00E-03      ;   956    1.7    1.00E-03      ;
859    1.75   1.00E-03      ;   908    1.7    1.00E-03      ;   957    1.7    1.00E-03      ;
860    1.75   1.00E-03      ;   909    1.7    1.00E-03      ;   958    1.7    1.00E-03      ;
861    1.75   1.00E-03      ;   910    1.7    1.00E-03      ;   959    1.7    1.00E-03      ;
862    1.75   1.00E-03      ;   911    1.7    1.00E-03      ;   960    1.7    1.00E-03      ;
863    1.75   1.00E-03      ;   912    1.7    1.00E-03      ;   961    1.7    1.00E-03      ;
864    1.75   1.00E-03      ;   913    1.7    1.00E-03      ;   962    1.7    1.00E-03      ;
865    1.75   1.00E-03      ;   914    1.7    1.00E-03      ;   963    1.7    1.00E-03      ;
866    1.75   1.00E-03      ;   915    1.7    1.00E-03      ;   964    1.7    1.00E-03      ;
867    1.75   1.00E-03      ;   916    1.7    1.00E-03      ;   965    1.7    1.00E-03      ;
868    1.75   1.00E-03      ;   917    1.7    1.00E-03      ;   966    1.7    1.00E-03      ;
869    1.75   1.00E-03      ;   918    1.7    1.00E-03      ;   967    1.7    1.00E-03      ;
870    1.75   1.00E-03      ;   919    1.7    1.00E-03      ;   968    1.7    1.00E-03      ;
871    1.75   1.00E-03      ;   920    1.7    1.00E-03      ;   969    1.7    1.00E-03      ;
872    1.75   1.00E-03      ;   921    1.7    1.00E-03      ;   970    1.7    1.00E-03      ;
873    1.75   1.00E-03      ;   922    1.7    1.00E-03      ;   971    1.7    1.00E-03      ;
874    1.75   1.00E-03      ;   923    1.7    1.00E-03      ;   972    1.7    1.00E-03      ;
875    1.75   1.00E-03      ;   924    1.7    1.00E-03      ;   973    1.7    1.00E-03      ;
876    1.75   1.00E-03      ;   925    1.7    1.00E-03      ;   974    1.7    1.00E-03      ;
877    1.75   1.00E-03      ;   926    1.7    1.00E-03      ;   975    1.7    1.00E-03      ;
878    1.75   1.00E-03      ;   927    1.7    1.00E-03      ;   976    1.7    1.00E-03      ;
879    1.75   1.00E-03      ;   928    1.7    1.00E-03      ;   977    1.7    1.00E-03      ;
880    1.75   1.00E-03      ;   929    1.7    1.00E-03      ;   978    1.7    1.00E-03      ;
881    1.75   1.00E-03      ;   930    1.7    1.00E-03      ;   979    1.7    1.00E-03      ;
882    1.75   1.00E-03      ;   931    1.7    1.00E-03      ;   980    1.7    1.00E-03      ;
883    1.75   1.00E-03      ;   932    1.7    1.00E-03      ;   981    1.7    1.00E-03      ;
884    1.75   1.00E-03      ;   933    1.7    1.00E-03      ;   982    1.7    1.00E-03      ;
885    1.75   1.00E-03      ;   934    1.7    1.00E-03      ;   983    1.7    1.00E-03      ;
886    1.75   1.00E-03      ;   935    1.7    1.00E-03      ;   984    1.7    1.00E-03      ;
887    1.75   1.00E-03      ;   936    1.7    1.00E-03      ;   985    1.7    1.00E-03      ;
888    1.75   1.00E-03      ;   937    1.7    1.00E-03      ;   986    1.7    1.00E-03      ;
889    1.75   1.00E-03      ;   938    1.7    1.00E-03      ;   987    1.7    1.00E-03      ;
890    1.75   1.00E-03      ;   939    1.7    1.00E-03      ;   988    1.7    1.00E-03      ;
891    1.75   1.00E-03      ;   940    1.7    1.00E-03      ;   989    1.7    1.00E-03      ;
892    1.75   1.00E-03      ;   941    1.7    1.00E-03      ;   990    1.7    1.00E-03      ;
893    1.75   1.00E-03      ;   942    1.7    1.00E-03      ;   991    1.7    1.00E-03      ;
894    1.75   1.00E-03      ;   943    1.7    1.00E-03      ;   992    1.7    1.00E-03      ;
895    1.75   1.00E-03      ;   944    1.7    1.00E-03      ;   993    1.7    1.00E-03      ;
896    1.75   1.00E-03      ;   945    1.7    1.00E-03      ;   994    1.7    1.00E-03      ;
897    1.75   1.00E-03      ;   946    1.7    1.00E-03      ;   995    1.7    1.00E-03      ;
898    1.75   1.00E-03      ;   947    1.7    1.00E-03      ;   996    1.7    1.00E-03      ;
899    1.75   1.00E-03      ;   948    1.7    1.00E-03      ;   997    1.7    1.00E-03      ;
900    1.75   1.00E-03      ;   949    1.7    1.00E-03      ;   998    1.7    1.00E-03      ;
901    1.7    1.00E-03      ;   950    1.7    1.00E-03      ;   999    1.7    1.00E-03      ;
902    1.7    1.00E-03      ;   951    1.7    1.00E-03      ;   1000   1.7    1.00E-03      ;
903    1.7    1.00E-03      ;   952    1.7    1.00E-03      ;           )
904    1.7    1.00E-03      ;   953    1.7    1.00E-03      ;
905    1.7    1.00E-03      ;   954    1.7    1.00E-03      ;

  * Temperature dependence (real):
  *    delta_n_T = n_0 * ( Cn_temp * (T-Tpar))
       Cn_temp       = 0    # [K^-1]
       Tpar   = 3.0000e+02  # [K]

  * Carrier dependence (real)
  *    delta_n_carr = - Cn_carr * (const.) * (n/m_e + p/m_h)
       Cn_carr       = 0    # [1]

  * Carrier dependence (imag)
  *    delta_k_carr = wavelength / (4*PI) * (Ck_carr_n*n + Ck_carr_p*p)
       Ck_carr       = 0.0000e+00 ,       0.0000e+00    # [cm^2]
```

```
  * Gain dependence (real)
  *    lin: delta_n_gain = Cn_gain * ( (n+p)/2 - Npar )
  *    log: delta_n_gain = Cn_gain * log ( (n+p)/(2 - Npar ) )
       Cn_gain       = 0    # [cm^3]
       Npar   = 1.0000e+18  # [cm^-3]
}


SpectralConversion
{ * Spectral Conversion Model
  * No default model, user has to define.
  * All wavelength parameters should be in nanometers.
  * Choice of Analytic or NumericalTable selected in Physics section of region
  *
  * ConversionEfficiency = float     * ratio of absorbed photons that are reemitted.
  * AbsorptionScaling = float        * scale absorption
  * EmissionScaling = float          * scale emission
  * Analytic (
  *   AbsorptionProfile = (
  *      Gaussian(lambda0 sigma peakvalue dc_offset lambda_range0 lambda_range1)
  *      Lorentzian(lambda0 width peakvalue dc_offset lambda_range0 lambda_range1)
  *      ...
  *   )
  *   EmissionProfile = (
  *      Gaussian(lambda0 sigma peakvalue dc_offset lambda_range0 lambda_range1)
  *      Lorentzian(lambda0 width peakvalue dc_offset lambda_range0 lambda_range1)
  *      ...
  *   )
  * )
  * NumericalTable (
  *   AbsorptionProfile = (
  *      lambda0 value0
  *      lambda1 value1
  *      ...
  *   )
  *   EmissionProfile = (
  *      lambda0 value0
  *      lambda1 value1
  *      ...
  *   )

  ConversionEfficiency = 1.0
}

************************** Lattice Heat Capacity: **************************
********************************************************************************
LatticeHeatCapacity
{ *  lumped electron-hole-lattice heat capacity
  * cv() = cv + cv_b * T + cv_c * T^2 + cv_d * T^3
       cv     = 2.73                          # [J/(K cm^3)]
       cv_b   = 0.0000e+00                    # [J/(K^2 cm^3)]
       cv_c   = 0.0000e+00                    # [J/(K^3 cm^3)]
       cv_d   = 0.0000e+00                    # [J/(K^4 cm^3)]
}

*************************** Thermal Conductivity: ***************************
********************************************************************************
Kappa
{ *  Lattice thermal conductivity

  Formula = 1
  * Formula = 1:
  * kappa() = kappa + kappa_b * T + kappa_c * T^2
```

```
       kappa  = 1.1  # [W/(K cm)]
       kappa_b       = 0.0000e+00                      # [W/(K^2 cm)]
       kappa_c       = 0.0000e+00                      # [W/(K^3 cm)]
}

*****************************  Hydro Parameters  ****************************
*****************************************************************************
EnergyRelaxationTime
{ *  Energy relaxation times in picoseconds
       tau_w_ele     = 0.2                       # [ps]
       tau_w_hol     = 0.2                       # [ps]

 * Below is the example of energy relaxation time approximation
 * by the ratio of two irrational polynomials.
 * If Wmax(interval-1) < Wc < Wmax(interval), then:
 * tau_w = (tau_w)*(Numerator^Gn)/(Denominator^Gd),
 * where (Numerator or Denominator)=SIGMA[A(i)(Wc^P(i))],
 * Wc=1.5(k*Tcar)/q (in eV).
 * By default: Wmin(0)=Wmax(-1)=0; Wmax(0)=infinity.
 * The option can be activated by specifying appropriate Formula equal to 2.
 *      Formula(tau_w_ele) = 2
 *      Formula(tau_w_hol) = 2
 *      Wmax(interval)_ele =
 *      tau_w_ele(interval)     =
 *      Numerator(interval)_ele{
 *        A(0)  =
 *        P(0)  =
 *        A(1)  =
 *        P(1)  =
 *        G     =
 *      }
 *      Denominator(interval)_ele{
 *        A(0)  =
 *        P(0)  =
 *        G     =
 *      }

 * Note: Energy relaxation times can be either molefraction dependent
 *       or energy dependent, but not both!

 *      Wmax(interval)_hol =
 *      tau_w_hol(interval)     =
}

AvalancheFactors
{ *  Coefficientss for avalanche generation with hydro
  *  Factors n_l_f, p_l_f for energy relaxation length in the expressions
  *  for effective electric field for avalanche generation
  *  eEeff = eEeff / n_l_f  ( or b = b*n_l_f )
  *  hEeff = hEeff / p_l_f  ( or b = b*p_l_f )
  *  Additional coefficients n_gamma, p_gamma, n_delta, p_delta
       n_l_f  = 0.8                              # [1]
       p_l_f  = 0.8                              # [1]
       n_gamma       = 0.0000e+00                      # [1]
       p_gamma       = 0.0000e+00                      # [1]
       n_delta       = 0.0000e+00                      # [1]
       p_delta       = 0.0000e+00                      # [1]
}

*************************** Bandgap  ************************************
*****************************************************************************
Bandgap
{ * Eg = Eg0 + alpha Tpar2 / (beta + Tpar) - alpha T2 / (beta + T)
```

```
  * Parameter 'Tpar' specifies the value of lattice
  * temperature, at which parameters below are defined
  * Chi0 is electron affinity. 4.4 for pure ZnO, 3.8 for ZnS
  * Eg0 varies based on stoichiometry
      Chi0   = 3.2                          # [eV]
      Bgn2Chi      = 0.5                          # [1]
      Eg0    = 3.3                          # [eV]
      alpha  = 7.40e-04                     # [eV K^-1]
      beta   = 6.00e+02                     # [K]
      Tpar   = 0.0000e+00                   # [K]
}


BandstructureParameters
{
  * Parameters for k.p bandstructure calculation:

  * Zincblende crystals:
  * Luttinger parameters gamma_1, gamma_2, gamma_3
  * Spin-orbit split-off energy so
  * Matrix element parameters for TE and TM modes ep_te and ep_tm

  * Wurtzite crystals:
  * Effective mass parameters A1, A2, A3, A4, A5, A6
  * Spin-orbit split-off energy so
  * Crystal-field split  energy cr
  * Matrix element parameters for TE and TM modes ep_te and ep_tm
  *
  *

      gamma_1       = 6.85 # [1]
      gamma_2       = 2.1  # [1]
      gamma_3       = 2.9  # [1]
      so     = 0.014       # [eV]
      ep_te  = 18.8 # [eV]
      ep_tm  = 12.4 # [eV]
      cr     = 0.019       # [eV]
      A1     = -7.2400e+00 # [1]
      A2     = -5.1000e-01 # [1]
      A3     = 6.73 # [1]
      A4     = -3.3600e+00 # [1]
      A5     = -3.3500e+00 # [1]
      A6     = -4.7200e+00 # [1]
}

QWStrain
{
  * Zincblende crystals:
  *   Parameters: a_nu, a_c, b, C_12, C_11
  *   StrainConstant eps (formula = 1) or lattice constant
  *   a0 (formula = 2) for energy shift of quantum-well
  *   subbands.
  *   a0(T) = a0 + alpha (T-Tpar)

  * Wurtzite crystals:
  *   Parameters: a_c, D1, D2, D3, D4, C_13, C_33
  *   Lattice constants a0 and c0 (formula 2 must be used)
  *   a0(T) = a0 + alpha (T-Tpar)
  *   c0(T) = c0 + alpha (T-Tpar)

        * Default formula  = 1    # [1]
      eps    = 0.0000e+00  # [1]
      a0     = 3.1890e-10  # [cm]
```

```
       alpha  = 0.0000e+00  # [cm/K]
       Tpar   = 3.0000e+02  # [K]
       a_nu   = 0.19 # [eV]
       a_c    = -4.0800e+00 # [eV]
       b_shear       = 0.9163      # [eV]
       c_11   = 11.879      # [1e-2 GPa]
       c_12   = 5.376       # [1e-2 GPa]
       d1     = -8.9000e-01 # [eV]
       d2     = 4.27 # [eV]
       d3     = 5.18 # [eV]
       d4     = -2.5900e+00 # [eV]
       c_13   = 1    # [1e-2 GPa]
       c_33   = 3.92 # [1e-2 GPa]
       c0     = 5.1850e-10  # [cm]
}


eDOSMass
{
  * For effective mass specificatition Formula1 (me approximation):
  * or Formula2 (Nc300) can be used :
       Formula       = 2    # [1]
  * Formula2:
  * me/m0 = (Nc300/2.540e19)2/3
  * Nc(T) = Nc300 * (T/300)3/2
       Nc300  = 1.8e18                          # [cm-3]

}

hDOSMass
{
  * For effective mass specificatition Formula1 (mh approximation):
  * or Formula2 (Nv300) can be used :
       Formula       = 2    # [1]
  * Formula2:
  * mh/m0 = (Nv300/2.540e19)2/3
  * Nv(T) = Nv300 * (T/300)3/2
       Nv300  = 2.2e19                          # [cm-3]
}

*****************************  Mobility Models: ******************************
* mu_lowfield^(-1) = mu_dop(mu_max)^(-1) + mu_Enorm^(-1) + mu_cc^(-1)
* Variable = electron value ,   hole value             # [units]
*******************************************************************************
ConstantMobility:
{ * mu_const = mumax (T/T0)^(-Exponent)
       mumax  = 3.000e+01 , 6.0000        # [cm2/(Vs)]
       Exponent      = 1 ,  1                    # [1]
}

DopingDependence:
{
  * For doping dependent mobility model three formulas
  * can be used. Formula1 is based on Masetti et al. approximation.
  * Formula2 uses approximation, suggested by Arora.
       formula       = 1 ,  1                          # [1]
  * If formula=1, model suggested by Masetti et al. is used:
  * mu_dop = mumin1 exp(-Pc/N) + (mu_const - mumin2)/(1+(N/Cr)^alpha)
  *                             - mu1/(1+(Cs/N)^beta)
  * with mu_const from ConstantMobility
       mumin1 = 85,  33                         # [cm2/Vs]
       mumin2 = 75,  0.00E+00                   # [cm2/Vs]
       mu1    = 50,  20                         # [cm2/Vs]
```

```
      Pc     = 6.50E+15,   5.00E+15            # [cm3]
      Cr     = 9.50E+16,   8.00E+16            # [cm3]
      Cs     = 7.20E+19,   8.00E+20            # [cm3]
      alpha  = 0.55,             0.55                # [1]
      beta   = 0.75,             0.7                 # [1]


  * If formula=2, model suggested by Arora is used:
  ***** Not Callibrated  *****
  ***** Parameters Below are for InN  *****
  * mu_dop = muminA + mudA/(1.+(N/N00)^AA),
  * where muminA=Ar_mumin*(T/T0)^Ar_alm; mudA = Ar_mud*(T/T0)^Ar_ald
  * N is net doping
  * N00=Ar_N0*(T/T0)^Ar_alN; AA = Ar_a*(T/T0)^Ar_ala
####   Ar_mumin      = 88,  54.3               # [cm2/Vs]
####   Ar_alm        = -6.70E-01,  -5.70E-01     # [1]
####   Ar_mud        = 2.20E+03,   4.07E+02      # [cm2/Vs]
####   Ar_ald        = -4.00E+00,  -2.23E+00     # [1]
####   Ar_N0         = 1.25E+17,   2.35E+17      # [cm^(-3)]
####   Ar_alN        = 1.9, 2.4                # [1]
####   Ar_a          = 0.98,       0.88                # [1]
####   Ar_ala        = -1.50E-01,  -1.46E-01     # [1]

}

HighFieldDependence:
{ * Caughey-Thomas model:
  * mu_highfield = mu_lowfield / ( 1 + (mu_lowfield E / vsat)^beta )1/beta
  * beta = beta0 (T/T0)^betaexp.
      beta0  = 1.7 ,       1.7                       # [1]
      betaexp       = 0.0000e+00 ,      0.0000e+00          # [1]

  * Smoothing parameter for HydroHighField Caughey-Thomas model:
  * if Tl < Tc < (1+K_dT)*Tl, then smoothing between low field mobility
  * and HydroHighField mobility is used.
      K_dT   = 0.2 ,       0.2                       # [1]
  * Transferred-Electron Effect:
  * mu_highfield = (mu_lowfield+(vsat/E)*(E/E0_TrEf)4)/(1+(E/E0_TrEf)4)
      E0_TrEf       = 1.5000e+05 ,      1.5000e+05          # [1]
      Ksmooth_TrEf  = 1 ,  1                  # [1]

 * For vsat either Formula1 or Formula2 can be used.
      Vsat_Formula  = 2 ,  2                  # [1]
 * Formula2 for saturation velocity:
 *            vsat = A_vsat - B_vsat*(T/T0)
 * (Parameter Vsat_Formula has to be equal to 2):
      A_vsat = 2.1000e+07 ,       2.1000e+07          # [1]
      B_vsat = 0 ,   0                          # [1]
      vsat_min      = 1.5000e+07 ,      1.5000e+07    # [1]
}


*****************  Recombination/Generation Models: ************************
* Variable = electron value ,   hole value            # [unit]
*******************************************************************************
Scharfetter * relation and trap level for SRH recombination:
{ * tau = taumin + ( taumax - taumin ) / ( 1 + ( N/Nref )^gamma)
  * tau(T) = tau * ( (T/300)^Talpha )          (TempDep)
  * tau(T) = tau * exp( Tcoeff * ((T/300)-1) ) (ExpTempDep)
      taumin = 0.0000e+00 ,       0.0000e+00          # [s]
      taumax = 1.0000e-11 ,       1.0000e-11          # [s]
      Nref   = 1.0000e+16 ,       1.0000e+16          # [cm^(-3)]
      gamma  = 1 ,  1                           # [1]
```

```
      Talpha = -1.5000e+00 ,      -1.5000e+00          # [1]
      Tcoeff = 2.55 ,      2.55                 # [1]
      Etrap  = 0.0000e+00                       # [eV]
}


*********************************************************************
*  Parameters for the recombination models below were taken
*  from GaAs and require calibration for accurate simulations
*********************************************************************
Auger * coefficients:
{ * R_Auger = ( C_n n + C_p p ) ( n p - ni_eff^2)
  * with C_n,p = (A + B (T/T0) + C (T/T0)^2) (1 + H exp(-{n,p}/N0))
      A      = 1.0000e-30 ,       1.0000e-30    # [cm^6/s]
      B      = 0.0000e+00 ,       0.0000e+00    # [cm^6/s]
      C      = 0.0000e+00 ,       0.0000e+00    # [cm^6/s]
      H      = 0.0000e+00 ,       0.0000e+00    # [1]
      N0     = 1.0000e+18 ,       1.0000e+18    # [cm^(-3)]
}

RadiativeRecombination * coefficients:
{ * R_Radiative = C (n p - ni_eff^2)
      C      = 2.0000e-10  # [cm^3/s]
}
```